Intermediate Mass Black Holes in Star Clusters: The Case of ω Centauri (NGC 5139)

Behrang Jalali

SIGILL·UNIVERSI·TAT·LUDOVIC·MAXIM·

München 2011

Intermediate Mass Black Holes in Star Clusters: The Case of ω Centauri (NGC 5139)

Behrang Jalali

Dissertation
an der Fakultät für Physik
der Ludwig–Maximilians–Universität
München

vorgelegt von
Behrang Jalali
aus Teheran, Iran

München, den 3 August 2011

Erstgutachter: Dr. Markus Kissler-Patig
Zweitgutachter: Prof. Dr. Barbara Ercolano
Tag der mündlichen Prüfung: 28 September 2011

To Ati, for everything we shared

Contents

Abstract xiii

Zusammenfassung xiv

1 Introduction 1

- 1.1 Motivation 1
- 1.2 Relationship of IMBHs with Formation and Evolution of Galaxies 2
  - 1.2.1 Main IMBH Formation Scenarios 4
  - 1.2.2 More on the Importance of IMBHs 8
- 1.3 Detection Methods of IMBHs in Star Clusters 9
- 1.4 Omega Centauri (NGC 5139) 10
- 1.5 Outline of the thesis 18
  - 1.5.1 New Central Kinematics for ω Centauri (Chapter 2) 18
  - 1.5.2 Direct N-body Simulations of ω Centauri (Chapter 3) 19
  - 1.5.3 Orbit-based Models (Chapter 4) 19
  - 1.5.4 Conclusions and Outlook (Chapter 5) 19

2 New Central Kinematics for ω Centauri 21

- 2.1 Light: Surface Brightness Profile with space and ground-based telescopes 21
- 2.2 Kinematics: using HST and VLT-FLAMES telescopes 25
  - 2.2.1 Proper motions: HST data 25
  - 2.2.2 Radial velocities: IFU data from VLT-FLAMES 28
- 2.3 Observations and Data Reduction 29
- 2.4 Kinematic Measurements 30
- 2.5 Isotropic Models and Discussion 37

3 Direct N-body Simulations of ω Centauri 39

- 3.1 Introduction 40
- 3.2 Observational Data 43
  - 3.2.1 The Center of ω Centauri 43
  - 3.2.2 Surface Brightness Data 43
  - 3.2.3 Kinematical Data 44
- 3.3 N-body modelling Method 45

3.3.1 Model Density Profile 47
3.3.2 Model Kinematic Profile 50
3.4 Results 50
3.4.1 No-IMBH Models 51
3.4.2 IMBH Models 57
3.5 Discussion and Conclusions 64

4 Orbit-based Models 67
4.1 Introduction 67
4.2 Data 68
4.3 Dynamical Model 69
4.4 Results for ω Centauri from line-of-sight velocities 75
4.4.1 IMBH mass 75
4.4.2 Anisotropy 75
4.5 Summary and Future work 77

5 Conclusions and Outlook 85
5.1 Evidence for a central IMBH in ω Centauri 85
5.2 The VLT-FLAMES kinematic survey of Galactic globular clusters 86

Acknowledgements 99

List of Figures

1.1 Black hole mass vs. velocity dispersion correlation for galaxies 3
1.2 A diagram for formation scenario of IMBHs 6
1.3 A diagram for formation scenario of SMBHs 7
1.4 A HST image of ω Centauri 11
1.5 Characteristic phase-space density of stellar systems versus total mass . . . 13
1.6 Projected mass density of stellar systems in terms of total mass 14
1.7 Absolute V-band magnitude vs. cluster half-light radius 16
1.8 Color-magnitude diagram of ω Centauri 17

2.1 Observed V-band surface brightness profile of ω Centauri 23
2.2 Central field of ω Centauri 24
2.3 Color-magnitude diagram for stars with proper motion measurements . . . 26
2.4 Observed proper motion dispersion profile of ω Centauri 27
2.5 VLT-FLAMES pointing map of ω Centauri 30
2.6 Spectra of normal stars 31
2.7 Spectra of hot and binary stars 32
2.8 Example of integrated spectra for the central bin 34
2.9 Model velocity dispersion profile of ω Centauri 35
2.10 χ^2 values as a function of IMBH mass for the Jeans isotropic models 36

3.1 Radial velocity dispersion profiles with the same initial $\log(c)$ 48
3.2 Radial velocity dispersion profiles with the same initial r_{hp} 49
3.3 Surface brightness profile for a model without an IMBH 52
3.4 Radial velocity dispersion profile for a model without an IMBH 53
3.5 Proper motion dispersion profile for a model without an IMBH 54
3.6 RV dispersion profile for models with different IMBH masses 55
3.7 SB profile for models with different IMBH masses 56
3.8 χ^2 map for the best-fit IMBH mass 58
3.9 Reduced combined χ^2 map for the best-fit model IMBH mass 59
3.10 Surface brightness profile for an IMBH model 60
3.11 Radial velocity dispersion profile for an IMBH model 61
3.12 Proper motion dispersion profile for an IMBH model 62
3.13 Stellar M/L profile for the best-fit models 63

4.1 Internal light profile for ω Centauri 70
4.2 A schematic diagram for the orbit-based superposition method 72
4.3 χ^2 contours in terms of IMBH mass and stellar M/L 73
4.4 Marginalized χ^2 values vs. different IMBH masses 74
4.5 σ_r/σ_t profile 76
4.6 Projected LOSVDs at several radii 83

5.1 Low mass end of M_{BH} versus σ correlation 87
5.2 Observed surface brightness profile of two globular clusters in our sample . 89
5.3 Observing strategy for the two observed targets 90

List of Tables

1.1 Main parameters of ω Centauri 10

2.1 Measured velocities and higher moments 33
2.2 Shot noise effect 34

3.1 Initial parameters in the N-body simulations 45
3.2 χ^2 values for the best-fit models 64

4.1 Components of internal velocities over angular bins 79
4.1 continued. 80

5.1 Characteristics of our sample globular clusters 88

Abstract

The main aim of this work is to determine whether the star cluster ω Centauri: hosts an intermediate-mass black hole (IMBH), as well as to investigate the dynamics of its central region. We perform direct N-body simulations on Graphics Processing Units (GPUs) and run orbit-based models which allow us to follow the temporal evolution of ω Centauri and to study its orbital structure.

To this aim, we take two-dimensional integral field spectroscopic data for a few Galactic globular clusters, including ω Centauri, with FLAMES at the ESO Very Large Telescope (VLT) on Paranal in Chile. In particular, we are interested in constraining the mass of a possible IMBH in the center of our proposed star clusters. IMBHs have recently received growing attention as these objects could play an important role in the building of nuclear clusters and the formation and growth of super-massive black holes.

Understanding the nature of IMBHs, in particular for masses $< 10^5 M_\odot$ (i.e. at the low mass end of the black hole mass versus velocity dispersion correlation) is a critical step towards a better understanding of the dynamics of their hosts: massive star clusters or dwarf galaxy nuclei.

We focus on one of the best studied cases to date: ω Centauri. This cluster is one of the most important targets in this context as it is suspected to be the stripped nucleus of a dwarf galaxy and hence to represent a transition object between globular clusters and nuclear clusters.

From our observations, we confirm the measured rise in the central velocity dispersion of this cluster up to 23 km/s as the signature of a central IMBH. On the modelling side, we could well reproduce the observed kinematics and also the light profile of this cluster applying both Jeans spherical isotropic models as well as evolutionary N-body simulations containing a central $5 \times 10^4 M_\odot$ IMBH. In addition, we perform axisymmetric orbit-based models that explore the anisotropy profile and therefore orbital structure of our star cluster. The preliminary result of this method also suggest a presence of $5 \times 10^4 M_\odot$ IMBH. We propose some further detailed work which could set tighter constraints on the initial conditions of ω Centauri as well as on the existence of a central IMBH.

Zusammenfassung

Im Vordergrund dieser Arbeit steht der Kugelsternhaufen ω Centauri sowie seine kinematischen Eigenschaften und seine Funktion als möglicher Entstehungs - und Beherbergungsort eines mittelschweren Schwarzen Loches (IMBH). Wir benutzen N-body Simulationen, die auf Graphic Processing Units (GPUs) laufen, in Kombination mit orbit-based Modellen, welche uns ermöglichen, die zeitliche Entwicklung und die Struktur des Kugelsternhaufens zu erforschen.

Für diesen Zweck benutzen wir zweidimensionale integral field unit Spektroskopien, die für eine Anzahl galaktischer Kugelsternhaufen, insbesondere ω Centauri, mit dem FLAMES instrument des Very Large Telescope (VLT) am Paranal in Chile aufgenommen wurden. Ganz besonders sind wir daran interessiert, die Masse des möglichen Schwarzen Loches im Zentrum dieser Kugelsternhaufen über die Kinematik zu bestimmen. IMBHs sind aufgrund ihrer möglichen Verbindung zu Nuklearen Sternhaufen und der Bildung von Supermassiven Schwarzen Löchern in den letzten Jahren immer mehr in den Vordergrund gerückt.

Ein genaues Studium dieser Art von Schwarzen Löchern erlaubt uns vor allem einen tieferen Einblick in die kinematischen Eigenschaften ihrer Geburtsorte - massiver Kugelsternhaufen. Diese früher als sehr einfach angenommene stellaren Systeme, enthüllen immer mehr ihre komplizierte Natur.

Die meisten Erkenntnisse über schwarze Löcher in Kugelsternhaufen liegen für ω Centauri vor. Es wird vermutet, daß es sich hierbei nicht um einen Kugelsternhaufen im ursprünglichen Sinne handelt, sondern vielmehr um eine ihrer äusseren Hülle beraubten Zwerggalaxie. Vielleicht bildet ω Centauri sogar das fehlende Glied zwischen Kugelsternhaufen und Zwerggalaxien.

In unseren Beobachtungen entdeckten wir eine starke IMBH-Signatur in Form eines Anstieges der Geschwindigkeitsdispersion in Richtung Zentrum auf 23 km/s. Mit unseren N-body simulationen und einfachen analytischen Jeans Modellen gelang es uns, die Daten gut zu reproduzieren und konsistent mit beiden Modellen ein zentrales Schwarzes Loch mit 5×10^4 Sonnenmassen vorauszusagen. Zusätzlich dazu wurden auch orbit-based Modelle erzeugt, um die anisotropie und die obritale Struktur des Haufens genauer zu untersuchen. Alle vorläufigen Ergebnisse dieser Methode weisen ebenfalls auf ein 5×10^4 Sonnenmassen schweres IMBH im Zentrum hin. Wir diskutieren weitere Methoden um diese Ergebnisse zu bestätigen und zu verfeinern und den Beweis für ein IMBH im Zentrum von ω Centauri zu festigen.

Chapter 1

Introduction

1.1 Motivation

Two classes of astrophysical black holes are well established: stellar mass black holes (BHs), and super-massive black holes (SMBHs). The first class is the end product of massive stars. In stellar evolution theory, using quantum mechanics and classical mechanics laws, stars initially more massive than 20 $M_\odot$ will collapse in a relatively short time scale, ~ 5 Myr, and depending on their initial mass will form a neutron star with up to 2-3 $M_\odot$ (Bombaci, 1996) or a stellar mass BH with a typical mass of 3-20 $M_\odot$ (Fryer, 1999).

Over the last forty years, the above process became very well accepted both theoretically and observationally for stellar mass BHs (Fryer, 1999). A BH with a companion star might accrete matter to form an X-ray binary (XRB). Cygnus X-1 is the first X-ray source which is accepted to be a BH candidate. Its estimated mass is about 8 $M_\odot$ (Iorio, 2008). Together with a companion super-giant star they form a high-mass X-ray binary system about 6,000 light years (~ 1.8 kpc) from the Sun. The super-giant star provides the material for accretion of the X-ray source via stellar winds (Gies & Bolton, 1986).

Today there are some dozens of stellar mass BHs known mostly with masses in the range of 5-15 $M_\odot$ (Charles, 2001). It is interesting to note that the predicted fraction of stellar mass BHs in a binary pair, which are also currently accreting, is very small. So most stellar mass BHs are single and remain therefore undetected. Our own Milky Way is estimated to contain a few 10^6 of these BHs (Brown & Bethe, 1994).

The second well established black hole category is the one of super-massive black holes, ranging from 10^6 to a few $10^9 M_\odot$ in mass. They are believed to sit in the centers of many, if not all, galaxies (Kormendy, 1993; Gebhardt et al., 2000a). Their existence is based on the strong observational evidences of active galactic nuclei (AGNs) in the center of some galaxies. Consequently, it is assumed that these powerful AGNs receive their energy from SMBHs as central engines (Rees, 1984).

One of the most well established SMBHs lies at the center of our own Galaxy. Schoedel et al. (2002), Ghez et al. (2003) and Gillessen et al. (2009) using Near–Infrared observations measure proper motions of stars in close orbits around the Galactic center, Sgr A^*.

They also indicate a rise in the stellar velocity dispersion profile continuously down to distances of 0.01 pc. Further, the density of more than $10^{12}M_{\odot}/pc^3$ within the resolved region is again tremendously high, and consequently ruling out most alternatives against a massive BH. More detailed discussions on alternative scenarios such as a cluster of smaller mass particles, for instance heavy white dwarfs or stellar-mass BHs, that are ruled out for the case of SMBH in the heart of the Milky Way are addressed in Maoz (1995, 1998) and Genzel et al. (1996).

Additionally, beyond our Galaxy, M87 was one of the first galaxies which shows dynamical evidence for the existence of a SMBH (see Kormendy & Gebhardt, 2001, for a review). In 1978, Sargent et al. (1978) report measurements of the central velocity dispersion, rising up to ∼ 400 km/s in its central region. There are other reasons in favor of the black hole scenario at the center of M87: its AGN features such as non-thermal radio emission and broad nuclear emission lines, and in particular a "jet" of relativistic particles that is being ejected from the nucleus. All of the above studies confirm the existence of a SMBH of a few $10^9M_{\odot}$ for this giant elliptical galaxy. Most recently, Gebhardt et al. (2011) derive a mass of $6.6 \times 10^9M_{\odot}$ for the SMBH using axisymmetic orbit-based method.

In the last decade, many correlations between the SMBH mass and host galaxy properties such as central velocity dispersion (Gebhardt et al., 2000a; Gültekin et al., 2009), bulge luminosity (Magorrian et al., 1998) and bulge mass (Häring & Rix, 2004) were discovered. Figure 1.1 shows one of such tight correlations.

In the early universe SMBHs were the most energetic objects. Quasi-stellar radio sources (quasars), and their activity in the form of matter accretion and outflows were tightly related to different phases of galaxy formation and evolution. In spite of the well accepted formation scenario for stellar mass black holes, there is no conclusive formation mechanism for this extremely super-massive objects.

The above two categories of BHs are very distinct from each other, with very different masses. The BHs in XRBs are clearly the remnants of very massive stars at the end of their lives. But how are the BHs in galactic nuclei formed, and how do they evolve?

1.2 Relationship of IMBHs with Formation and Evolution of Galaxies

Many plausible formation scenarios for SMBHs are proposed. One of the possible formation mechanisms for SMBHs is through merging of IMBHs. IMBHs are supposed to have masses of a few 100 to a few $10^5M_{\odot}$. Therefore, it is possible that IMBHs and SMBHs are intimately related in the universe. It is likely that some IMBHs in galaxy centers could not have the chance to grow further and form a SMBH. Thus some galaxies may have an IMBH in their center. For instance, Filippenko & Ho (2003) show that there is a black hole with about $10^4 - 10^5M_{\odot}$ mass at the center of NGC 4395, one of the nearest known type 1 Seyfert bulgeless galaxies. Similarly, Barth et al. (2004) report the existence of an IMBH in a dwarf Seyfert 1 Galaxy POX 52.

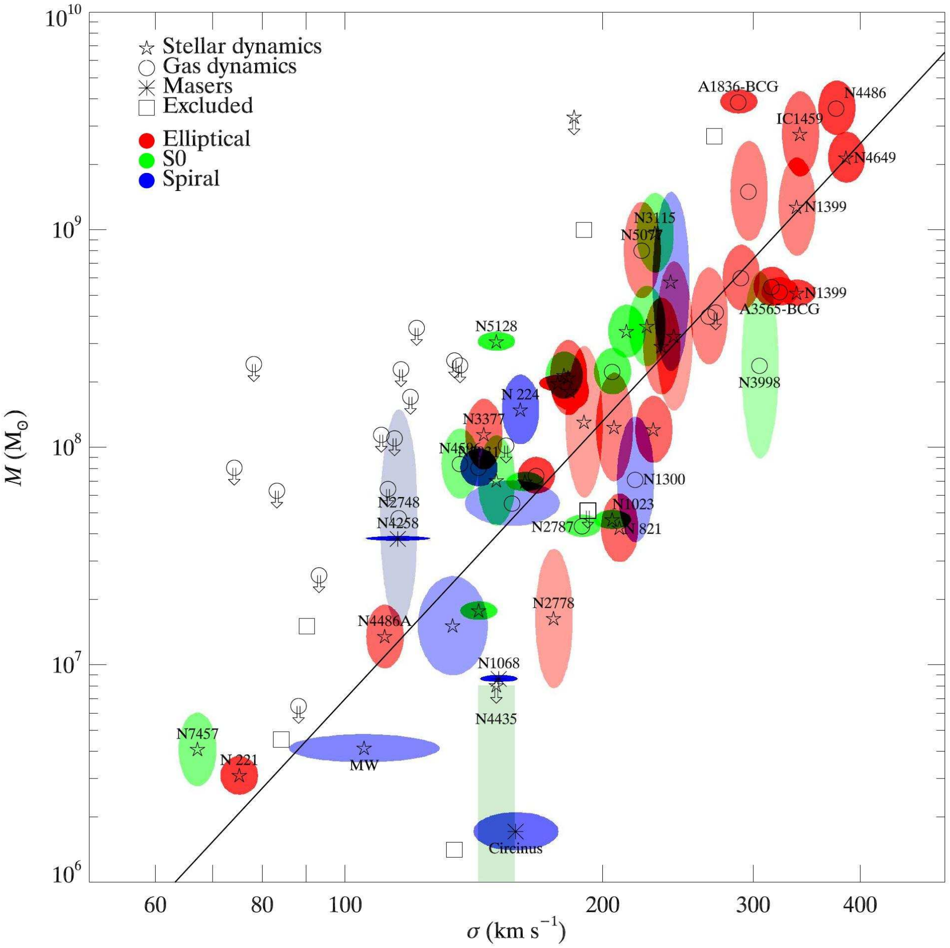

Figure 1.1: The black hole mass vs. velocity dispersion relation for galaxies with dynamical measurements (Gültekin et al., 2009). The method of BH mass measurement is indicated by different symbols: stellar dynamics (pentagrams), gas dynamics (circles), masers (asterisks). Arrows indicate 3σ upper limits to BH mass. The Hubble type of the host galaxy is marked by the color of the error ellipse. The best fit relation to the full sample is plotted by the line: $M_{BH} = 10^{8.12} M_\odot (\frac{\sigma}{200\ km/s})^{4.24}$.

Schneider et al. (2002) and Volonteri et al. (2003) studied the IMBH formation from population III stars which they propose to end up with a SMBH. They suggest that in a hierarchical assembly of galaxies from smaller systems, IMBHs in the center of small units sink to the center by dynamical friction. They then merge to form SMBHs. Haiman & Loeb (2001) find that this is a possible solution for building some $10^9 M_\odot$ black holes in the early universe which is required observationally by the detection of quasars at high redshift, $z \sim 6$ (Fan et al., 2001). This mechanism might not be responsible for all SMBHs since Hughes & Blandford (2003) show that supermassive BHs grown by mergers generally have little spin which then could not explain the observed powerful radio jets. An IMBH seed could also grow to a SMBH via accretion as an alternative to merging. Feedback from the energy output in the central region may limit the growth of the black hole (Haehnelt et al., 1998) and also the growth of the host galaxy (Silk & Rees, 1998). Thus, such scenarios including IMBHs can explain observed correlations between SMBHs and bulge mass and bulge velocity dispersion which would imply that BH growth and galaxy formation regulate each other.

1.2.1 Main IMBH Formation Scenarios

IMBHs themselves could have formed in different ways and at different cosmological epochs. They might have formed as remnants of Population III stars, the first generation of stars in the universe, or as the result of dynamical evolution processes in dense star clusters. However, it might also be possible that some IMBHs have formed as part of the formation process of SMBHs in some galaxies which then did not grow enough to build up a final SMBH.

In the early universe the stellar initial mass function (IMF) is thought to have been very different from the present-day IMF (Larson, 1998). First generation stars in the universe (population III) contained only Hydrogen and Helium, therefore zero metallicity. The general belief about the population III stars is that their IMF was top-heavy, i.e. a typical mass was about 100 $M_\odot$ instead of about 1 $M_\odot$ at the present time (Fryer et al., 2001).

Not surprisingly, the evolution of population III stars also depend on their initial masses. Stars with the initial masses of above $\sim 250 M_\odot$ could directly collapse into massive BHs since nuclear energy is not sufficient to prevent gravitational collapse. The remnant mass is about half of the initial one, so producing an IMBH (Heger & Woosley, 2002). Madau & Rees (2001) estimate the population of IMBHs formed by such population III stars. They predict that IMBHs could have formed at $z \sim 10-20$ which is the peak of mass distribution of these stars in the early universe. Such IMBHs could act as seeds for SMBHs formation.

Another way of forming IMBHs is in different environments such as in star clusters. Many groups propose that IMBHs could form by successive merging of massive stars in (young) dense stellar systems. Ebisuzaki et al. (2001) indicate that massive stars have higher merging rates, due to larger cross sections and because of a higher density in the central part of the cluster into which they sank due to mass segregation. They argue that such conditions could lead to merging instability (Lee, 1987) or a runaway growth of the most massive star in the core of the cluster. Portegies Zwart et al. (1999) show that for R 136, a compact star cluster in the Large Magellanic Cloud, physical collisions between stars are frequent. They show that the growth rate of this runaway merger is much larger than estimates based on simple cross-section arguments, because the most massive star is found in the core and tends to form a binary with other massive stars there. They predict that a very massive ($M > 100 M_\odot$) star forms on a short time scales (< 4 Myr), and such massive star could be found in the Hertzsprung-Russell diagram as a blue straggler. Once a BH form by such mergers, it will continue merging with other stars and keep growing. In M82 and the Milky Way there are about 100 such clusters in the central part (200 pc) which might host an IMBH (Portegies Zwart et al., 2006).

Ebisuzaki et al. (2001) explain the processes in details and show how an IMBH could form in such young star clusters (Figure 1.2). The main issue for such runaway scenario to occur is the race between two timescales: dynamical friction, to bring the most massive stars into the core, and mass loss of the massive stars. Basically, dynamical friction for massive stars should be shorter than their lifetime.

Usuda et al. (2001) estimate the total mass and the size of MGG-11 cluster found in the star-burst M82 galaxy to be $\sim 5 \times 10^6 M_\odot$ and 5 pc, respectively. For this object $\sim 5\%$ of the total cluster mass would be confined in a ~ 0.5 pc. Dynamical friction would be less than 10 Myr and, therefore, it could bring the most massive stars in the core and runaway merging of the stars can occur. Thus MGG-11 is a strong candidate to host an IMBH. There are some other bright massive clusters in the vicinity of this object. M82 has shown continuous star-burst activity over the last 200 Myr. Thus it is plausible that at least 100 clusters similar to MGG-11 were formed and could have formed IMBHs (see also Portegies Zwart et al. (2006) for more detailed description of MGG-11 cluster).

As is mentioned before, one of the main motivations to look for IMBHs, is that they could act as seed masses for the formation of SMBHs. In Ebisuzaki et al. (2001), they propose an idea in which IMBHs that formed in dense star clusters could spiral into the central part of the host galaxy and finally merge together to build a SMBH. Figure 1.3 shows this process schematically which basically is again the competition between two timescales: 1) the cluster orbital decay, to sink into the galaxy center and 2) the cluster evaporation due to two-body relaxation processes.

It is shown in Ebisuzaki et al. (2001) that clusters initially 1 kpc away from the galactic center can reach the center within 1 Gyr. Portegies Zwart & McMillan (2002) also estimate the evaporation timescale of a compact cluster in a tidal field that is around 2-3 half-mass relaxation times which in turn, for clusters such as MGG-11, would be a few giga-years. Therefore, since it is predicted that about 100 clusters hosting IMBHs could exist in M82, a massive black hole with about $10^5 M_\odot$ mass could be formed if we assume each IMBH has a mass of ~ 5000 $M_\odot$.

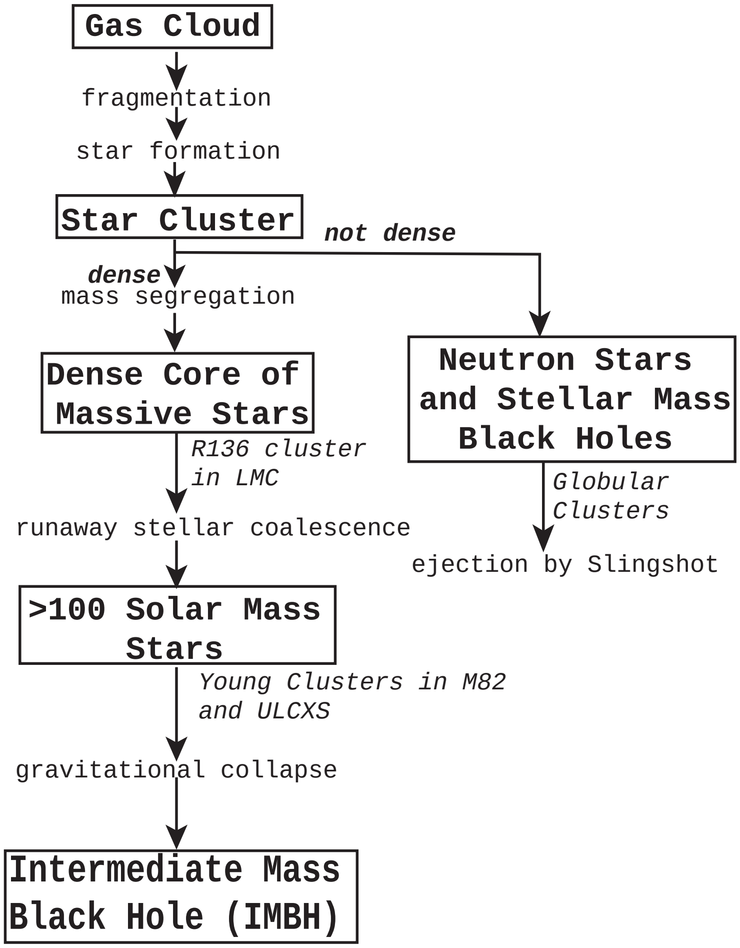
Gas Cloud
fragmentation
star formation
Star Cluster
not dense
dense
mass segregation
Dense Core of Massive Stars
R136 cluster in LMC
runaway stellar coalescence
>100 Solar Mass Stars
Young Clusters in M82 and ULCXS
gravitational collapse
Intermediate Mass Black Hole (IMBH)
Neutron Stars and Stellar Mass Black Holes
Globular Clusters
ejection by Slingshot

Figure 1.2: A schematic picture for the formation of IMBHs in a dense star cluster (Ebisuzaki et al., 2001). If the formed star cluster is dense enough, massive stars could sink into the core of the cluster before they explode as supernovae. Runaway mergers of those massive stars, then, will lead to the formation of an IMBH. Such young dense cluster are observed in LMC (R136) and M82 galaxy (MGG-11).

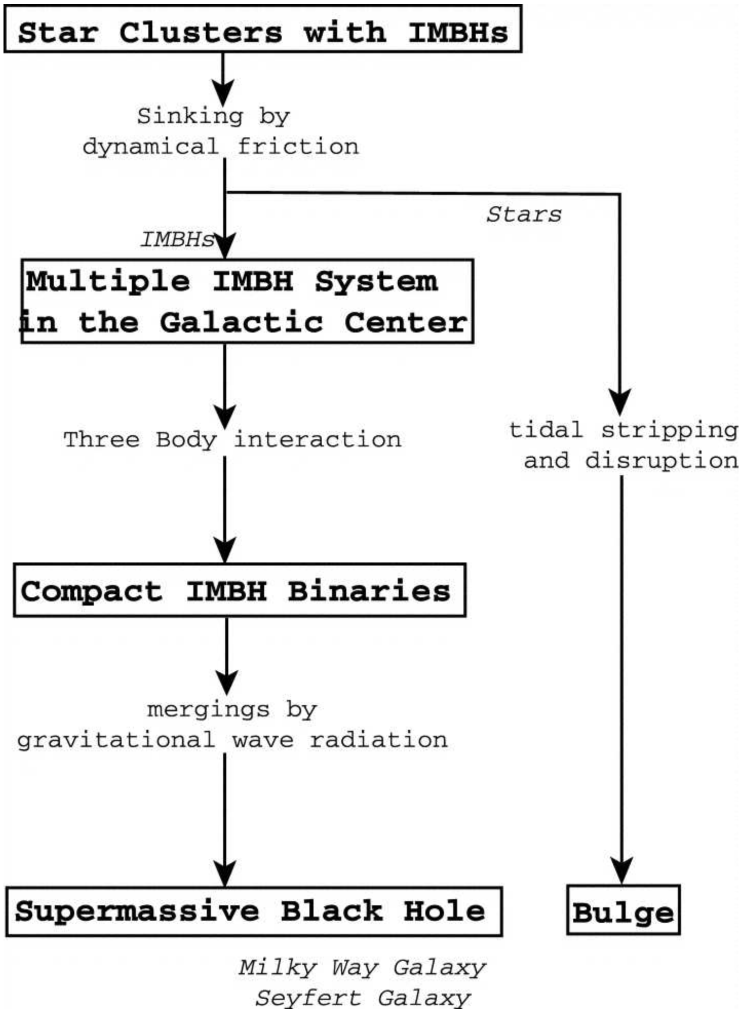
Star Clusters with IMBHs
Sinking by dynamical friction
Stars
IMBHs
Multiple IMBH System in the Galactic Center
Three Body interaction
tidal stripping and disruption
Compact IMBH Binaries
mergings by gravitational wave radiation
Supermassive Black Hole
Bulge
Milky Way Galaxy
Seyfert Galaxy

Figure 1.3: This diagram shows the proposed mechanism by Ebisuzaki et al. (2001) for the formation of super massive black holes. Young dense clusters which host an IMBH could sink into the center of galaxies if the dynamical friction timescale is shorter than evaporation of those clusters. Ultimately those IMBHs in the center of a galaxy could merge through gravitational radiation and form a SMBH.

1.2.2 More on the Importance of IMBHs

It is interesting to consider IMBHs as candidates for the missing baryonic dark matter in the universe. It is well established that the matter density of the Universe is $\Omega_m \sim 0.3$ with an additional $\Omega_\Lambda \sim 0.7$ in a so-called dark energy form. The baryonic matter density contributes as $\Omega_{baryonic} \sim 0.04$ (assumed $H_0 = 70$ km/s/Mpc) - as derived by comparing Big Bang nucleosynthesis with the observed abundances of light elements. The famous (non-baryonic) dark matter is the difference of Ω_m and $\Omega_{baryonic}$. However, this is not the only missing matter since the visible baryonic matter is at most $\Omega_{visible} \sim 0.02$. Thus half of the baryonic matter is in a dark form (Fukugita et al., 1998). The candidates, and the constraints on them, for such a baryonic dark matter are intensively reviewed by Carr & Lidsey (1993). In this context, the possibility of a population of IMBHs (for instance as remnant of population III stars) is particularly interesting to consider as an important candidate for a baryonic dark matter form (Lacey & Ostriker, 1985).

Another astrophysical importance of IMBHs is due to their gravitational emissions. Compact remnants such as stellar mass BH, neutron stars or white dwarfs that pass close to IMBHs will emit gravitational waves. For stars bound to the IMBH this will lead to mergers driven by gravitational waves. Baumgardt et al. (2004c) show that due to the mass of the IMBH, the frequency of gravitational wave emission is too low to be detected by ground-based gravitational wave detectors like Laser Interferometer Gravitational-Wave Observatory (LIGO). Space-based gravitational wave detectors such as Laser Interferometer Space Antenna (LISA) is required to detect in-spiral events for IMBHs. Miller (2003) also estimates the signal strengths of binaries containing intermediate-mass black holes in dense stellar clusters. He predicts a few detection per five years of integration for such massive BHs during the last phase of their in-spiral if IMBHs lie in the Galactic globular clusters (GCs).

As another remarkably important issue, IMBHs could be responsible for at least some of the luminous X-ray sources. The Eddington luminosity for an accreting object of mass M is $1.3 \times 10^{38} (\frac{M}{M_\odot})$ erg/s. As an example, the Eddington luminosity of a neutron star or a stellar mass BH is about 10^{38} to 10^{39} erg/s, and is in a range of 10^{42} to 10^{44} erg/s for bright Seyfert galaxies. Interestingly, X-ray observations with Chandra and ROSAT (Colbert & Ptak, 2002) demonstrate that there are some luminous sources with (isotropic) luminosities higher than those for stellar compact objects and below the ones of AGNs. Thus, those intermediate luminous objects are called ultra-luminous X-ray sources (ULXs). ULXs are usually not in the center of galaxies, so they are not related to less active AGNs. They are not candidates to be supernovae since they do not have a radio counter part (Zezas & Fabbiano, 2002), and particularly they show variability (Fabbiano et al., 2003).

Therefore, the origin of these ULXs could be linked to the accreting compact objects. If the emitted luminosity is assumed to be isotropic and at the Eddington limit, then such ULXs are IMBHs in the mass range of 15-1000 $M_\odot$. This interpretation for ULXs has some problems. King et al. (2001) show that there is no well known binary evolution that produce the required characteristics. ULXs are not usually associated with star clusters. Observations of the M82 galaxy (Matsumoto et al., 2001), and the Antenna galaxy show that ULXs are associated with star forming regions. In the Antenna galaxy, ULXs are often observed close to - but not coincident with - star clusters. However, IMBHs are too massive for being ejected XRBs (Miller & Hamilton, 2002; Portegies Zwart & McMillan, 2002). An alternative interpretation for ULXs rather than being IMBHs, is that those luminous objects are only an unusual class of XRB. Mild beaming (King et al., 2001) has been proposed in this context.

The most recent claim for an accreting IMBH with very high luminosity is HLX-1 in the outskirts of the edge-on spiral galaxy ESO 243-49 (Godet et al., 2009). Its X-ray luminosity, assuming isotropic emission, is found to be 1.1 $\times 10^{42}$ erg/s, an order of magnitude larger than the previously known brightest ULXs (Miniutti et al., 2006). HLX-1 has therefore been interpreted as an accreting intermediate-mass black hole with a minimum mass of 500 $M_{\odot}$. Wiersema et al. (2010) report a spectroscopic confirmation of the association of HLX-1 with the galaxy ESO 243-49, at a distance of 95 Mpc. Thus the claimed alternative interpretation of HLX-1 being a Galactic neutron star in a X-ray binary at a Galactic distance of only 2.5 kpc is ruled out. Furthermore, using the Magellan telescope, Soria et al. (2010) have discovered an unresolved optical counterpart within HLX1's positional error circle. They obtain an intrinsic brightness magnitude comparable to that of a massive globular cluster for the optical counterpart. HLX-1 could, therefore, be an accreting IMBH in a star cluster which, similar to G1 or ω Centauri, may itself be the stripped nucleus of a dwarf galaxy that passed through ESO 243-49.

1.3 Detection Methods of IMBHs in Star Clusters

This thesis is focused on measuring the mass of an IMBH, it is therefore appropriate to introduce some of the detection methods especially for IMBHs in star clusters.

GCs normally do not contain considerable amount of gas or dust, and consequently accretion events are not expected to cause a strong signal. Hence, the detection of radio or X-ray emission does not play a major role so far in GCs. However, using Very Large Array (VLA) radio telescope, Ulvestad et al. (2007) detect a radio source within an arcsecond of the center of G1 cluster in Andromeda galaxy that is consistent with the accretion of an IMBH. In their paper, they also show that the radio/X-ray ratio is a few hundred times higher than the one expected for a high-mass X-ray binary in this cluster.

Furthermore, recently Lu & Kong (2011) use the correlation found in Merloni et al. (2003), for AGNs and stellar mass black holes, between X-ray luminosity, black hole mass and radio flux to estimate black hole masses in several Galactic GCs with some assumptions on gas properties in GCs and accretion models. They estimate a few $10^3 M_{\odot}$ for the IMBH in ω Centauri. For almost all of their sources the estimated black hole mass is below the ones derived with dynamical measurements.

Considering all the above, accretion events might be a good method for detection but do not constrain the mass of an IMBH accurately due to large uncertainties in the gas and dust fraction as well as accretion efficiency. The best method for measuring the mass of the possible black hole is via observing and modelling the dynamics. Observationally, as

Table 1.1: Some of the main parameters of ω Centauri as well as of typical globular clusters and dwarf galaxies

	ω Centauri	Globular clusters	Dwarf galaxies
Mass ($\times 10^6 M_\odot$)	2.5	0.1	100
Luminosity (M_V)	-10	-8	-8 to -13
Half-Light Radius (pc)	6	2	10-100
Global M/L_V	3	2	10
Central σ (km/s)	23	10	>10
Dark Matter	×	×	$\surd$
Δ [Fe/H] (dex)	1	0	0.1-1.5
Δ Age (Gyr)	3	0	>1
Galactocentric Distance (kpc)	6	2-100	>100
Central Surface Brightness ($V/''^2$)	16.7	15-20 (Harris 2010)	25
$\log(T_{r_h})$ (Gyr)	10	8 to 9	>10

NOTES. – All parameters for ω Centauri and GCs are from Harris (1996), except age and metallicity spread for ω Centauri from Hilker et al. (2004), and its mass from van de Ven et al. (2006). Global M/L_v and central σ for globulars and ω Centauri are taken from Pryor & Meylan (1993). Most of the parameters for dwarf galaxies are from Mateo (1998). The Central brightness, luminosity, and effective radius values are from Bender et al. (1992).

we show in the next Chapters, one should detect a rise in the central part of the velocity dispersion profile (indicating a massive concentration), and also a cusp in stellar density (such as the one at the center of our Galaxy), to further apply dynamical models such as Jeans models or N-body simulations to measure the mass of an IMBH.

1.4 Omega Centauri (NGC 5139)

This thesis focuses on ω Centauri, thus I will briefly highlight here some of its main properties, and proposed theories for its formation and evolution. Further, I describe its current dynamical status, and in particular summarize some motivations that led us to choose this object as the best target for detecting an IMBH.

Being as bright as 4th magnitude, ω Centauri (or NGC 5139) has been known since ancient times. It was listed in Ptolemy's catalog as a star, and received its "Omega" designation from Beyer in his catalog of stars. Edmund Halley, in 1677, was the first to document its non-stellar appearance, listing it as a "luminous spot or patch in Centaurus" (Sawyer Hogg, 1947). ω Centauri is very luminous, and is in fact rightfully called the jewel of the southern hemisphere. Its apparent size is twice the size of the full Moon. Sir John Herschel wrote in the 1830s: "The noble globular cluster Omega Centauri is beyond all comparison the richest and largest object of its kind in the heavens. The stars are literally innumerable, and as their total light affects the eye hardly more than a star of 4th magnitude, the minuteness of each star may be imagined" and classified it as a globular cluster. I summarize the main properties of ω Centauri, as well as a comparison with a classical globular cluster and a dwarf galaxy in Table 4.1. Figure 1.4 shows an image of this system taken by HST.

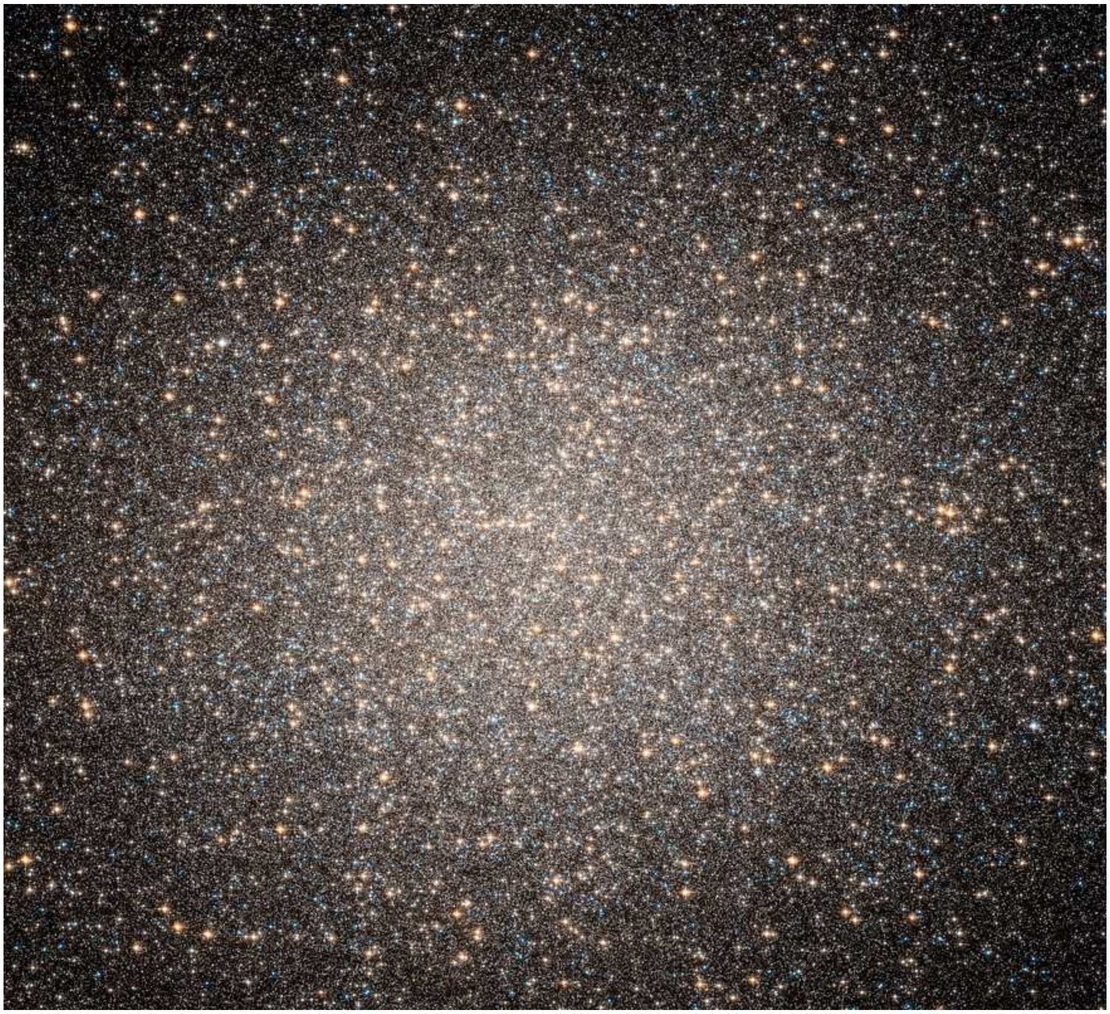

Figure 1.4: An image of ω Centauri showing only the core of this very large (R_{core} ~3 pc) Milky Way cluster, taken by the Advanced Camera for Surveys (ACS) on Hubble Space Telescope (credits from the NASA/ESA Hubble Space Telescope).

As prescribed above, one might think about ω Centauri as a normal globular cluster in the first place. However, as we show in the following such a classification is not very trivial for ω Centauri. It could as well be classified as the stripped nucleus of a dwarf galaxy.

According to Sparke & Gallagher (2006), GCs are an ensemble of gravitationally bound, old stars which do not contain dark matter. In addition, they are basically objects that have simple stellar populations (SSPs), i.e. their stars have the same age, and more or less the same chemical compositions.

However, in the last decade it turned out that beside the gravitationally bound condition, and lack of dark matter, none of the other above properties are met completely for most of the Galactic GCs. One should note that there are few extensive observations and modelling efforts to actually constrain the existence of dark matter especially in the outskirts of these objects (Abramowski et al., 2011).

ω Centauri's chemical abundances have long been known to be unusual for a globular cluster. The wide spread in the globular's metallicity distribution function suggests a complex formation process (Hilker et al., 2004). Also it is found by Hilker et al. (2004) that there is an age spread of 3 billion years in the stars within ω Centauri. One would not expect star formation to occur at such different times in a normal globular cluster. Therefore, I review the arguments for which ω Centauri could be classified either as a typical GCs or as an accreted dwarf galaxy.

There are multiple reasons to believe that ω Centauri is a normal ordinary GC. Firstly, it follows the basic definition of a globular cluster as mentioned above, i.e. it is certainly a collection of bound stars, albeit loosely bound, concerning its low concentration and huge radial extension. Moreover, as is shown in Figure 1.5, ω Centauri as well as G1 (the largest GC in the Andromeda galaxy, with similar properties as ω Centauri), nicely follow the fundamental plane scaling relation for most GCs in the Milky Way and GCs in other galaxies such as NGC 5128. This figure shows the characteristic phase space density inside the half-mass radius, f_e, against mass of the stellar systems. Walcher et al. (2005) define f_e using the half-mass radius r_h, total mass M and measured velocity dispersion σ according to be:

$$f_e = \frac{\rho_h}{\sigma^3} = \frac{M}{2} \frac{1}{\frac{4}{3}\pi r_h^3 \sigma^3} \propto r_h^{-2} \sigma^{-1}. \tag{1.1}$$

The projected effective radii r_e could be derived from 3D half-mass radii r_h by the approximate relation $r_e = 0.75\ r_h$ (Spitzer, 1987, page 12). As is stated in Walcher et al. (2005), the change of slope in this figure defines two group of systems, galaxies and star clusters, where ω Centauri as well as nuclear clusters fall on the sequence of massive star clusters.

Furthermore, from spectroscopic signatures, GCs are known to show star-to-star variations in the abundances of the light elements such as C, N, O, Na, and Mg. Typical GCs show a Na-O anti-correlation (Gratton et al., 2001). D'Antona et al. (2011) show that ω Centauri also shows this Na-O anti-correlation. In addition to the wide spread in the metallicity distribution for ω Centauri, this system shows very clear and pronounced distinct multiple populations in its color magnitude diagram. These two properties are now being discovered in many (massive) GCs.

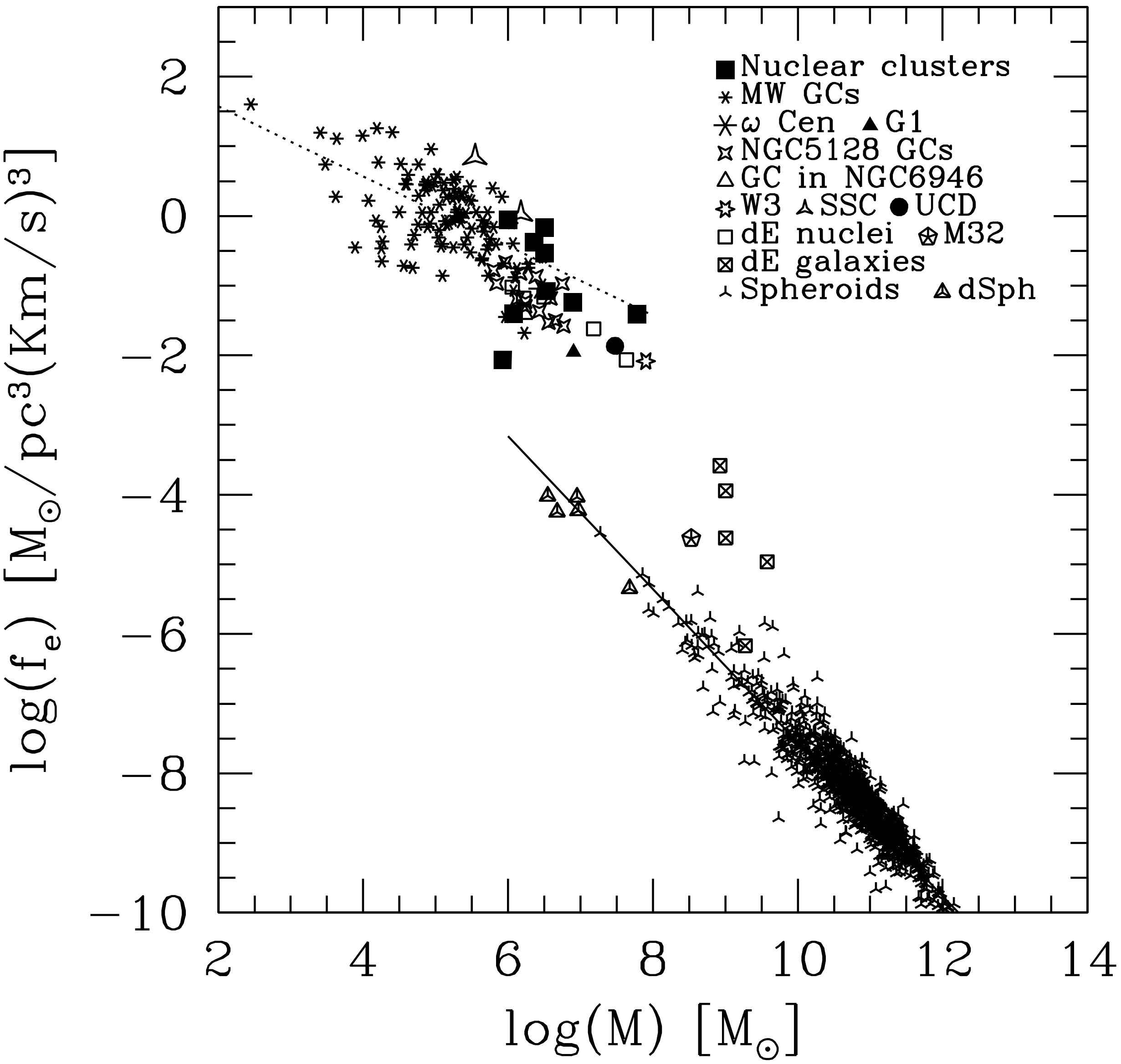

Figure 1.5: The two families of stellar systems, according to Walcher et al. (2005), shown in a plane of characteristic phase-space density, f_e, versus total mass, M, inside the half-mass radius of each system, r_h (see text for details). All the shown objects around the two lines obey the virial theorem, but systems around the solid line follow a Faber & Jackson (1976) relationship of the form $M \propto \sigma^{3.33}$. Interestingly, ω Centauri (close to G1) and G1 lie in the region populated by GCs and nuclear clusters.

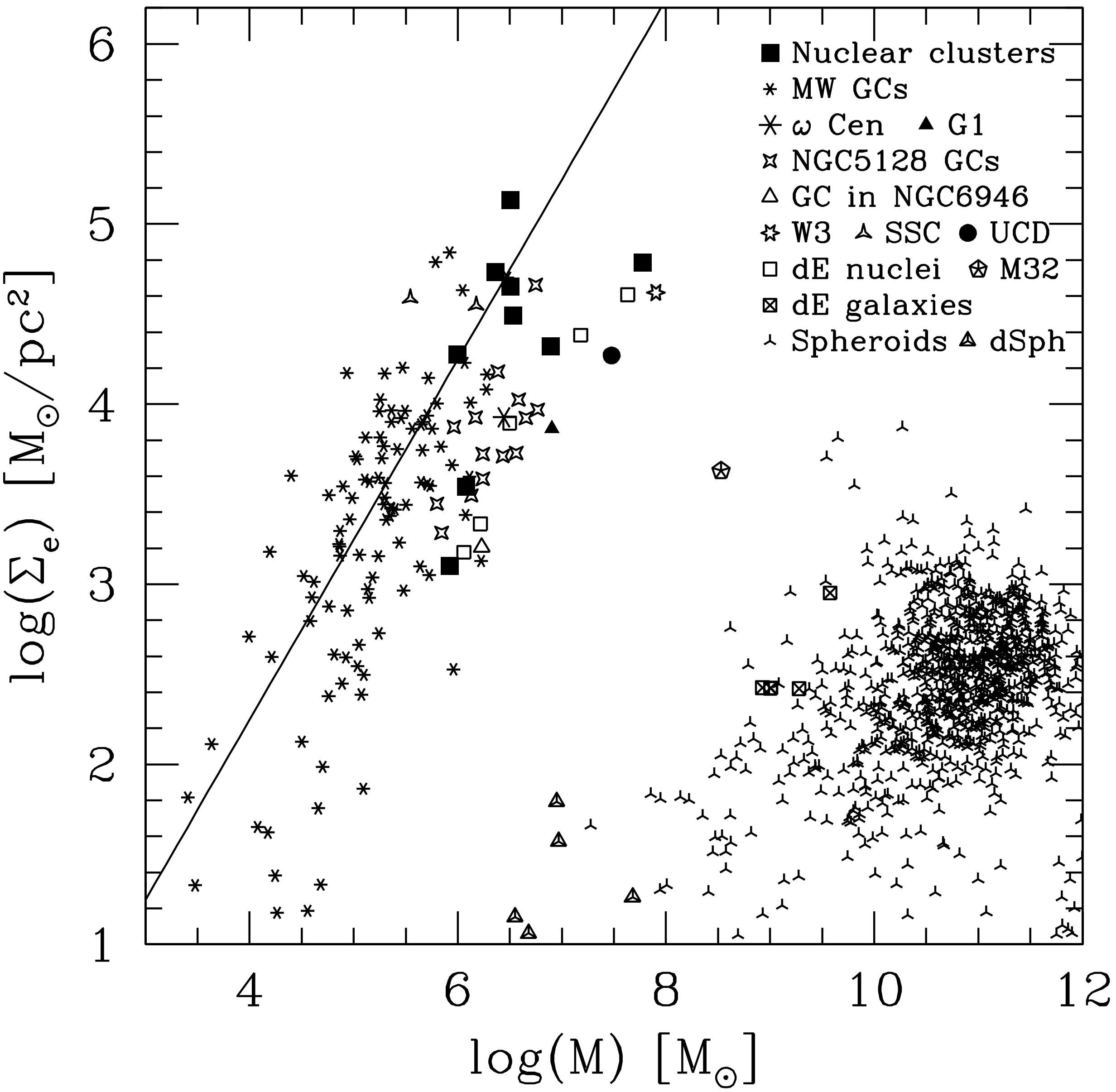

Figure 1.6: This plot, taken from Walcher et al. (2005), presents mean projected mass density inside the effective radius in terms of the total mass (symbols are consistent with the previous Figure). In this plot the position of ω Centauri and G1 are more similar to dSphs and nuclear clusters in mass, although they are well separated from bulges.

On the other hand, ω Centauri could as well be classified as a dwarf galaxy, relying on the properties mentioned in Table 4.1. Its total mass, luminosity, and internal age spread lie in the range of the ones for dwarf galaxies. This can also be seen in Figure 1.6 (Walcher et al., 2005), where from the point of view of the total mass ω Centauri lies in the region of low mass dwarf spheroidal galaxies (dSphs), while its high surface mass density brings it back to the region of GCs and nuclei of dwarf ellipticals. It is also interesting from a dynamical point of view to note that its central velocity dispersion is higher than for any other Galactic star clusters.

This anomaly can also be recognized in the Figure 1.7 which depicts the similarities of ω Centauri and M54 - as a nuclear cluster of Sagittarius dwarf galaxy. ω Centauri has a very blue extended horizontal branch (EHB), and it has been shown by Georgiev et al. (2009) that star clusters with EHBs tend to be very massive. Georgiev et al. (2009) claim that star clusters evolve to lower concentration and lose a significant amount of mass when being captured by a massive galaxy such as the Milky Way.

Moreover, ω Centauri has an orbit that is not normal for typical Galactic GCs, and is unlikely to have formed at its current position. ω Centauri's orbit is retrograde, $r_{apocenter} =$ 6.4 kpc, and flat, $|z|_{max} \sim 1$ kpc (Dinescu et al., 1999). The orbital period ($\tau \sim 100$ Myr) is shorter than those for most GCs and dSphs. ω Centauri's orbit contrasts sharply with halo GCs, which typically co-rotate with the Galaxy, and have highly radial, large r_a orbits. Thus, ω Centauri is very unusual as a globular cluster, but could be fairly well explained as a former nuclear star cluster in a dwarf galaxy.

Another reason why ω Centauri deviates from the classical definition of a GC is seen by looking at its color-magnitude diagram (Figure 1.8). ω Centauri is the first Galactic star cluster where multiple stellar populations have been discovered almost over its entire magnitude range. The metallicity spread on the giant branch has been discovered and studied from the ground since many decades (Freeman & Rodgers, 1975), but only with the Hubble Space Telescope (HST) it became feasible to uncover the multiple populations down to the faint main sequence stars. Anderson (2002) using HST found multiple turn-offs and a bifurcated main sequence. Bedin et al. (2004) exploited larger fields and different filters, again observed by HST, and confirmed the double main sequence populations. The double main sequence, the multiple turnoffs and sub-giant branches, and multiple population sequences along the red giant branch of this cluster, illustrated in Fig. 1.8, show a fascinating picture of ω Centauri as a complex object which has a puzzling origin. ω Centauri resembles dwarf galaxies in terms of stellar populations, traceable multiple sequences, and the significant spread in age and metallicity (Hilker et al., 2004).

The chemical composition of ω Centauri shows a large range in $[\frac{Fe}{H}]$ metallicity and in age (Norris & Da Costa, 1995). $[\frac{\alpha}{H}]$ is high for most of the $[\frac{Fe}{H}]$ range which implies that feedback from SN II is predominant, and is similar to local group dwarf galaxies.

Thus, we can assume an extended star formation history for ω Centauri, which could have experienced self-enrichment similar to the one seen in dwarf galaxies.

From the dynamical point of view, Noyola et al. (2008) suggest an intermediate mass black hole of about $4 \times 10^4 M_{\odot}$ in ω Centauri. Such a claim has been made for dwarf galaxies like M32 (van der Marel et al., 1998), M54 in Sagittarius (Ibata et al., 2009) and

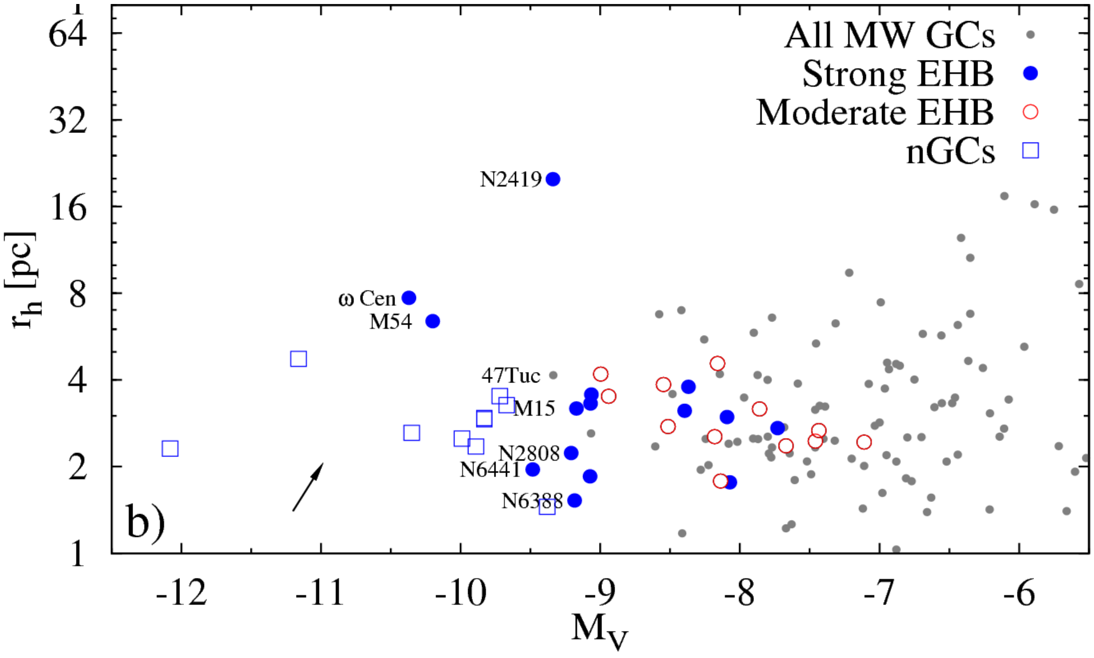

Figure 1.7: Absolute V-band magnitude vs. cluster half-light radius for different stellar systems: Galactic GCs, nuclear globular clusters (nGC) in dwarf galaxies and Galactic globular clusters with extended horizontal branches (Georgiev et al., 2009). The arrow shows the expected direction of evolution of the clusters from tidal stripping by accretion which increase the half-light expansion and cause the mass loss.

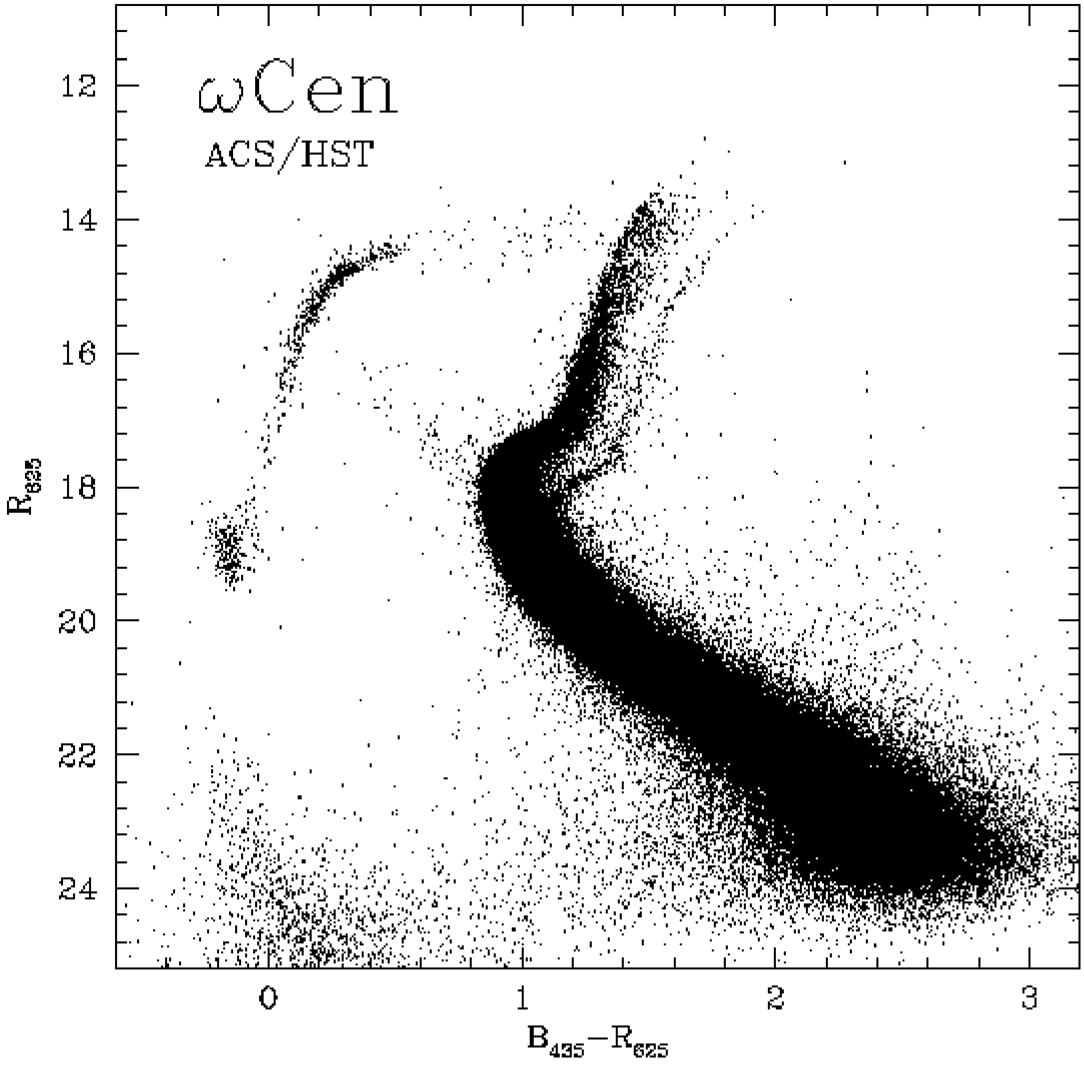

Figure 1.8: The color-magnitude diagram of ω Centauri for more than 400,000 stars identified in the nine ACS fields (Ferraro et al., 2004). The second pronounced red giant branch stars, called SGB-a, is clearly visible. This diagram shows that this object is very complex and clearly differs from many other Galactic GCs.

POX 52 (Barth et al., 2004), as well as for G1 in the Andromeda galaxy (Gebhardt et al., 2005; Ulvestad et al., 2007).

Further, in-spite of the normal M/L for ω Centauri (consistent with its stellar populations) it is worth to add a note about the dark matter content of this object.
Mashchenko & Sills (2005) and Baumgardt & Mieske (2008) show mechanisms by which low-mass groups of baryons, such as the progenitor of ω Centauri, could strip off their initial dark matter halos during the interaction with a massive galaxy.

Thus, as described briefly above, a plausible scenario for ω Centauri could be that it formed in a dark matter halo, enriched itself by heavy elements over about 3 Gyr via SN II feedback, and got accreted onto the Galaxy. It then lost its gas and thus the ability to form stars and stripped off its stellar envelope as well as its dark matter halo.

We can thus speculate that, a few Gyr ago, ω Centauri looked like M54 in Sagittarius, and in a few Gyr from now its stars will be dissolved in the inner halo field of the Milky Way.

In spite of all the debates on its nature and the actual formation scenario, ω Centauri is indeed the best target for studying its central parsecs and looking for a possible central massive black hole, because it is one of the most massive, most luminous, and most spatially extended Galactic "stellar systems". On top of that, it has a very high central velocity dispersion, indicating a possibility for a massive concentration in its central region.

1.5 Outline of the thesis

In the first Chapter, I briefly introduced the importance of IMBHs, for formation and evolution of galaxies as well as astrophysical consequences, and indicated some possible formation scenarios for them. Moreover, I showed that star clusters such as ω Centauri are among the best sites to look for detecting an IMBH.

I presented some of the main properties of ω Centauri and showed that in fact it is hard to classify this object as a normal globular cluster as it could also be the remnant of an accreted dwarf galaxy. Clearly, ω Centauri is the most interesting Galactic star cluster and a unique target to study its central dynamics with the aim to find an IMBH.

In the following chapters I present the data and techniques that I use to accomplish this goal.

1.5.1 New Central Kinematics for ω Centauri (Chapter 2)

In Chapter 2, I describe the kinematic measurements we obtain for a couple of the Milky Way's star clusters, including ω Centauri, using the VLT-FLAMES integral field spectrograph. Integral field spectroscopy (IFS) provides two-dimensional maps of the line-of-sight velocities. The two-dimensional maps give necessary information to better constrain the kinematics of stellar systems.

Furthermore, I present velocities of stars on the plane of the sky (proper motions) taken from space using the Hubble Space Telescope. Proper motions provide additional components of velocities necessary for our goal in better understanding the central dynamics of our object.

1.5.2 Direct N-body Simulations of ω Centauri (Chapter 3)

Chapter 3 presents the results of N-body simulations tailored to the properties of ω Centauri. In these simulations we follow the dynamical evolution of stars (including stellar evolution) directly star-by-star, and investigate in details the effect of an IMBH on the dynamical evolution of model clusters. The models are compared to our newly acquired VLT-FLAMES data, as well as to the rich data from the literature.

Using N-body simulations allows us to follow the evolutionary track of stellar systems under some certain canonical assumptions, and compare the plausible final dynamical states of our model cluster with the observations.

1.5.3 Orbit-based Models (Chapter 4)

In Chapter 4, I apply the orbit-based modelling method assuming axisymmetry to study the detailed orbital structure of ω Centauri. Further, using this approach one can better investigate the degeneracy between mass-to-light ratio and black hole mass for stellar systems.

I address the preliminary results that we obtain using the light profile and line-of-sight velocities, described in Chapter 2. I will use proper motions as additional information on the kinematics to better constrain the black hole mass.

1.5.4 Conclusions and Outlook (Chapter 5)

In this final Chapter, I summarise the main findings of this thesis and propose a few lines of future research. I give a glance on a sample of Galactic star clusters that we have kinematic data for.

Further, on the modelling side, I lay out some ideas for more detailed studies that will hopefully provide a better understanding of the presence of IMBHs in star clusters and also clarify the situations with respect to the current alternatives to IMBHs in these stellar systems.

Chapter 2

New Central Kinematics for ω Centauri

Based on Noyola, E., Gebhardt, K., Kissler-Patig, M.,
Lützgendorf, N., Jalali, B., de Zeeuw, P. T., Baumgardt, H.
2010, ApJL, 719, 60

In this chapter, I present the available density and kinematic data for ω Centauri which we will compare in the next two chapters with our models to constrain the central dynamics of this object. I also briefly explain our integral field spectroscopy survey obtained with VLT-FLAMES in ARGUS mode, aimed at studying the demography of potential IMBHs in a sample of Galactic star clusters.

As we described in the first Chapter, two-dimensional kinematic data provide a rich information to study the dynamics of stellar systems. It is also used in many astrophysical environments such as star formation regions and galaxies. We describe in this chapter such a 2D kinematic study for one of the objects in our sample, ω Centauri. In addition, we demonstrate the power of HST spatial resolution for obtaining light profiles of our objects which is crucial to construct dynamical models.

2.1 Light: Surface Brightness Profile with space and ground-based telescopes

To investigate the dynamical status of stellar systems, it is necessary to use a surface brightness profile (SBP) as it is representing a (luminosity) density profile of the system as a function of radius. The SBP for ω Centauri was the subject of many studies already before the 70's from ground-based facilities. Meylan (1987) and Trager et al. (1995) compile the SBP for this object from various sources. Gascoigne & Burr (1956) and Da Costa (1979) use aperture photometry for the central regions and King et al. (1968) apply star counts for larger radii. This compiled data covered a radial range of $10''$ to $\sim 2500''$ from the center (~ 0.3 to 50 pc at ω Centauri distance).

However, only with the Hubble Space Telescope (HST) resolution it is possible to reliably detect individual stars within $10''$ radius and obtain the light profile for the most inner region, where ground-based observations suffer from sever crowding.

Figure 2.1 shows the SBP for ω Centauri with respect to a center that is determined in van der Marel & Anderson (2010, hereafter vdMA10). Note that, in Chapter 3 and Chapter 4 we derive the SBP with respect to another center that we find from multiple arguments, and that we adopt for model-data comparisons (see for instance Figure 3.3 in chapter 3).

In spite of the general agreement on the SBP values for large radii on this profile, there is not agreement yet for the central $10''$. This is partly because of different techniques used to determine the center and also to derive the SBP itself. This discrepancy arises because ω Centauri has a very large core, which also shows a rather flat distribution of stars. The core size is about 2.5 pc (see Table 1 in chapter 1) which at the distance of ω Centauri (4.8 kpc; van de Ven et al., 2006, hereafter vdV06) is about $100''$ and is considerably larger than other Galactic star clusters. These facts make it quite challenging to agree on a center position very precisely.

Noyola et al. (2008, hereafter NGB08), for instance, apply a technique where they count the number of stars in eight concentric sectors around several trial centers. They calculate the standard deviation of the sum of stars for this sectors. After repeating the procedure for a grid of center coordinates, they find a center which shows the minimum standard deviation (for more details see Noyola & Gebhardt, 2006). NGB08, then, use integrated light from Advanced Camera Surveys (ACS) on HST to determine the SBP inside $40''$. In that study, they report a shallow cusp, with a central logarithmic slope of ~ -0.08, that they interpret as an indicator for the presence of an IMBH (see below).

As an alternative to the above approach, Anderson & van der Marel (2010, hereafter, AvdM10) again use HST but with a larger field, $10' \times 10'$, and try various methods to find the center, and then they derive a SBP. Their center lies $\sim 12''$ away from the center found by NBG08 and previous studies (Figure 2.2). vdMA10 see a rather flat core instead of a shallow cusp, and as we see in the next sections they find a relatively flat velocity dispersion profile with respect to their determined center.

Both studies have their own advantages and disadvantages. Without going into detail, as we see in the next two chapters the behavior of the central part of the surface brightness and kinematic profiles make a pronounced difference on the interpretations for the presence of a central massive object such as an IMBH, and consequently its mass.

Interestingly, Baumgardt et al. (2004a,b, 2005) find that star clusters with an IMBH will have a shallow cusp in the SBPs. Further, Baumgardt et al. (2004b) find that star clusters starting from multimass King profiles, and containing an IMBH will expand more after a Hubble time compared to clusters without an IMBH as a result of energy generation in the cusp around the black hole. Therefore, the clusters with an IMBH will be among the least concentrated globular clusters at the present time. Additionally, the more massive

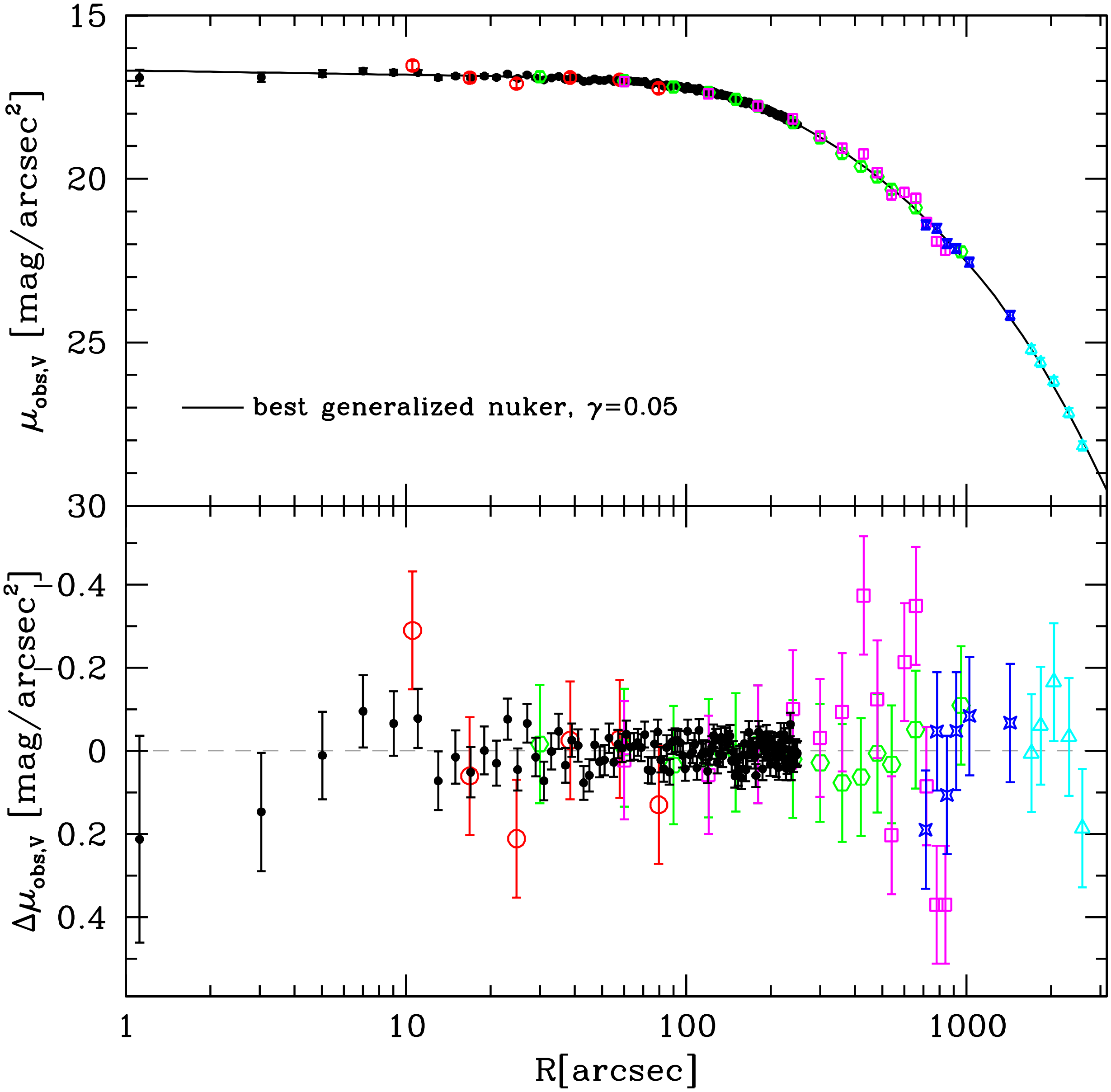

Figure 2.1: V-band surface brightness profile of ω Centauri vs. projected distance to the center (taken from vdMA10). The solid black points in the central region are star counts data from the HST (AvdM10). The bigger open symbols are from the compilation of ground-based data in Trager et al. (1995) described in the text.

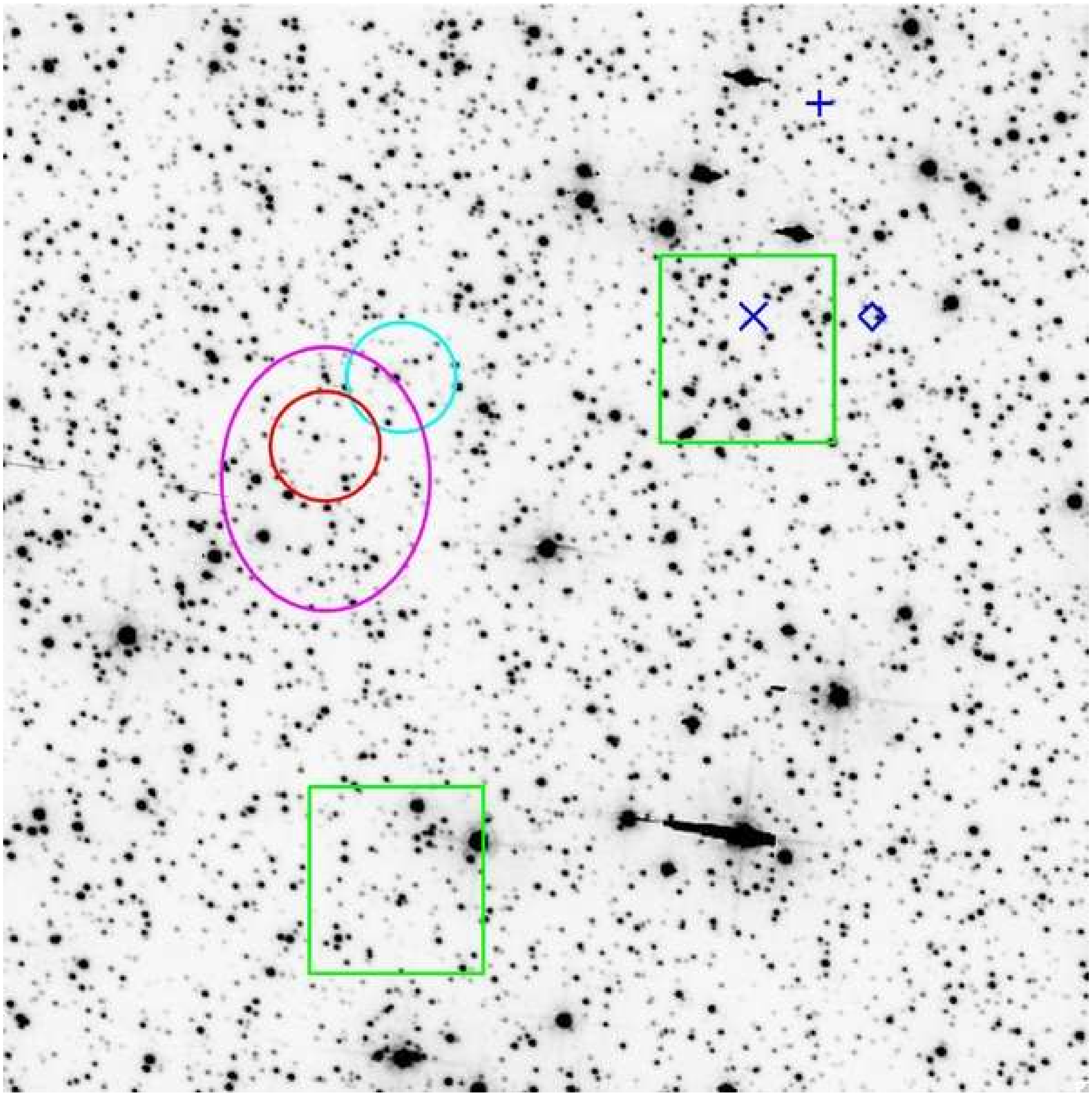

Figure 2.2: This Figure (taken from AvdM10) shows the central $30'' \times 30''$ of ω Centauri on an HST image. The symbols are different centers in the literature: In blue, plus is Harris (1996), diamond is van Leeuwen et al. (2000), and cross is NGB08. The green boxes are the two fields observed by Gemini-GMOS in NGB08. The centers determined in AvdM10 are marked by circles and the ellipses (sizes indicate the 68.3% confidence regions) using various independent methods: HST star counts (red), HST proper motions (magenta), and 2MASS unresolved light (cyan).

the central IMBH is, the steeper the cusp in the velocity dispersion will get, and thus detecting the IMBH will be easier. According to their models, if ω Centauri started much more concentrated and its current size is due to an expansion because of initial stellar mass loss and two-body relaxation, then the mass of the central IMBH would have to be larger than 1000 $M_{\odot}$ (in their models), since the half-mass radius of this object is much larger than predicted by their models. However, this criterion is not a reliable indicator for an IMBH since other physical mechanisms such as a tidal field could cause the size expansion of the clusters.

Another interesting issue in the SBP of AvdM10 is that King models (King, 1966) alone could not reproduce the observations for ω Centauri at large radii, and the model surface brightness drops quicker than the observed profile at radii around $1000''$. In the N-body simulations we find similar a behavior for the model SBP in Chapter 3.

2.2 Kinematics: using HST and VLT-FLAMES telescopes

2.2.1 Proper motions: HST data

A proper motion study with HST is an important tool to uncover cluster memberships, to measure or calibrate distance and to further constrain the anisotropy profile of star clusters. In addition, by using proper motions one could of course study the dynamics of clusters as well as study the kinematics of different stellar populations.

AvdM10 use images with a 2-years and a 4-years baseline taken by the Hubble Space Telescope's Advanced Camera for Surveys (ACS), and construct a catalog with more than 10^6 stars which allows them to measure reliable proper motions for about 53,000 stars. This makes their study the largest proper motions catalog for any Milky Way star cluster to date. As an example, the next largest proper motion data-set available for a globular cluster is 47 Tucanae with $\sim 14,000$ proper motions measurement.

As it is shown in Figure 2.3 most of the reliable proper motions are for stars around the main sequence turn off, in the B-magnitude range of 18 to 22 mag. In the next two chapters, we use their proper motions, transformed with respect to our new kinematic center (next section), to compare our results with. We also use the proper motion uncertainties in terms of magnitude in their Table 4 which we interpolate linearly and apply in our N-body analysis to compute magnitude weighted proper motion velocities in our models.

vdMA10 combined the proper motions on major and minor axes to derive the total one-dimensional proper motions. In Figure 2.4, the black points are the HST 1D proper motion dispersions. Different models, core versus cusp, with different anisotropy assumptions led to different IMBH masses. AvdM10 found less shallow cusp in their SBP, and also rather flat velocity dispersion profile with respect to the center they found. vdMA10, consequently, have an upper limit on the mass of possible IMBH $< 12,000 M_{\odot}$.

Besides the center determination and photometric profiles, AvdM10 also find that the different stellar populations of ω Centauri do not show different proper motion kinematics.

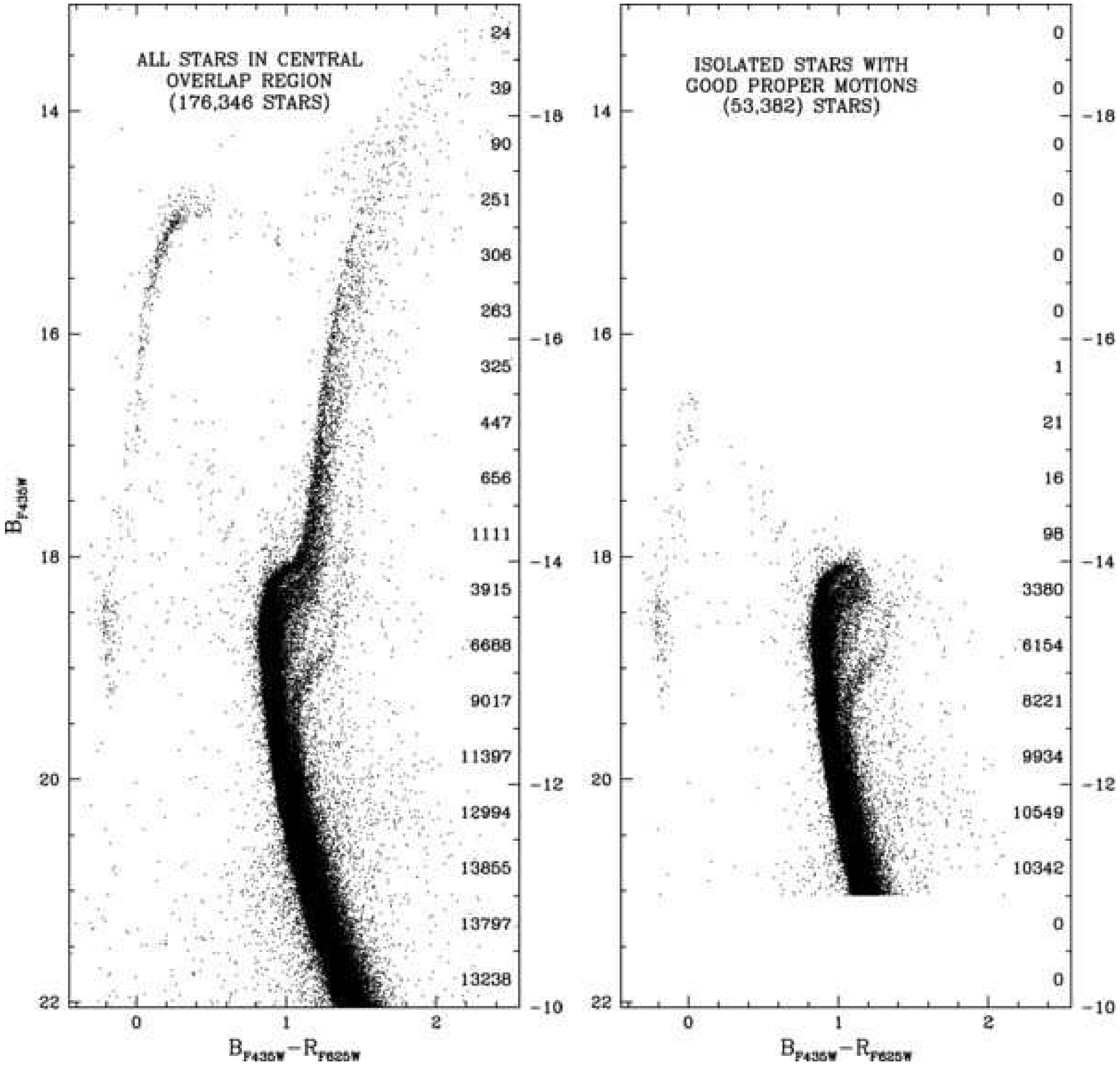

Figure 2.3: Color-magnitude diagram (CMD) of all stars in the HST fields (central regions of GO-9442 and GO-10775), and stars which AvdM10 measure reliable proper motions. The number of stars in each 1 mag bin is presented on the right of each CMD.

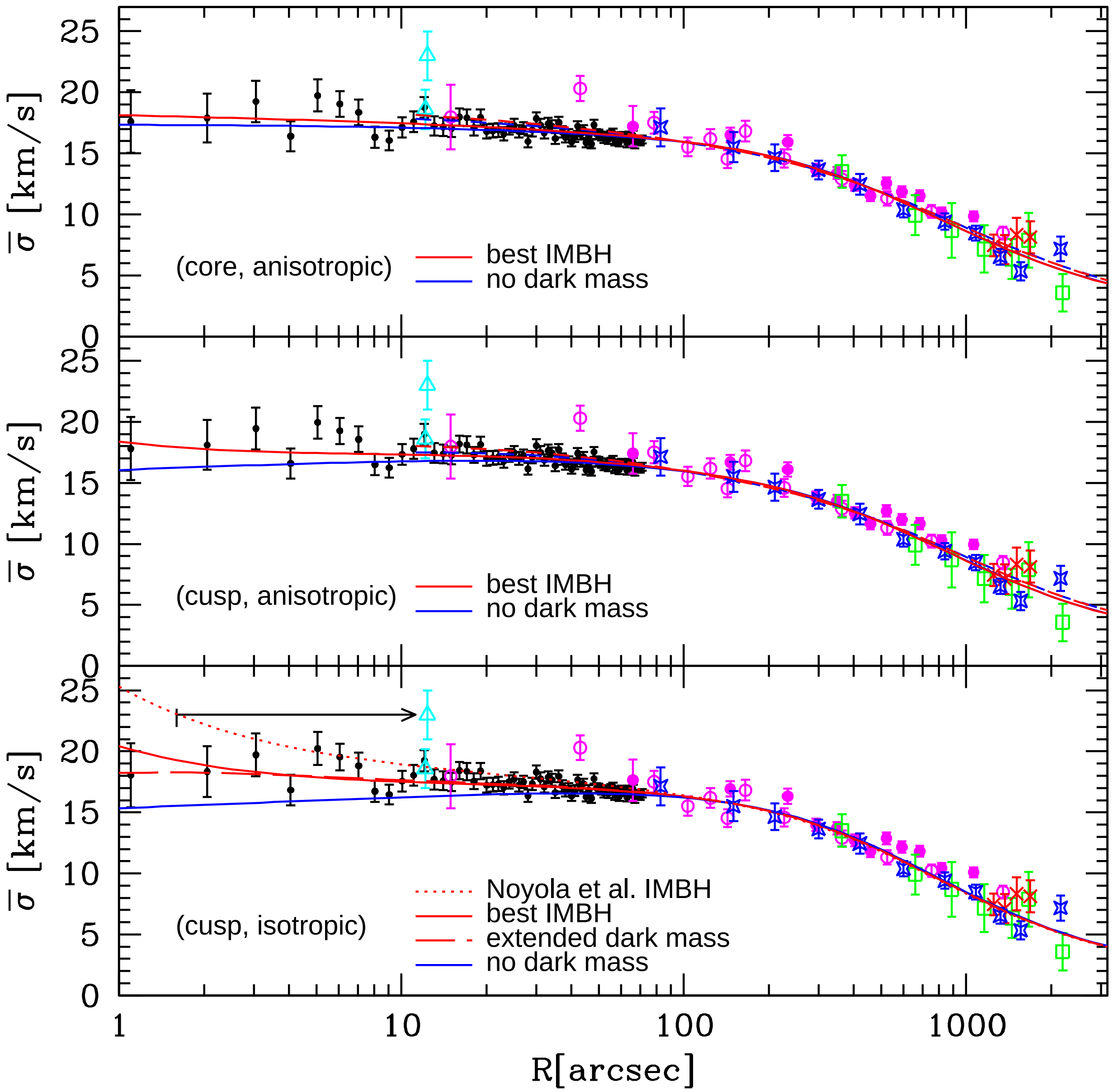

Figure 2.4: Proper motion dispersions versus projected distance to the cluster center (vdMA10). Black points are measured proper motions in the central region using HST (see AvdM10 and references therein for detailed description of different symbols). Magenta points are ground-based proper motions from vdV06. The lines in each panel are models assuming different anisotropy profiles and core/cusp parameters. In the next two Chapters, we use this data-set as well as our obtained line-of-sight velocity dispersions with respect to our kinematic center to study the presence of an IMBH.

This is a very interesting result considering the fact that this cluster has multiple populations of stars, with different masses which could also have different mass functions. In the same context, the half-mass relaxation time is about 10 Gyr (Harris, 1996) which shows that this system has not reached the energy equipartition phase yet.

2.2.2 Radial velocities: IFU data from VLT-FLAMES

We use VLT-FLAMES to obtain new integrated spectra for the central region of ω Centauri. We combine these data with existing measurements of the radial velocity dispersion profile taking into account a new derived center from kinematics and two different centers from the literature. The data support previous measurements, in NGB08, performed for a smaller field of view, and show a discrepancy with the results from the large proper motion data set, in vdMA10. We see a rise in the radial velocity dispersion in the central region to 22.8 ± 1.2 km/s, which provides a strong sign for a central black hole. Isotropic dynamical models for ω Centauri imply black hole masses ranging from 3.0 to $5.2 \times 10^4 M_\odot$ depending on the center. The best-fitted mass is $(4.7 \pm 1.0) \times 10^4 M_\odot$.

As explained in chapter 1, intermediate-mass black holes (IMBHs) may bridge the gap between stellar mass black holes and super-massive black holes found in the center of most galaxies. Their existence is appealing in various ways: they could extend the $M_{BH} - \sigma$ relation for galaxies (Gebhardt et al., 2000a; Ferrarese & Merritt, 2000) down to dwarf galaxies and globular clusters, and present a potential connection to nuclear star clusters (Seth et al., 2010). They could also be the seeds for super-massive black holes and alleviate problems with difficulties to account for the rapid growth necessary to explain massive QSOs at high red shift (Tanaka & Haiman, 2009).

The existence of an IMBH at the center of ω Centauri (NGC 5139) has been controversial. NGB08 obtain line-of-sight velocity dispersion measurements using the Gemini-GMOS integral field unit (IFU). They find a velocity dispersion rise toward the center implying the presence of a $(4 \pm 1) \times 10^4 M_\odot$ black hole when compared to spherical isotropic dynamical models. In contrast,vdMA10, using proper motions from *HST*-ACS imaging, find a lower black hole mass of $(1.8 \pm 0.3) \times 10^4 M_\odot$ for an isotropic model and their profile with a central cusp. Their anisotropic model sets an upper limit of $7.4 \times 10^3 M_\odot$. The comparison is complicated by the fact that the cluster centers between NGB08 and AvdM10 are separated by $\sim 12''$ (about $\frac{1}{10}$ of the core radius).

As described in the previous chapter, the nature of ω Centauri is under discussion. This object has been regarded as the largest globular cluster in the Galactic system, but the clear metallicity spread (Norris & Da Costa, 1995; Sollima et al., 2005), as well as a double main sequence (Bedin et al., 2004; Piotto et al., 2005) has led to the suggestion that it might be the stripped core of a dwarf galaxy (Freeman, 1993; Meza et al., 2005; Bekki & Norris, 2006). ω Centauri has a large central velocity dispersion of 22 ± 4 km/s (Meylan et al., 1995), as well as a fast global rotation of 8 km/s (Merritt et al., 1997), at 11 pc from the center. It is the most flattened Galactic globular cluster (White & Shawl, 1987), and has a retrograde orbit around the galaxy (Dinescu et al., 2001). Using both radial velocities and proper motions van de Ven et al. (2006) calculate a total mass of $2.5 \times 10^6 M_\odot$, making ω

Cen the most massive Galactic globular cluster.

The extrapolation of the $M_{BH} - \sigma$ relation for galaxies (Tremaine et al., 2002) predicts a $1.3 \times 10^4 M_\odot$ black hole for ω Cen. At a distance of 4.8 ± 0.3 kpc (van de Ven et al., 2006), the sphere of influence of such a black hole is $\sim 5''$. In this chapter, we present new VLT-ARGUS data that we compare to previous measurements.

2.3 Observations and Data Reduction

We obtain central kinematics data of ω Centauri using the ARGUS IFU with FLAMES on the Very Large Telescope (VLT). With a central σ around 20 km/s, a spectral resolving power of R ∼10,000 is sufficient to measure the dispersion from integrated stellar light. The Ca-triplet region (8450–8700Å) is well suited for kinematic analysis. The LR8 setup of the GIRAFFE spectrograph (Pasquini et al., 2002), covering the range 820–940 nm at R ∼10,400 in ARGUS mode, is ideally suited for our study.

The ARGUS IFU was used in the 1:1 magnification mode providing a field of view of $11.5'' \times 7.3''$, sampled by$0.52'' \times 0.52''$ pixels. The FLAMES observations were taken during two nights (2009 June 15 and 16). Eight different pointings were obtained at and around the two contended center determinations (see Figure 2.5). While the pointings aimed at including both centers, position inaccuracies in the guide star catalogs made us miss the second from AvdM10. The final set of observations consists of three exposures for the first ARGUS pointings (around the NGB08 center) and two exposures for the seven other pointings, with exposure times of 1500s for the first two, 1020s for the next two (90° tilted, see Fig. 2.5) and 900s for the four peripheral pointings (±45° tilted).

The first reduction steps are done with the GIRAFFE pipeline (based on the Base Line Data Reduction Software developed by the Observatoire de Genève). The pipeline recipes *gimasterbias, gimasterdark, gimasterflat* and *giscience* produce bias corrected, dark subtracted, fiber-to-fiber transmission and pixel-to-pixel variations corrected spectra. Sky subtraction and wavelength calibration are performed with our own tools, which test the wavelength solution with arc exposures and skylines.

We reconstruct the ARGUS data cubes to images in order to determine the exact location of the pointings with respect to reference *Hubble Space Telescope (HST)* images. We use a large Advanced Camera for Surveys (ACS) mosaic of ω Centauri (GO-9442, PI: A. Cool), which we convolve to ground-based observed spatial resolution. The reconstructed ARGUS images are matched to the convolved ACS image and used to assign the correct location and position angle from both centers to each pixel and to identify pixels which are dominated by single stars (i.e., not suited to derive a velocity dispersion).

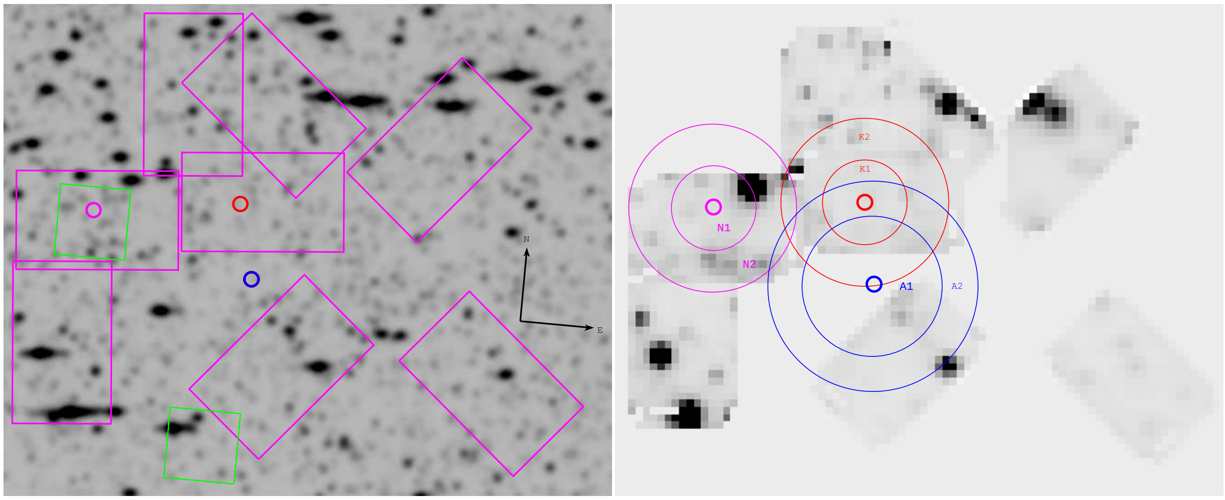

Figure 2.5: Left: Area of the eight pointings observed with ARGUS overlaid on a convolved *HST*-ACS image of ω Centauri (about $30'' \times 40''$). The two explored centers (magenta circle: NGB08, blue circle: AvdM10), the new kinematic center (red), and the previous GMOS IFU pointings (green squares) are marked for comparison. Right: reconstructed ARGUS images for the eight pointings. The overlaid circles show the two central annuli in which the velocity dispersion is measured as a function of radius.

2.4 Kinematic Measurements

Measuring kinematics of globular clusters from integral field spectroscopy is challenging. For details, we refer to NGB08. A key aspect to consider is the fact that bright stars might dominate the integrated light and increase the "shot noise" of the velocity dispersion. In order to minimize the shot noise from bright stars, we can choose which pixels to combine for the integrated light measure of the velocity dispersion.

In Figures 2.6 and 2.7, some of the spectra are shown as an example. There are hot stars with strong Paschen-series lines present (see Fig. 2.8). We exclude regions dominated by these stars and those dominated by bright stars. We identify these regions by including one of these stars in the velocity template library and then exclude those regions which have a significant contribution, ~5% of the pixels are excluded in this way. We also exclude those regions dominated by bright stars. After these two cuts, about 85% of the pixels remain to derive kinematics. To further minimize the effect from bright stars, we divide each spectrum by its mean value, thereby giving all pixels equal weight when combining.

We consider the shot noise from having a small number of stars contribute to a spatial bin. We calculate the shot noise using the HST R-band photometry from AvdM10. We use Monte Carlo simulations to generate a mock velocity data set in a given spatial bin, using magnitudes of present stars. We then estimate a velocity dispersion weighted by the fluxes of the stars. After 1000 realizations, we get sample velocity dispersion estimates from which we obtain the scatter, and hence the shot noise.

We rely on both centers by NGB08 and AvdM10, which differ by $12''$. AvdM10 claim

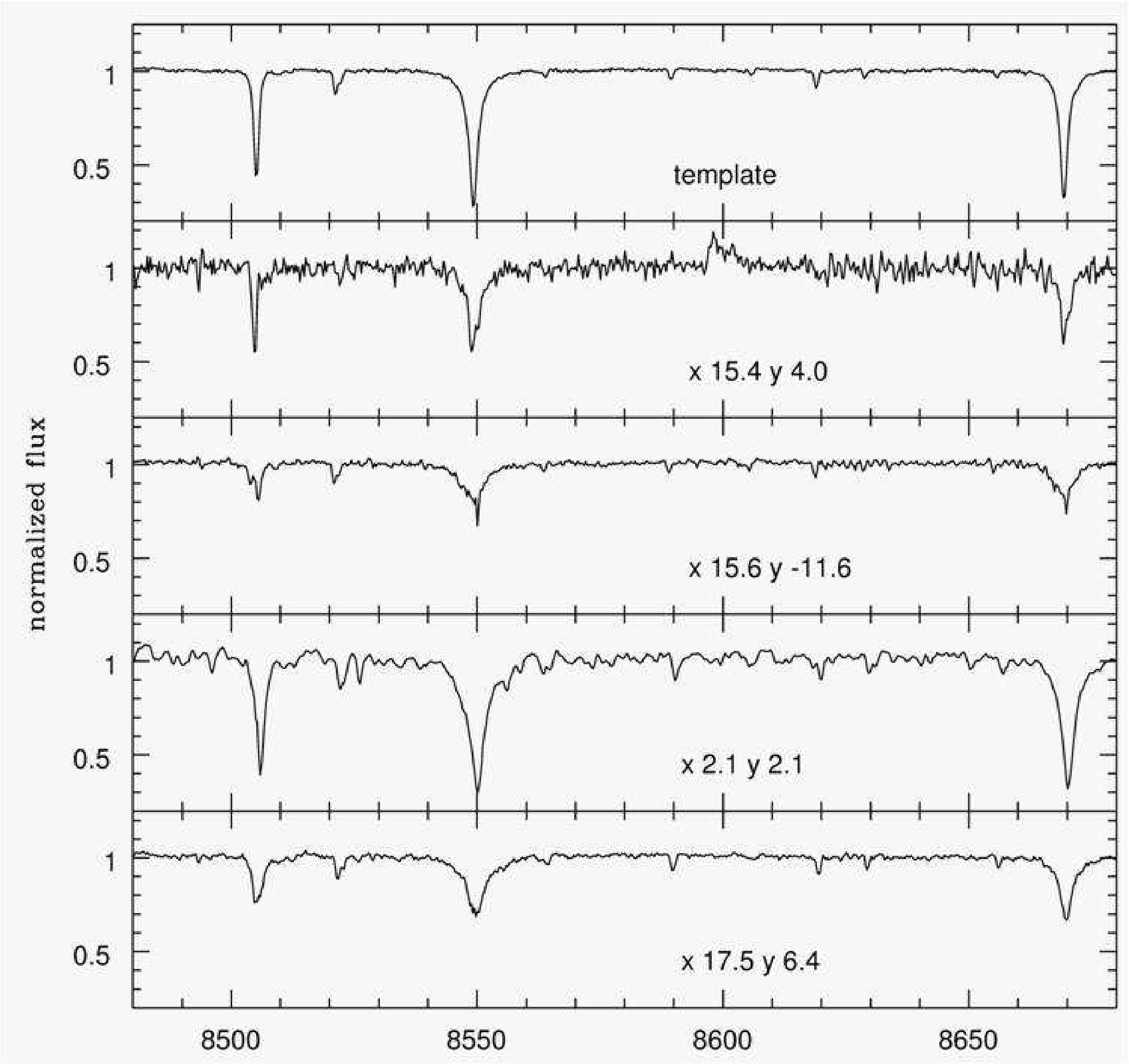

Figure 2.6: A few examples showing a spectral template (top), and some normal as well as binary candidate stars in our ω Centauri data.

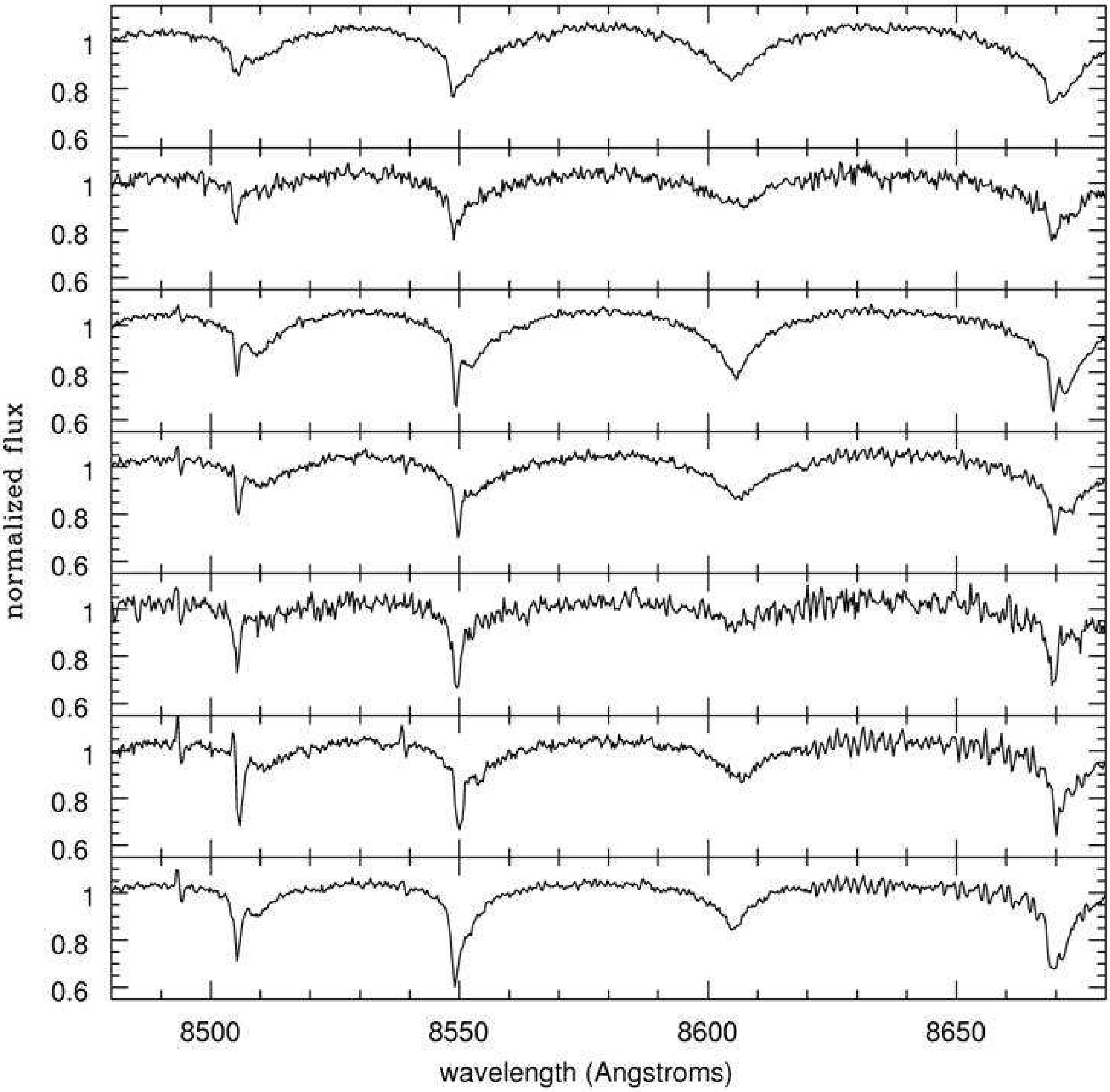

Figure 2.7: An ensemble of hot stars found in our spectra.

Table 2.1: Velocities and higher moments (dispersion, h3 and h4) with respect to three recent centers.

Bin	$R('')$	$V(km/s)$	$\Delta V(km/s)$	$\sigma(km/s)$	$\Delta\sigma(km/s)$	h_3	Δh_3	h_4	Δh_4
K1	2.0	1.1	0.5	22.8	1.2	0.05	0.03	-0.05	0.01
K2	4.5	-1.1	0.4	21.3	0.8	0.03	0.03	-0.05	0.01
K3	8.0	3.0	0.4	19.8	0.9	0.01	0.03	-0.04	0.01
K4	12.7	2.3	0.4	18.8	0.7	-0.01	0.02	-0.04	0.01
K5	18.3	1.9	0.4	18.9	0.7	-0.00	0.03	-0.05	0.01
N1	1.9	-0.6	0.4	20.1	2.1	0.00	0.02	-0.05	0.01
N2	4.5	1.4	0.5	22.7	1.5	-0.01	0.04	-0.06	0.01
N3	8.2	1.3	0.4	19.5	0.8	-0.01	0.04	-0.05	0.01
N4	14.0	1.0	0.4	19.8	0.9	0.01	0.03	-0.04	0.01
N5	25.5	3.9	0.4	18.4	0.5	0.01	0.03	-0.05	0.01
A1	3.1	8.7	0.3	17.9	1.7	0.01	0.03	-0.04	0.01
A2	6.0	-2.2	0.4	21.5	1.0	0.05	0.03	-0.05	0.01
A3	8.8	-0.5	0.5	22.8	1.2	0.00	0.03	-0.08	0.01
A4	12.6	4.2	0.4	16.9	0.4	0.03	0.02	-0.06	0.01
A5	16.9	0.6	0.4	18.5	1.0	-0.01	0.04	-0.04	0.01

that the center of NGB08 is biased toward bright stars and that these stars do not trace the center well. On the other hand, using corrected star counts biases one away from bright stars. Thus, there may be reasons to expect increased noise for the center position in both techniques. Given that we have two-dimensional (2D) kinematics, we can provide another center based on kinematics by running a kernel of $5''$ across the field and estimating the velocity dispersion within that kernel. From the 2D dispersion map there is a clear peak at the location highlighted in Fig. 2.5. It lies about $10''$ from NGB08 and $3.5''$ from AvdM10. We make dynamical models using the three centers.

We use five annuli centered on each center for the dynamical analysis. We combine the pixels within each annulus using a biweight estimator (Beers et al., 1990). The average radius of the annuli are given in Table 2.1, they are chosen to provide a signal-to-noise ratio of at least 40 in each bin. The central annulus has about 60 pixels and the outer has 500. The shot noise in any of the outer annuli is below 3% of the velocity dispersion. In the central bins, the shot noise is 3% for the kinematic center, 6% for AvdM10 and 9% for NGB08. The uncertainties include the velocity correspondence for shot noise Table 3.1 added in quadrature with the measured uncertainties.

In order to extract the kinematics from the spectra, we use the technique described in Gebhardt et al. (2000b) and Pinkney et al. (2003), also employed in NGB08. This technique provides a non-parametric estimate of the LOSVD. Starting from velocity bins of 8 km/s, we adjust the height of each LOSVD bin to define a sample LOSVD. This LOSVD is convolved with a template. The parameters, bin heights and template mix are changed to minimize the χ^2 fitted with the data spectrum. For the template, we use two

Table 2.2: Shot noise effect and its velocity correspondence with respect to different centers. We add such velocity in quadrature to the uncertainty of velocity dispersions.

different centers	shot noise	velocity (km/s)
Our Kinematic	3%	0.5
Noyola08	9%	1.8
AvdM10	6%	1.4

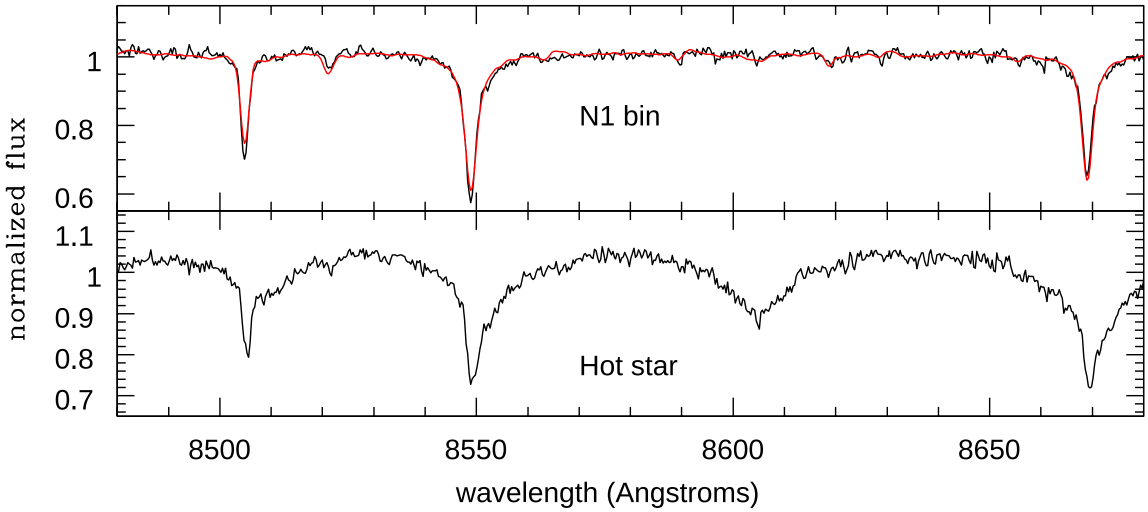

Figure 2.8: Examples of integrated spectra for the central bin N1 (top), as well as for one of the hot stars (bottom). The black line shows the combined spectra, and the red line shows the fit used for kinematics

individual stars within the IFU; these are a normal late-type giant star, and a hot star (shown in Fig. 2.8). The program then determines the relative weight of these two stars.

The non-parametric LOSVD estimate requires a smoothing parameter (see Gebhardt et al. (2000b) for a discussion) in order to produce a realistic profile, otherwise, adjacent velocity bins can show large variations. We use the smallest smoothing value just before the noise in the LOSVD bins becomes large (similar to a cross-validation technique). In addition to a non-parametric estimate, we fit a Gaussian–Hermite profile including the first four moments. The second moment of both the Gauss–Hermite profile and the non-parametric LOSVD is similar, which implies that we have a good estimate for the smoothing value. We first fit all individual 4700 pixels in all dithered positions of the IFU. This step allows us to identify those pixels where hot stars provide a significant contribution. We then exclude those pixels from the combined spectra. The top spectrum in Fig. 2.8 shows the spectral fit to the central radial bin.

The uncertainties for the LOSVD come from Monte Carlo simulations. For each spectrum,

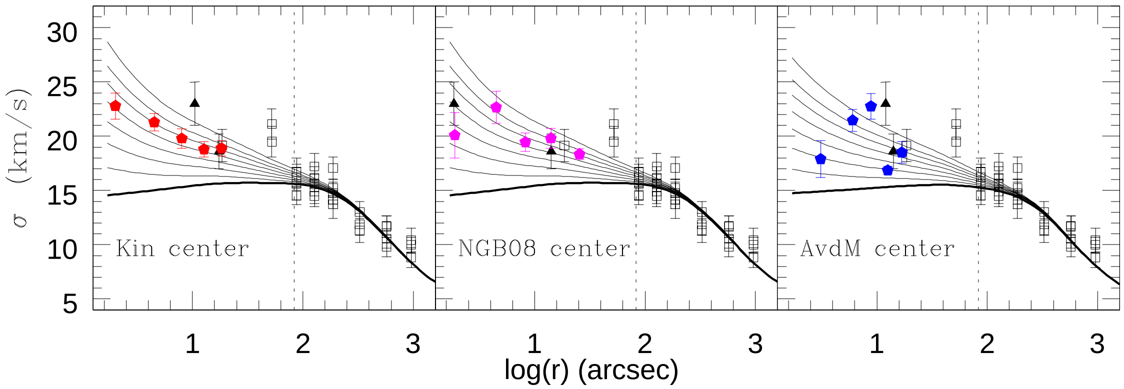

Figure 2.9: Velocity dispersion as a function of radius. The dashed line marks the core radius. The open squares are measurements taken from van de Ven et al. (2006). The solid lines show isotropic spherical models assuming various black holes masses (0,1,2,3,4,5,6, and 7.5×10^4 $M_\odot$). The left panel shows the measured σ assuming the new kinematic center (filled red pentagons), while the middle and right panels show the same for the NGB08 and AvdM10 center. Black triangles mark the kinematic measurements from NGB08.

we generate a set of realizations from the best-fitted spectrum (template convolved with the LOSVD), and add noise according to the rms of the fit. We then fit a new LOSVD, varying the template mix. From the run of realizations we take the 68% confidence band to determine the LOSVD uncertainties.

Given that ω Centauri contains stars with different spectral types, we also allow the equivalent widths to be an additional parameter. This parameter allows for mismatch between the stars chosen as templates and different regions of the cluster. We have tried a variety of different template stars and find no significant changes. Table 2.1 presents the first four moments (v, σ, h_3, and h_4) of a Gauss-Hermite expansion fitted to the non-parametric LOSVD. We note that the LOSVDs have statistically-significant non-zero h_4 components, which are important for the dynamical modelling in terms of constraining the stellar orbital properties.

Fig. 2.9 shows velocity dispersions from the LOSVDs for spectra combined around all centers. Every case shows an increase in the dispersion compared to data outside 50″, while isotropic models without a black hole expect a drop in the central velocity dispersion. The dispersion profile obtained for the kinematic center shows a smooth rise, the one for the NGB08 center is still relatively smooth, while the profile for the AvdM10 center shows larger variation. While the larger scatter is not evidence that the two previous centers are not proper, it is suggestive.

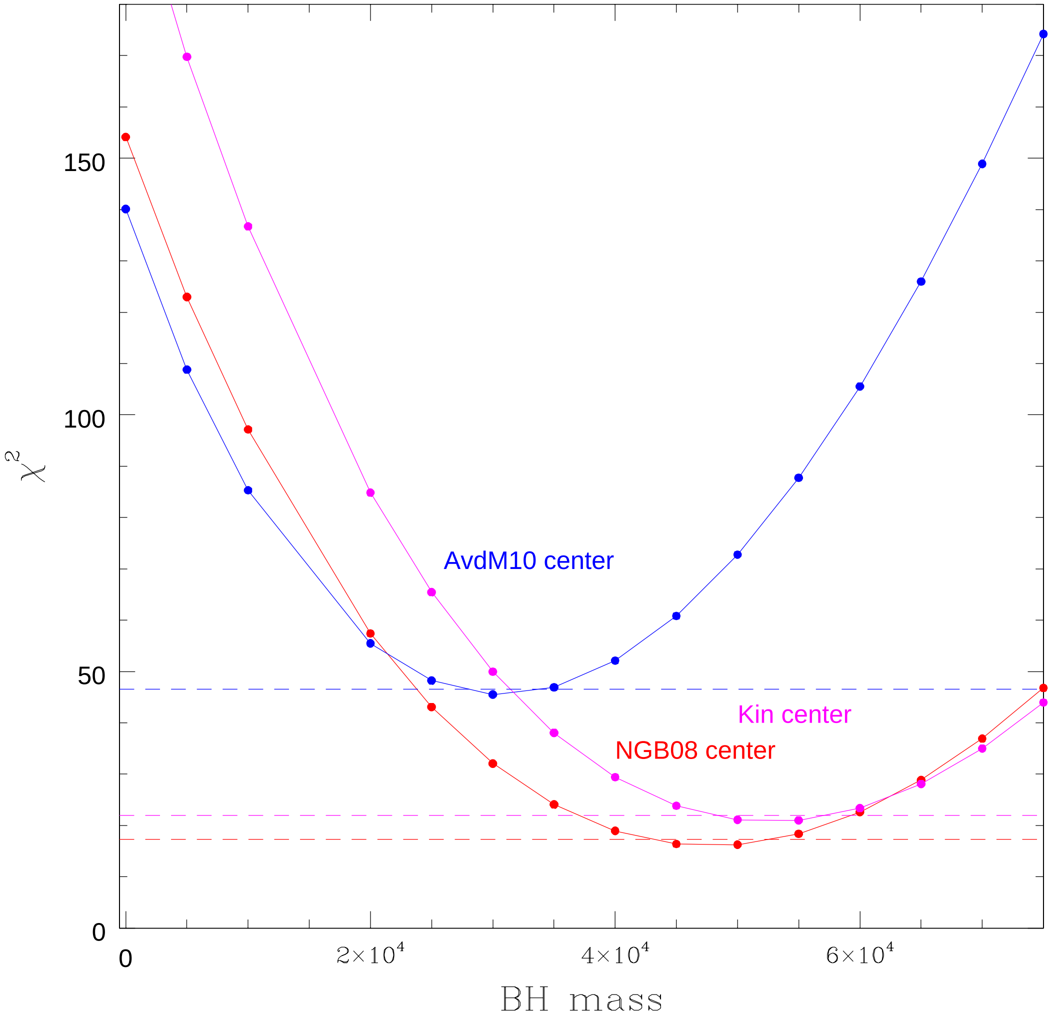

Figure 2.10: χ^2 as a function of IMBH mass for our isotropic, spherical model fits to the data, shown for the three cases: the kinematic center (magenta curve), the AvdM10 center (blue curve), and the NGB08 (red curve). In both cases the best fit is obtained with a black hole of a few 10^4 $M_\odot$, while a better fit is achieved assuming our original center.

2.5 Isotropic Models and Discussion

A detailed comparison with N-body simulations and orbit based models is in preparation (see Chapters 3 and 4). These models can also consider possible velocity anisotropy and contribution of dark remnants, as well as include a comparison with the large proper motion data-set in AvdM10. In this chapter, we limit ourselves to a comparison of the present data with isotropic models. These models have represented the projected quantities for globular clusters extremely well, starting with King (1966) all the way to a recent analysis by McLaughlin et al. (2006), where the conclusion is that clusters are isotropic within their core. Thus, while isotropy needs to be explored in detail, it provides a very good basis for comparison.

For the details of the isotropic analysis, we refer to NGB08, essentially following the non-parametric method described in Gebhardt et al. (1996). The surface brightness profile is the one obtained in NGB08, which is smoothed and deprojected assuming spherical symmetry in order to obtain a luminosity density profile (Gebhardt et al., 1996). By assuming an M/L ratio, we calculate a mass density profile, from which the potential and the velocity dispersion can be derived. We repeat the calculation adding various central point masses ranging from 0 to $7.5 \times 10^4 M_\odot$ while keeping the global M/L value fixed. Since vdMA10 obtain a density profile from star counts, we use their Nuker fit to the star-count profile to create a similar set of models. We note that the M/L value needed to fit the kinematics outside the core radius is 2.7 for both profiles. For comparison, van de Ven et al. (2006) found an M/L value of 2.5.

As could be seen in Fig. 2.6 binaries could potentially bias a velocity dispersion measured from radial velocities, which is not an issue for proper motions. Carney et al. (2005) estimate an 18% binary fraction for ω Centauri (with large uncertainties); this implies that at any given time, the observed fraction is about a few percent due to chance inclination and phase (Hut et al., 1992). Also, Ferraro et al. (2006) find no mass segregation for this cluster tracing the blue straggler population with radius. Both facts imply that the expected binary contamination is low (a few percent), which at most would cause a few percent increase in the measured velocity dispersion (i.e., within our errors).

Figure 2.9 shows the comparison between the different models and the measured dispersion profiles. As in our previous study, the most relevant part of the comparison is the rise inside the core radius. As can be seen, an isotropic model with no black hole predicts a slight decline in the velocity dispersion toward the center which is not observed for any of the assumed centers. The calculated χ^2 values for each model are plotted in Fig. 2.10, as well as a line showing $\Delta\chi^2 = 1$. The χ^2 curve implies a best-fitted black hole mass of several $10^4 M_\odot$ in every case, but with lower χ^2 for the NGB08 center. Specifically, a black hole of mass of $(5.2 \pm 0.5) \times 10^4 M_\odot$ is found for the kinematic center $(4.75 \pm 0.75) \times 10^4 M_\odot$ for the NGB08 center, and of $(3.0 \pm 0.4) \times 10^4 M_\odot$ for the AvdM10 center.

The velocity dispersion at $100''$ is well measured at around 17 km/s. The radial velocities inward show a continual rise in the dispersion with smaller radii to the central value around 22.8 km/s, which is statistically significant. This rise is now seen in multiple radial velocity data-sets. It is this gradual rise that provides the significance for a central black hole. The proper motion data of AvdM10 show a slight rise in the velocity dispersion, but not all the way into their center. It is unclear why the two dispersion measurements differ.

To summarise, we take kinematic data using one of the most advanced integral unit spectrographs, VLT-FLAMES, and measure the line-of-sight velocity dispersion in the central $10''$ of ω Centauri. This unique kinematic data-set is fundamentally crucial for studying the fingerprints of a potential $10^4 M_\odot$ IMBH, in particular we resolve its influence radius which at the distance of our cluster and assuming the central velocity dispersion of 23 km/s is $\sim 5''$.

In the next Chapter, we present the results of our N-body simulations which demonstrate again the importance of the central line-of-sight velocity dispersion we obtain in this Chapter to distinguish beween different BH masses. We simulate a cluster of 5×10^4 stars taking into account their stellar evolution, and with different IMBH masses. We follow the dynamical evolution of such model clusters up to 12 Gyr (the age of this object) to compare the results with the kinematic information as well as the light profile of this cluster (measured on HST images).

In Chapter 4, we use the obtained kinematics in this chapter to derive the line-of-sight velocity distributions (LOSVDs) of ω Centauri in the central region. We perform orbit-based models to construct trail potential fields appropriate for our cluster's parameters, and compare the model LOSVDs with the ones extracted from the data to constrain the mass of possible IMBH for this stellar system and also to investigate its orbital structure.

Chapter 3

Direct N-body Simulations of ω Centauri

Based on Jalali et al. (2011),
"A Dynamical N-body Model for the Central Region of ω Centauri",
submitted to A&A

Abstract

Supermassive black holes (SMBHs) are fundamental keys to understand the formation and evolution of their host galaxies. However, the formation and growth of SMBHs are not yet well understood. One of the proposed formation scenarios is the growth of SMBHs from seed intermediate-mass black holes (IMBHs, 10^2 to $10^5 M_\odot$) formed in star clusters. In this context and also with respect to the low mass end of the $M_\bullet - \sigma$ relation for galaxies, globular clusters are in a mass range that make them ideal systems to look for IMBHs. Among Galactic star clusters, the massive cluster ω Centauri is a special target due to its central high velocity dispersion and also its multiple stellar populations.

We study the central structure and dynamics of the star cluster ω Centauri to examine whether an IMBH is necessary to explain the observed velocity dispersion and surface brightness profiles.

We perform direct N-body simulations on GPU and GRAPE special purpose computers to follow the dynamical evolution of ω Centauri. The simulations are compared to the most recent data-sets in order to explain the present-day conditions of the cluster and to constrain the initial conditions leading to the observed profiles.

We find that starting from isotropic spherical multi-mass King conditions and within our canonical assumptions, a model with a central IMBH mass of 2% of the cluster stellar

mass, i.e. a $5. \times 10^4 M_\odot$ IMBH, provides a satisfactory fit to both the observed shallow cusp in surface brightness and the continuous rise towards the center of the radial velocity dispersion profile. In our isotropic spherical models, the predicted proper motion dispersion for the best-fit model is the same as the radial velocity dispersion one.

We conclude that with the presence of a central IMBH in our models we reproduce consistently the rise in the radial velocity dispersions. Furthermore, we always end up with a shallow cusp in the projected surface brightness of our model clusters containing an IMBH. In addition, we find that the M/L ratio starts to rise for all models from the half-light radius inward due to the segregation of heavy-mass compact remnants and is about 1.3 times as large at $10''$ than at the half-light radius. Considering our initial parameter space, it is not possible to explain the observations without a central IMBH for ω Centauri. To further strengthen the presence of an IMBH as a unique explanation of the observed light and kinematics more detailed analysis such as investigating the contribution of primordial binaries and different anisotropy profiles should be studied which we intend to do in the future.

3.1 Introduction

There is no doubt about the existence of supermassive black holes (SMBHs) at the center of most galaxies. However, the formation and growth of SMBHs is poorly understood. One of the proposed scenarios is the growth of SMBHs from seed intermediate-mass black holes (IMBHs, 10^2 to $10^5 M_\odot$) (Ebisuzaki et al., 2001; Tanaka & Haiman, 2009). IMBHs in star clusters might form through the runaway merging of massive stars (Portegies Zwart & McMillan, 2002; Portegies Zwart et al., 2004). IMBH formation in star clusters could help to explain the supermassive black hole formation and growth in the center of galaxies. For instance, Portegies Zwart et al. (2006) simulate the inner 100 pc of the Milky Way to study the formation and evolution of the population of star clusters and IMBHs in the bulge. They find that 10% of the clusters born within 100 pc of the Galactic center undergo core collapse during their inward migration and form IMBHs via runaway stellar merging. The IMBHs continue their inward drift towards the Galactic center after the dissolution of the host clusters. Portegies Zwart et al. (2006) predict that a region within 10 pc of the Galactic center might be populated by 50 IMBHs of about 1000 $M_\odot$ mass. They also predict that there is a steady population of several IMBHs within a few milliparsecs of the Galactic center. This population merges with a rate of about one per 10 Myr with the central SMBH, which is sufficient to build the accumulated majority of the SMBH mass. In the same context, nuclear star clusters co-exist with massive black holes (Seth et al., 2008, 2010). The star cluster ω Centauri (NGC 5139) in our galaxy might be a bridge between smaller systems such as classical globular clusters and larger systems like nuclear star clusters.

If IMBHs form in large numbers in star clusters then one might expect that some star clusters in the Milky Way or other nearby galaxies contain central black holes. The structural parameters of globular clusters harboring IMBHs are studied in Baumgardt et al. (2004a,b, 2005) and Vesperini & Trenti (2010). Care should be taken when interpreting cluster morphological parameters as IMBH indicators. For instance, Hurley (2007) shows that without an IMBH and only by heavy stellar mass black hole binaries one could explain large cores observed in some Galactic star clusters. Baumgardt et al. (2005) show that core-collapsed globular clusters with steep surface brightness profiles are not good candidates for harboring central black holes. They find that a cluster hosting an IMBH appears to have a relatively large core with a projected surface brightness only slightly rising toward the center. It should be noted that Vesperini & Trenti (2010) argue that shallow cusps in the central surface brightness profile may not be a unique IMBH indicator (see also Noyola & Baumgardt (submitted) for a different interpretation). Baumgardt et al. (2005) show that the velocity dispersion of the visible stars in a globular cluster with a central black hole remains nearly constant well inside the apparent core radius. Further, they report that in a cluster containing an IMBH, the influence of the black hole becomes significant only at a fraction $\frac{5}{2} \cdot \frac{M_{BH}}{M_C}$ of the half-mass radius (where M_{BH} and M_C are the mass of the IMBH and the cluster), i.e. deep within the core, which will affect only a small number of stars.

The star cluster ω Centauri (NGC 5139), with an estimated mass of $2.5 \times 10^6 M_\odot$ (van de Ven et al., 2006, hereafter vdV06) and a tidal radius of about 70 pc (Harris 1996), is the most massive and one of the most spatially extended Galactic star clusters. It has one of the highest central velocity dispersions among the Milky Way star clusters with about 22 km/s (Meylan et al., 1995; Noyola et al., 2010, hereafter N10). Furthermore, vdV06 measure a rotation of 8 km/s at a radius of about 11 pc from the center using radial velocities. In addition, ω Centauri is one of the first Galactic globular clusters that have multiple stellar populations among both red giant branch stars (Freeman & Rodgers, 1975) and main sequence stars (Anderson, 2002; Bedin et al., 2004). The nature of this cluster is therefore a matter of debate, it could either be a giant globular cluster or the core of a stripped dwarf galaxy (Freeman, 1993; Meylan, 2002; Bekki & Norris, 2006). The above spectacular properties, in addition to a shallow cusp in the surface brightness profile (Noyola et al., 2008, hereafter NGB08) and a central sharp rise in the radial velocity dispersion (N10), make ω Centauri an interesting candidate for harboring a black hole.

ω Centauri's dynamics is among the best studied of any Galactic star cluster. vdV06 determine its dynamical distance, inclination, mass-to-light ratio, and the intrinsic orbital structure by fitting axisymmetric dynamical models to the ground-based proper motions of van Leeuwen et al. (2000) and line-of-sight velocities from independent data-sets. They find that ω Centauri shows no significant radial dependence of M/L, consistent with its relatively long relaxation time. Their best-fit dynamical model has a stellar V-band M/L of 2.5 ± 0.1 (solar units) and an inclination $i = 50^\circ \pm 4^\circ$, which corresponds to an average intrinsic axial ratio of 0.78 ± 0.03. These models do not include any kinematical data in the central $10''$. Giersz & Heggie (2003) use Monte Carlo simulations to model ω Centauri with simple spherical models (neglecting rotation and binary stars). They fit the surface brightness and radial velocity dispersion relatively well, though again, neither the data nor the model have sufficient resolution in the central 1 pc ($\sim 43''$ at 4.8 kpc).

There are several well established correlations between the central black hole mass of galaxies and other parameters of host galaxies such as velocity dispersion (Ferrarese & Merritt, 2000; Gebhardt et al., 2000a; Gültekin et al., 2009), bulge mass and bulge luminosity (Magorrian et al., 1998; Häring & Rix, 2004). If we extrapolate the Magorrian et al. (1998) relation to the globular cluster mass regime, it predicts an IMBH of about $1.5 \times 10^4 M_\odot$ for ω Centauri assuming a total cluster mass of $2.5 \times 10^6 M_\odot$. NGB08 find a $(4 \pm 1) \times 10^4 M_\odot$ IMBH applying isotropic Jeans models and a $(3 \pm 1) \times 10^4 M_\odot$ IMBH using axisymmetric orbit-based models. More recently, N10 provide new central kinematics of ω Centauri and suggest a $(5.2 \pm 0.5) \times 10^4 M_\odot$ IMBH assuming spherical isotropic Jeans models with respect to a newly determined kinematic center. In contrast, van der Marel & Anderson (2010, hereafter vdMA10), using HST proper motions find a $(8.7 \pm 2.9) \times 10^3 M_\odot$ IMBH assuming cusp models and an upper limit of $7.4 \times 10^3 M_\odot$ at 1σ confidence assuming core models (flat central density), while isotropic models imply an IMBH mass of $(1.8 \pm 0.3) \times 10^4 M_\odot$. One of the main reasons for the discrepancy is the different cluster centers these two groups used. In addition to the center determination, underestimating the rotation, particularly in the central parsec, could have an important effect on velocity dispersion measurements.

In this chapter, we compare the most up-to-date observed surface brightness and kinematic profiles of ω Centauri with direct N-body simulations in the same way as observers do. This means the same luminosity weights and magnitude cut-offs as in the observations are applied to compute the velocity dispersion and surface density profiles from the models. Similar studies have been performed earlier for the globular cluster M15 in the Milky Way and G1 in M31 by Baumgardt et al. (2003a,b). Direct N-body simulations of M15 explain the observations with a concentration of dark remnants, such as massive white dwarfs and neutron stars in the central regions through mass segregation. Therefore, the presence of an IMBH was not necessary in order to explain the observations. The same conclusion is made by van den Bosch et al. (2006) for M15 using Schwarzschild model. In the case of G1, Baumgardt et al. (2003b) reproduce the observations by assuming a merger history for G1. However, Gebhardt et al. (2005) provide additional support for the presence of a $2 \times 10^4 M_\odot$ IMBH. The black hole scenario for G1 is also supported by detections of radio and x-ray sources in the cluster (Ulvestad et al., 2007; Pooley & Rappaport, 2006).

Here, we examine different IMBH masses (including the no black hole case) in our N-body models with the aim of reproducing the observations for ω Centauri. Only N-body models allow realistic inclusion of relaxation and stellar evolution effects and changes in M/L with radius due to mass segregation. The possible disadvantage of N-body models is that one is restricted to a small number of models since they are time consuming to construct. Therefore we restrict ourselves to isotropic models and only run a three dimensional grid in logarithmic concentration ($\log(c)$), projected half-mass radius (r_{hp}) and IMBH mass space for the scope of this paper. Although axisymmetry and anisotropy models are important to include in any modelling, according to vdV06 ω Centauri is close to isotropic and spherical within the central few core radii.

In Section 3.2, we describe the data used in this work to compare with the N-body results. The general recipe for our N-body models is discussed in Section 3.3. In Section

3.4 we explain our model results, in particular we discuss the profiles of the no-IMBH and IMBH models and compare them with the observations. We draw our conclusions and discuss possible future work in Section 3.5.

3.2 Observational Data

3.2.1 The Center of ω Centauri

The determination of ω Centauri's center is crucial in order to understand and model its dynamics. However, the exact location of the center has been controversial due to the large flat core of the cluster (core radius $\sim 100''$) and the different methods used to estimate its location.

The center of ω Centauri has been determined by several authors. Recent determinations are done by NGB08 and Anderson & van der Marel (2010, hereafter AvdM10). NGB08 determine the center of ω Centauri using star counts by excluding the faintest stars due to incompleteness. This method can be biased towards bright stars. In an independent study AvdM10 determine the center with different methods including star counts and proper motions. In this case, the authors use star lists corrected for the presence of bright stars assuming a symmetry axis. This measurement can be biased due to the quality of the correction and the location of symmetry axis. Their result differs from the NGB08 position by $\sim 12''$. AvdM10 also determine the center of ω Centauri using HST proper motion data, which they report to be in agreement with their star count method within the uncertainties. AvdM10 might have underestimated the rotation contribution in their local filter window in the proper motion measurements. They try to estimate global rotation but were limited in the amount they could detect. Their evaluated center based on proper motion could possibly be offset from the true center due to this effect.

Due to the above discrepancy, N10 argue that using the kinematic center rather than the density center is the better choice as starting point for models. For our N-body models we use the kinematical center derived in N10.

3.2.2 Surface Brightness Data

Meylan (1987) and Trager et al. (1995) compile the surface brightness data for ω Centauri from different sources in the literature: aperture photometry of the central regions from Gascoigne & Burr (1956) and Da Costa (1979) and star counts for larger radii from King et al. (1968). The star counts are characterized by a magnitude limit of B=19 mag. We use the star catalog of AvdM10 to perform star counts in the central regions ($R < 20''$) with respect to the kinematic center described above. We use stars brighter than 19.5 mag and an adaptive kernel density estimator for the star counts. The magnitude cut was applied to limit the incompleteness. Our profile center was stable for this magnitude cut-off (fainter magnitude cut-offs cause the density center to shift towards the Anderson center). We adjust our star count profile to the Meylan (1987) and Trager (1995) profiles at larger radii, as taken from NGB08. In NGB08 a surface brightness profile was obtained with integrated light from HST-ACS data within the central 40″ with respect to their center (details explained in Noyola & Gebhardt (2006) and Noyola & Gebhardt (2007)). We use their data from radii larger than 20″, i.e. the data from 20″ to 40″ comes from integrated light measurements and the inner 20″ comes from star counts.

3.2.3 Kinematical Data

N10 obtain kinematics in the central region of ω Centauri using integral field spectroscopy. They measure the velocity dispersion from integrated light using VLT-FLAMES with a spectral resolution of ~10,000 in the Ca-triplet wavelength. They tile around the two proposed centers by NGB08 and AvdM10 with eight pointings. Furthermore, we use Gemini-GMOS data which NGB08 obtain with integrated light using the same approach as for the VLT-FLAMES data. We use the integrated light velocity dispersion with respect to the kinematic center as presented in Table 1 of N10.

vdV06 collect individual velocity measurements at larger radii from four different sources (Suntzeff & Kraft (1996); Mayor et al. (1997); Reijns et al. (2006); Xie and Gebhardt (private communication)). Almost all of the above authors measure the velocities of luminous (giants) stars. vdV06 perform many tests such as cluster membership, excluding velocities with large uncertainties and also corrections for perspective rotation, in order to pick only suitable velocities for dynamical modelling. They bin the measurements and obtain the velocity moments in a set of apertures in the plane of the sky. We use the velocity dispersions presented in their Table 4 for comparison with our simulations.

Proper motions are very useful to better constrain the internal dynamics of star clusters, in particular the degree of anisotropy. In addition to ground-based data from vdV06, HST proper motions are available from AvdM10. These authors use isolated stars brighter than the apparent magnitude 21 in their high quality sample for proper motions. In total, they have about 72,000 stars in two fields: one on the cluster center and one positioned adjacent to the first field along the major axis. The central field covers the central 147″ in radius, and the major axis field covers radii between about 100″ to 347″. They use 25,167 stars at $R < 71''.7$, aiming at having the complete position angle coverage in order to calculate average kinematical quantities over circular annuli. However, they stress that the whole data set is usable but is excluded in their main study because of sparse position angle coverage at larger radii.

To compare with the N-body models in this work, we use the proper motions on the minor and major axes available in Table 4 of AvdM10 transformed with respect to the kinematic center in N10. We measure the proper motion dispersion along each axis using a maximum likelihood technique in radial bins taking uncertainties into account (Pryor & Meylan, 1993).

Throughout this work, we assume a heliocentric distance of 4.8 ± 0.3 kpc for ω Centauri (vdV06). Therefore, 1 pc corresponds to 42.97″ in our simulations.

Table 3.1: Initial parameters and some observed properties used in our models.

Property	Symbol	Values
Num. of stars	N^a	5×10^4
Structure	–	King (1996)
Initial concentration	$\log(c)$	0.3 - 0.8
Initial half-light radius	initial r_{hp}	12.2 - 14.4 pc
Initial mass function	Kroupa 2001	0.1 - 100 $M_\odot$
Tidal field	–	none
Primordial binaries	–	none
Primordial mass segregation	–	none
Mean metallicity	$[Fe/H]$	-1.62 (Harris 1996)

[a] see Section 3.3 for scaling description.

3.3 N-body modelling Method

We started running simulations on GRAPE special purpose computers at ESO using the NBODY4 code (Aarseth, 1999) in order to model the star cluster ω Centauri. It became possible in the middle of this project, however, to take advantage of the recently installed GPU cluster of the University of Queensland which speeds up the simulations by a factor of about 10. We could probe a larger initial parameter space considerably cheaper in computational time. All the results of our models for ω Centauri are based on simulations using the NBODY6 code (Aarseth, 2003) on the GPU cluster.

We follow the method described in Baumgardt et al. (2003a,b, 2005) to model the dynamical evolution of ω Centauri. We set up our model clusters following a spherical isotropic King model (King, 1966) in virial equilibrium. The initial stellar masses are drawn from a Kroupa (2001) initial mass function (IMF) with lower and upper mass limits of 0.1 and 100 $M_\odot$, respectively. This standard IMF is supported in Section 3.4 by reproducing well the M/L profile, consistent with other independent studies. Primordial binaries are not included in our simulations. This assumption considers the very high velocity dispersion of ω Centauri that makes the contribution of a reasonable small fraction of primordial binaries shallower. In addition, including primordial binaries computationally is very time consuming and we will investigate it in a separate project. We also do not include initial mass segregation. Furthermore, we do not consider the tidal field of the Galaxy since we are interested in the very central part of the cluster. Neglecting the influence of the tidal field, the evolution of our modeled clusters is driven mainly by two-body relaxation and stellar evolution. We note that, mass loss has little effect on the current velocity dispersion profile if the mass loss occurred early in the evolution. In our simulations, stellar evolution is modeled according to Hurley et al. (2000). We assume $[Fe/H] = -1.62$ dex as the mean cluster metallicity (Harris, 1996). The assumed neutron star and black hole retention fraction is set to 10% for both no-IMBH models and models with an IMBH. The initial parameters in our simulations are summarized in Table 3.1.

ω Centauri has a mass of $\sim 2.5 \times 10^6 M_\odot$ and therefore $\sim 5 \times 10^6$ stars. Since direct N-body simulations can at the moment handle only clusters with up to 10^5 stars (see e.g. Hasani Zonoozi et al., 2010), we perform simulations of smaller-N clusters (but more extended in size) and scale our results up to ω Centauri such as to have the same relaxation time and size as our observed cluster after 12 Gyr of evolution. The relaxation time of a cluster with mass M and half-mass radius r_h is given by Spitzer (1987) as:

$$T_{r_h} = 0.138 \frac{\sqrt{M}\; r_h^{3/2}}{\langle m \rangle \sqrt{G}\; \ln(\gamma N)} \quad , \tag{3.1}$$

where $\langle m \rangle$ is the mean mass of the stars in the cluster, N is the number of stars, and γ is a factor in the Coulomb logarithm, approximately equal to 0.02 for multi-mass clusters (Giersz & Heggie, 1996). The scaling factor for the positions is given by

$$r_{scale} = \frac{r_{hpocen}}{r_{hpsim}} \;, \tag{3.2}$$

where r_{hpocen} is the projected half-light radius of ω Centauri (5.83 pc at 4.8 kpc distance, Harris, 1996) where the integrated cluster light reaches half its maximum value and r_{hpsim} is the projected half-light radius of model clusters. In order to have the same relaxation time as the observed cluster, we have to scale up the mass of our clusters to a mass M_{ocen} which satisfies the following equation:

$$\left(\frac{M_{sim}}{M_{ocen}}\right)^{1/3} \left(\frac{\ln(\gamma M_{ocen})}{\ln(\gamma M_{sim})}\right)^{2/3} = \frac{r_{hpocen}}{r_{hpsim}} \;. \tag{3.3}$$

Here M_{ocen} is the bound mass of the models at the end of our simulations (T = 12 Gyr). Since the size and mass of the model clusters are re-scaled, we also scale the velocities of the stars by a factor:

$$v_{scale} = \left(\frac{r_{hpsim}}{r_{hpocen}}\right)^{1/2} \left(\frac{M_{ocen}}{M_{sim}}\right)^{1/2} \quad , \tag{3.4}$$

where subscripts “ocen” and “sim” denote the actual values for ω Centauri and those in the simulations, respectively (see Baumgardt et al., 2003b). In eq. (3.4), the first factor is needed due to the reduction of distances between stars while the second factor takes care of the increase in cluster mass when scaling our models to ω Centauri. Due to eqs. (3) and (4) models starting with larger initial r_{hpsim} will end with a higher cluster mass and therefore higher velocities (see Section 3.4).

We perform all simulations with 5×10^4 stars, which before scaling gives us an initial cluster mass of $3.5 \times 10^4 M_\odot$ and a final cluster mass of $2.0 \times 10^4 M_\odot$. Usually the bound stars are about 99% of the initial number of stars.

In order to find the initial conditions of ω Centauri that lead to the present-day observed kinematics and surface brightness profile, we set up clusters with different initial half-mass radii, different concentration parameters, defined as $\log(\frac{r_t}{r_c})$ where r_t is the tidal radius and

r_c is the core radius, and different IMBH masses and evolve them with NBODY6 up to an age of 12 Gyr. Then, we estimate how closely each model cluster reproduce the observed profiles using χ^2. We calculate χ^2 for the surface brightness, the radial velocity, and the proper motion dispersion profiles of each model to compare with the data using

$$\chi^2 = \sum_{i=1}^{N} \left(\frac{\mathcal{M}_i - \mathcal{D}_i}{\sqrt{(\Delta\mathcal{M}_i)^2 + (\Delta\mathcal{D}_i)^2}} \right)^2 . \tag{3.5}$$

$\mathcal{M}_i$, $\mathcal{D}_i$, $\Delta\mathcal{M}_i$ and $\Delta\mathcal{D}_i$ are the model and data points and their relevant uncertainties. N is the number of data points for the radial velocity dispersion, the proper motion dispersion and the surface brightness profiles. We calculate the absolute χ^2 values for all the χ^2 maps in the next section. We use χ^2 values only to quantify judgments on different model profiles in comparison with observed ones. We calculate the χ^2 values for all models within the inner $400''$ ($\sim$ 10 pc) since we do not consider tidal fields and this in turn affects the number of stars at larger radii. We aim to simultaneously reproduce the observed velocity dispersions and surface brightness profiles. Therefore, we apply the following relation to obtain the reduced combined χ^2 values of radial velocity, and proper motion dispersion and surface brightness for each model:

$$\chi^2 = \frac{\chi^2_{rv} + \chi^2_{pm} + \chi^2_{sb}}{N_{rv} + N_{pm} + N_{sb}} , \tag{3.6}$$

“rv”, “pm” and “sb” stand for radial velocity dispersion, proper motion dispersion and surface brightness, respectively. N_{rv}, N_{pm}, and N_{sb} are 38, 218, and 32 over $400''$. We note that the large difference between number of data points will cause a non-smooth total χ^2 space between different models and consequently results in small absolute χ^2 differences, as we see in Section 3.4.2.

We vary the initial parameters to compare the resulting profiles with observations of ω Centauri. We vary the IMBH mass between 0% to 3% of the model stellar mass. In total we compute about 100 models to find the initial conditions which reproduce the observations of ω Centauri best. The final obtained quantities (e.g. number density and velocity) are calculated by superimposing 10 snapshots in the case of no-IMBH models and 20 snapshots in the case of IMBH models to improve the statistics. The snapshots start from 11 Gyr with a 50 Myr step.

3.3.1 Model Density Profile

For each model we calculate the surface brightness and kinematic profiles including radial velocity and proper motions, using similar magnitude limits as observers use for ω Centauri. In order to determine the surface brightness profile, the density center of our model clusters is determined using the method of Casertano & Hut (1985). We then count the number of bound stars in two-dimensional circular annuli around the density center. We use the infinite projection method of Mashchenko & Sills (2005) and average each quantity over all (infinite) orientations for each bin based on geometric arguments. Infinite projection gives significantly better statistics over using only a finite number of projections, especially in the inner cluster parts. We convert the star counts per parsec squared to numbers per arcsecond squared using the assumed distance to ω Centauri. We bin the stars around

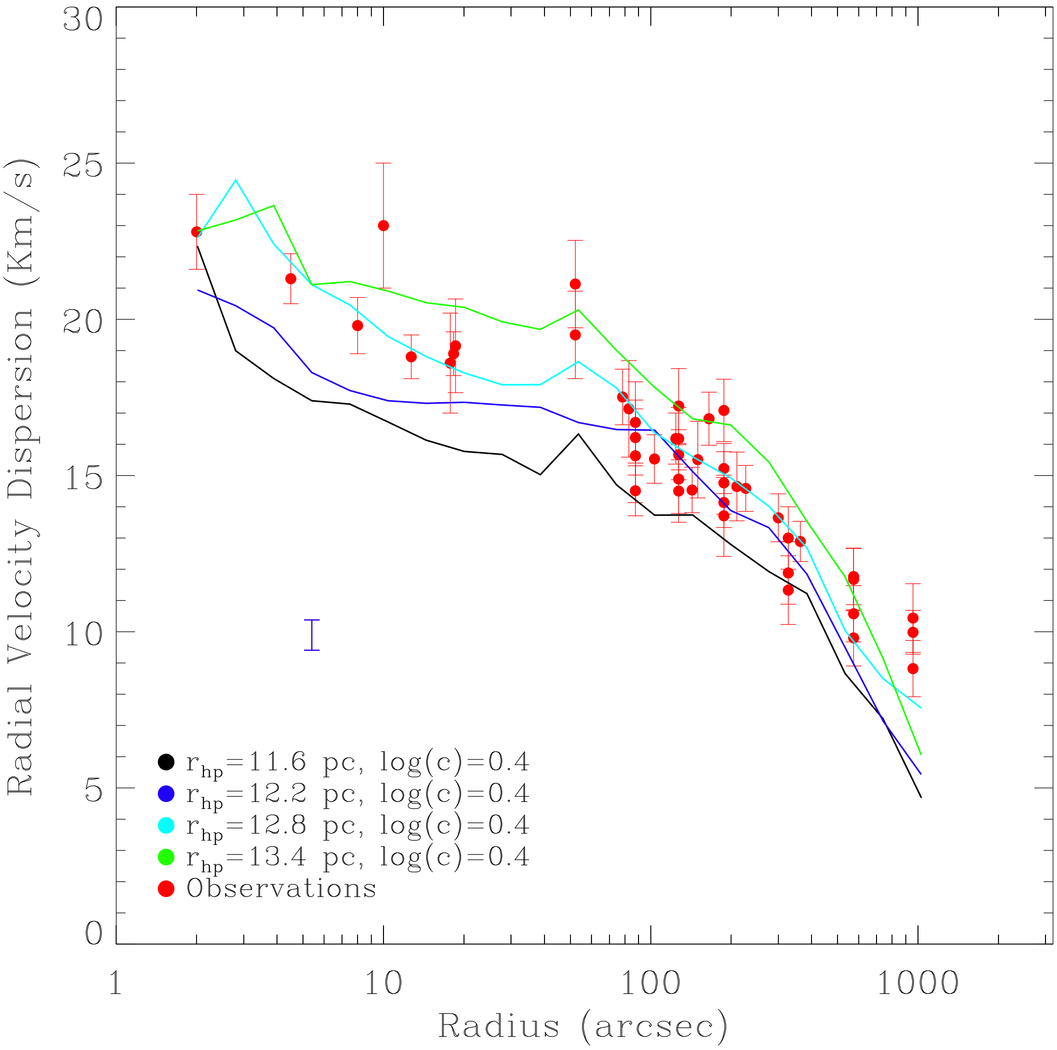

Figure 3.1: Radial velocity dispersion profiles as a function of radius for models with an IMBH mass of 2% of the stellar mass with the same initial concentration factor. Red points are the observed data taken from different sources (section 3.2.3). Black, magenta, light blue and green are models with initial half-light radius (r_{hp}) of 11.6, 12.2, 12.8 and 13.4 pc, respectively. A typical uncertainty for models at 5″ is indicated in blue. Higher initial r_{hp} models end up with a higher velocity dispersion across all radii but with roughly the same overall shape because of their higher total cluster mass as described in section 3.4.

the (density) center in 20 annuli of equal logarithmic width between 2.0″ and 1000″. We separately calculate the surface number density of all stars (including dark remnants) and only bright stars.

In order to compare the models with the observations, we only consider stars brighter than V=22 magnitude. We convert model bolometric luminosities to V-band luminosities

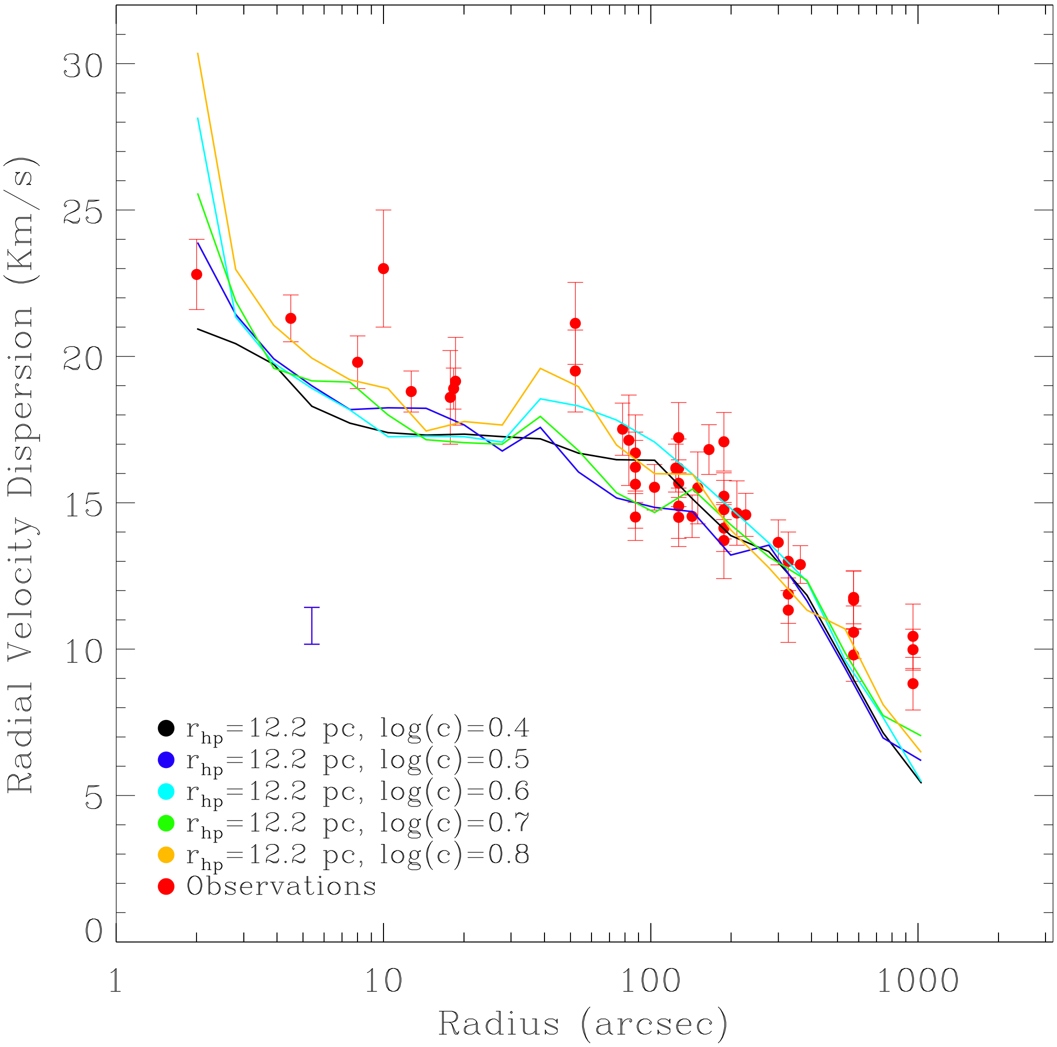

Figure 3.2: Radial velocity dispersion profiles as a function of radius for models with an IMBH mass 2% of the stellar mass with the same initial r_{hp}. Observational data are shown as red points, and a sample uncertainty is shown in blue as in Figure 3.1. Black, magenta, light blue, green and orange points are models with initial log(c)=0.4 to 0.8. All models have the same dispersion outside the core radius (∼ 100″) while clusters with higher concentration show higher velocity dispersion towards the center, as explained in section 3.4.

assuming the stellar temperature model of Eggleton et al. (1989). Using the distance modulus of ω Centauri, we obtain V-band magnitudes that can be directly compared to the measurements (e.g. magnitude cuts). AvdM10 measure the observed surface brightness profile using HST multi-epoch data with the magnitude cut of B∼22 mag (section 3.2 and their Figure 1). Our magnitude cutoff of V=22 magnitude is also consistent with the combined data in Meylan (1987) and Trager et al. (1995). The adopted cutoff in our simulations is also applied to maximize the number of stars in each bin for better number statistics. We then convert the star counts to magnitude per arcsecond squared. We match our surface brightness profile with the observed one by shifting it by an additional zero point. We calculate the zero point for each model profile with a χ^2 minimization in order to compare our profile directly to the observed surface brightness profile.

3.3.2 Model Kinematic Profile

We calculate the velocity dispersion profile of our model clusters again using all stars and using only bright stars similar to how the surface brightness profile was calculated. First, we determine the velocity dispersion using all stars including compact remnants. Second, we use only stars brighter than a certain magnitude limit, adopted to be the same as the observational one. In the case of radial velocities, the observed kinematical data within the central $30''$ are obtained using integrated light (IFU data), so we similarly measure in the models the luminosity weighted velocity dispersions. We avoid very bright stars in the central region as in the observations, in order to prevent shot noise effects. Therefore, we only consider stars fainter than V-magnitude of 15 (similar to the observational cut off) inside $30''$. For radial velocities at larger radii, we consider stars brighter than an apparent magnitude of V=18 magnitude since the observed data were mainly obtained from individual giant stars. For proper motions, we consider stars within the magnitude range of $18 < V < 22$ magnitude which is found suitable for proper motion measurements in AvdM10. We assign magnitude weights to the velocities of stars within this magnitude range following Table 4 of AvdM10 to measure the proper motion velocities.

3.4 Results

In order to find a model which has simultaneously an excellent fit of the observed surface brightness and velocity dispersion profiles of ω Centauri, we run a grid of models with different initial conditions. We describe below some general phenomena in order to illustrate the effect of each initial parameter on the profiles of the evolved clusters. We use as an example the IMBH model with 2% mass of the total cluster mass. We first consider variations of the initial r_{hp} while the cluster logarithmic concentration $\log(c)$ is fixed. The model cluster final mass is a free parameter as discussed for eq. (3.3). Since the final r_{hp} is fixed to the ω Centauri one (4.18 arcmin in the 2003 version of Harris (1996)), increasing the initial radius will produce a more massive cluster after scaling, since we scale such as to keep the relaxation time constant (see eq. 3.3). Hence, at a fixed initial cluster concentration, by increasing the initial r_{hp} the whole radial velocity dispersion profile will scale up, as can be seen in Fig 3.1. In this figure, at a fixed logarithmic concentration $\log(c) = 0.4$ one can see that a cluster which starts with an initial r_{hp} of 11.6 pc has a much lower velocity dispersion profile than the observed one at almost all radii. In contrast, the cluster with the same concentration but higher initial r_{hp} of 13.4 pc has a higher dispersion profile than the observed one, while the general shape of the profiles usually follows the same pattern. This also shows that relaxation is not very important for ω Centauri.

We now discuss the effect of varying initial concentration c on the final kinematic profiles after 12 Gyr of evolution. Clusters with higher concentrations have more mass in the central regions and therefore a higher central velocity dispersion. In Figure 3.2, we show this effect by presenting one family of models with fixed initial r_{hp} (12.2 pc) but varying concentrations (see the color code in the caption). In this example, all clusters in the family of $r_{hp} = 12.2$ pc have almost the same velocity dispersion at large radii, but different central velocity dispersions as a function of their concentrations.

3.4.1 No-IMBH Models

We first run a sparse grid of models between $0.5 < \log(c) < 1.5$ and $10.0 < r_{hp} < 15.0$ pc in order to identify the best fitting model. We find that models with initial $\log(c) \sim 0.8$ and $r_{hp} \sim 12$ pc give the best fit. We produce a finer grid of models between $0.6 < \log(c) < 1.0$ and $11.6 < r_{hp} < 13.4$ pc for the no black hole case. As explained in section 3.3, we calculate the χ^2 values of velocity dispersion and surface brightness profiles to choose the best-fitting no-IMBH model. We find that the model with initial $\log(c) = 0.9$ and initial $r_{hp} = 12.8$ pc produces the best fit to the data of ω Centauri.

Figure 3.3 shows the surface brightness profile of bright stars with V $<$ 22 magnitude for the model with $\log(c) = 0.9$ and $r_{hp} = 12.8$ pc and no central black hole. In this model, the surface brightness of bright stars reproduces the observational data well but predicts slightly lower values in the central $10''$ where NGB08 saw a shallow cusp, which can be interpreted as an evidence of an IMBH. Fig. 3.4 shows the radial velocity dispersion profile for the above no-IMBH model. Except for the innermost part, the model agrees relatively well with the data within the uncertainties but in the central $100''$ the no-IMBH model lies significantly below the observational data. The proper motion dispersion profile for the no-IMBH best-fit model is shown in Fig. 3.5.

We note that whether the no-IMBH model does a good or a poor fit depends on the adopted center since in vdMA10 there is no shallow cusp in the observed surface brightness profile. Further, the observed proper motion data around the proposed center by AvdM10 would be better fitted by the no-IMBH models although the central $10''$ values are still slightly above the best no-IMBH models.

Models starting with higher r_{hp} than 12.8 pc cannot match the radial (and proper motion) velocity dispersion profile beyond $\sim 50''$, they always lie higher than the data at larger radii when we attempted to match the inner region. In other words, higher initial r_{hp}, meaning higher model cluster mass, increase the whole model profile. Therefore, models with an initial r_{hp} higher than 12.8 pc are ruled out. Similarly, models with 11.6 pc initial

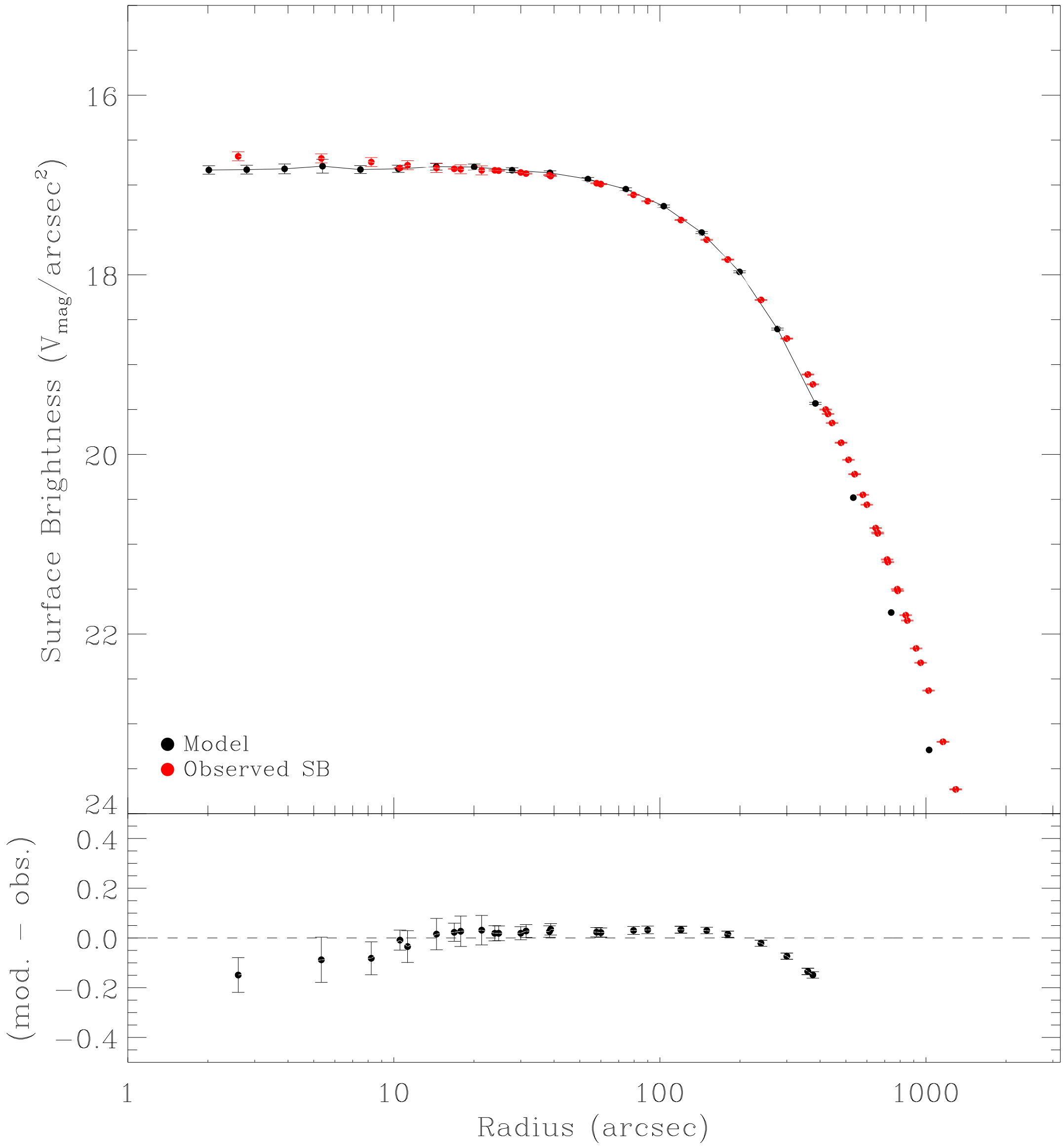

Figure 3.3: Upper panel: V-band surface brightness profile as a function of radius. The red points are the observed V-band surface brightness relative to the kinematic center in N10. The black points are the best no-IMBH model. This model fits the surface brightness data relatively well inside 400″, except inside the central 10″, where it follows below the observations. The model points are connected inside 400″ over which we calculate the χ^2 values. Lower panel: residual of our model with respect to the observed profile.

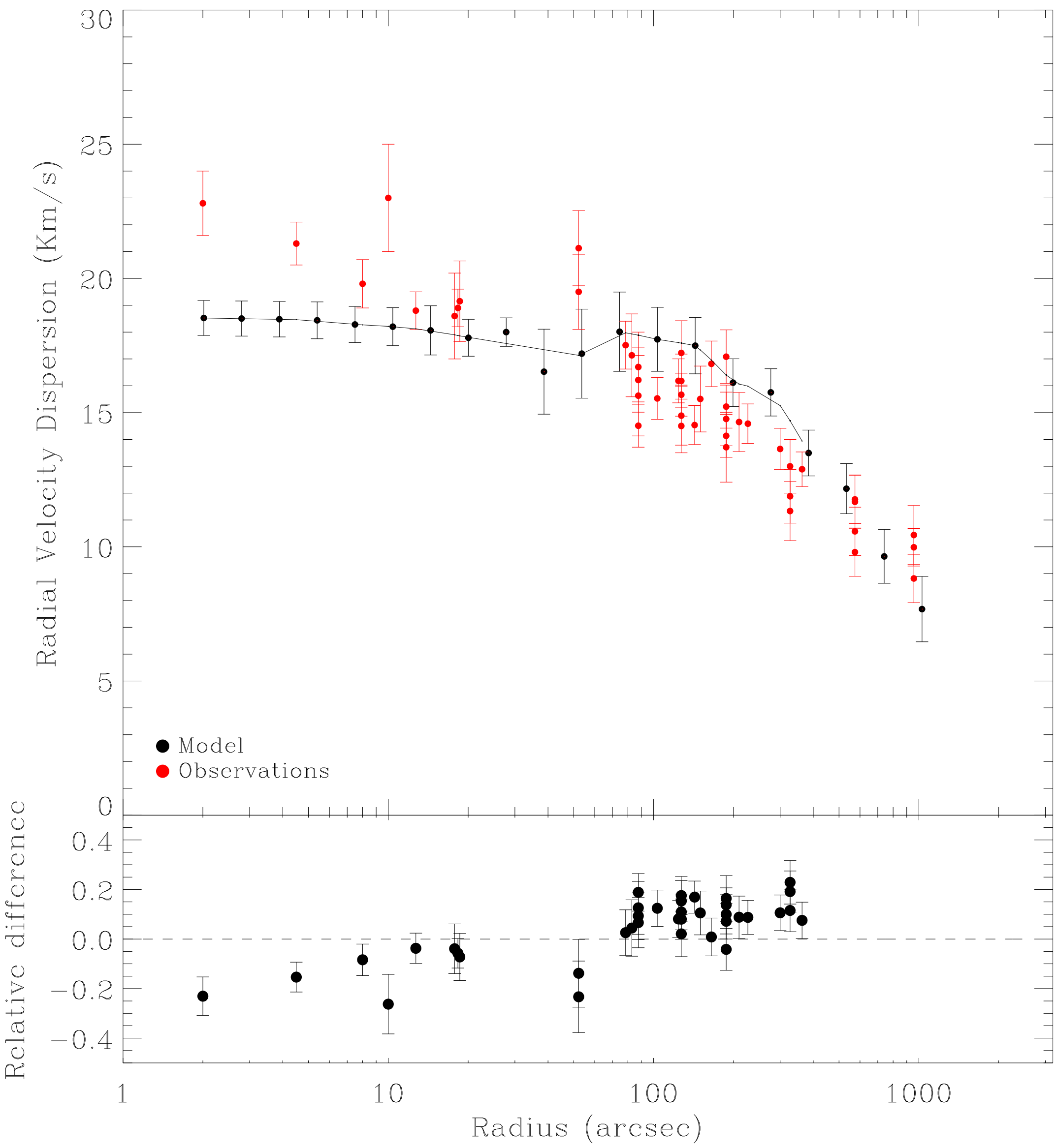

Figure 3.4: Upper panel: Radial velocity dispersion profile vs. radius. The red points are the observed velocity dispersion relative to the kinematic center, taken from N10. The velocity dispersion of the best-fit no-IMBH model is shown in black. The model obviously does not fit the data around the center (for details see section 3.4.1). Lower panel: the relative difference of our model and the observed profile.

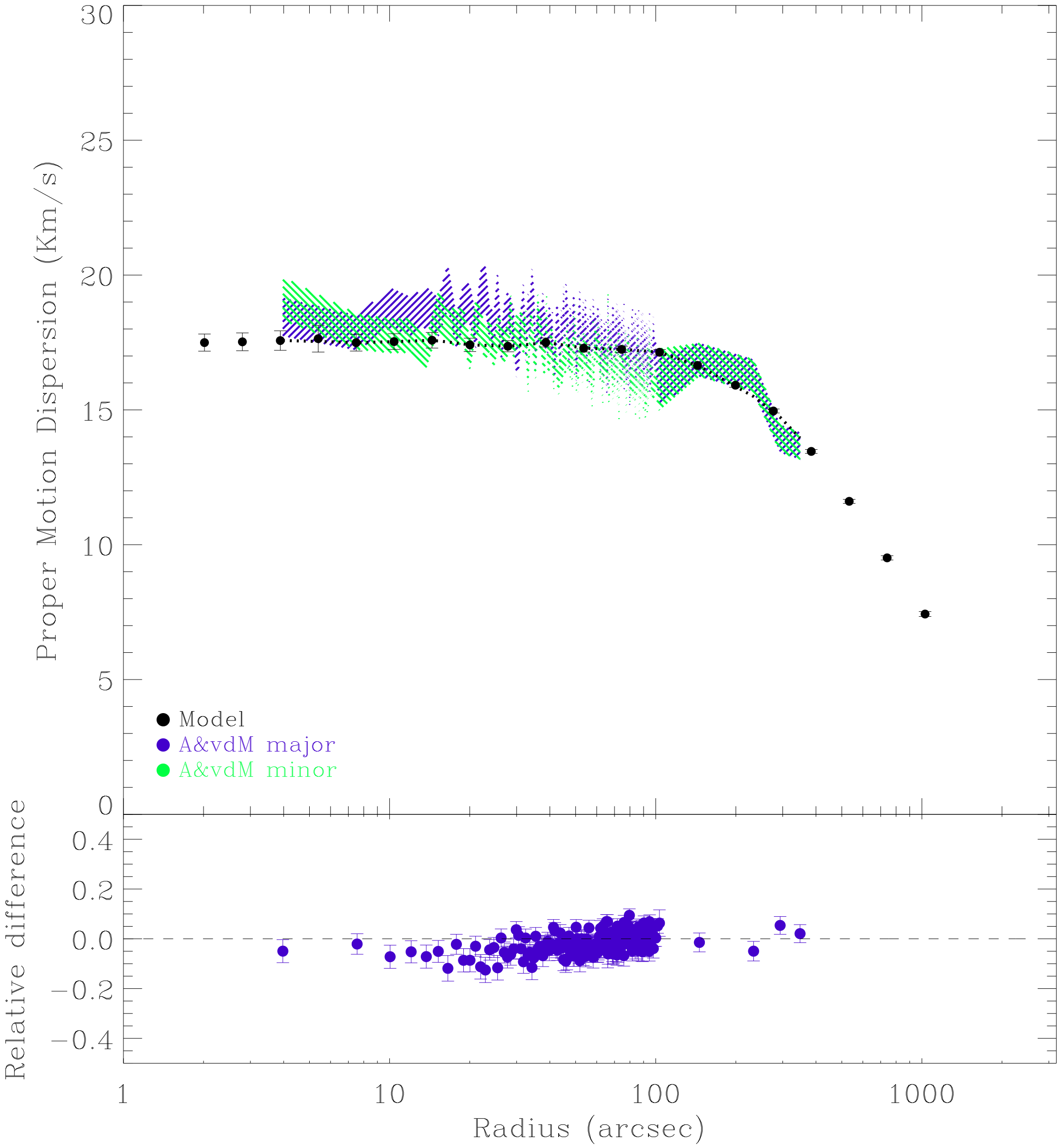

Figure 3.5: The proper motion velocity dispersion profile vs. radius. The best-fit no-IMBH model is shown in black. Shaded magenta and green are the observed proper motions for major and minor axes taken from vdMA10 but with respect to the kinematic center. The Lower panel shows the residuals and displays the major axis data only, for clarity.

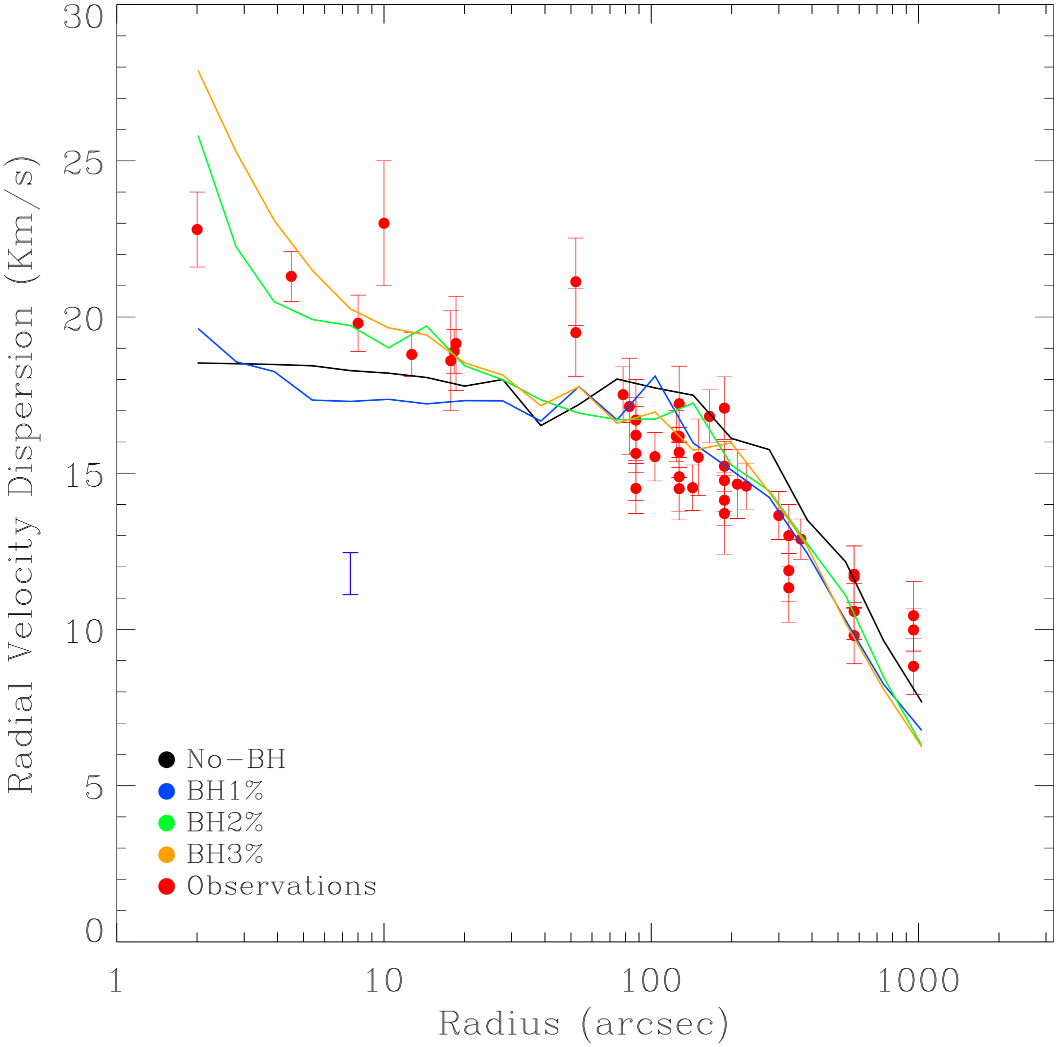

Figure 3.6: Velocity dispersion profile with different central black hole masses. The red points are the observed dispersion. The black line is the best no-IMBH model which obviously cannot reproduce the data in the inner parts. The blue, green and yellow lines represent models with black hole masses of 1%, 2% and 3% of the cluster total mass. A typical uncertainty at 5″ is shown in blue on top of models for visual clarity. The green line is the velocity dispersion profile for the best-fit black hole model, containing 2% of the initial cluster stellar mass (section 3.4.2).

r_{hp} do not reproduce the observations either. However, the majority of the data points used to compute the radial velocity dispersion is at radii larger than $\sim 100''$ while for the proper motion dispersion it is at radii smaller than $\sim 100''$. This can lead to a slightly different best-fit model depending on the radial range over which the model is evaluated. Given eq. (3.3), we use the data at large radii to choose the best cluster mass scaling. For

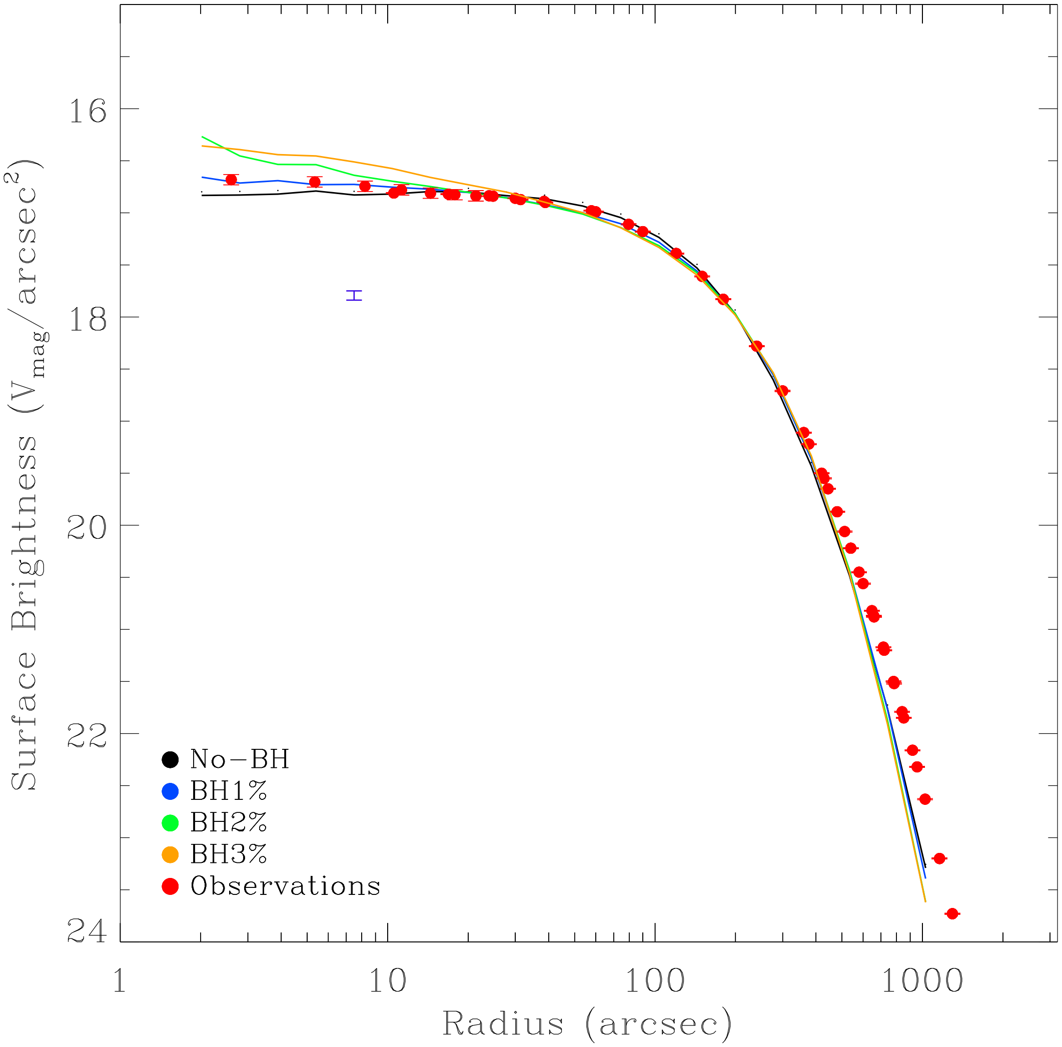

Figure 3.7: Surface brightness profile of models with different central black hole masses. Symbols and colors are the same as Fig 3.6. The red points are the observed profile (section 3.2). The black line is the best no-IMBH model which falls slightly below the observed data. The blue, green and yellow lines represent models with black hole masses of 1%, 2% and 3% of the cluster total mass.

instance, the model with $\log(c) = 0.9$ and $r_{hp} = 12.8$ pc better fits the proper motions than the $\log(c) = 0.8$ and $r_{hp} = 12.2$ pc which better fits the radial velocity dispersion. The latter provides a good fit to the data, but the total χ^2 is slightly larger than for the former since the number of proper motion data points is much larger (218 points) than the number of data points for radial velocity data (38 points), giving a higher weight to the proper motion fit.

Note that the model radial velocity profiles systematically show a slight discontinuity starting at $30''$ as can be seen e.g. in Figure 3.4. The jump is due to the way we measure our model radial velocity dispersions: since we follow the same method as the observational studies (see Section 3.3.2), we measure the luminosity weighted velocities for stars fainter than 15 mag in the inner $30''$, as opposed to the velocities of individual stars brighter than 18 mag at larger radii. Consequently, we have fewer stars/measurements at larger radii, and the uncertainties get slightly larger than for the central values. Furthermore, stars that contribute to the velocity dispersion measurement in the inner part are more massive than at larger radii which causes slightly smaller velocity dispersions in the inner $20''$ than at $50''$.

3.4.2 IMBH Models

Since models without an IMBH could not represent the data well, we run models including central black holes of various masses with the hope of improving the fit to the data. In this set of simulations, we start from isotropic King model conditions with concentrations in the range $0.3 < \log(c) < 0.8$ and initial r_{hp} in the range of $11.6 < r_{hp} < 13.4$ pc. Apart from the central black hole mass, all the other parameters such as NS retention fraction and stellar mass range are the same as for the no-IMBH models. Furthermore, since we find that the IMBH model that reproduces the observed profiles best has lower concentration and higher r_{hp} than the no-IMBH models, we explore a larger parameter space in order to determine the best set initial conditions leading to the present-day observations. For each initial configuration, we run the simulations as described in Section 3.3. For models with a central black hole, we calculate the kinematic and surface brightness profiles as described in the Sections 3.3.1 and 3.3.2. Hence, all the model-data comparisons are done following the same magnitude and radial cut-offs as for the no-IMBH models.

In the case of IMBH models the IMBH could move around the cluster during the simulations, and we center the final model clusters on the central black hole. In our simulations, IMBH models contain black hole masses of 1%, 2% and 3% of the final stellar mass of the cluster. For reference, a 1% IMBH would lie slightly above the Magorrian et al. (1998) relation. If we adopt a mass of $\sim 2.5 \times 10^6 M_\odot$ for ω Centauri (vdV06), the IMBH masses we use are equivalent to black hole masses of about $2.5 \times 10^4 M_\odot$, $5.0 \times 10^4 M_\odot$ and $7.5 \times 10^4 M_\odot$ respectively. However, the exact masses of our models depend on the initial r_{hp} due to the scaling of radii (see eq. 3.3), and will slightly differ from the above values. We calculate and analyze the χ^2 maps for models including the above IMBH masses. We find the best-fit models for each grid including a 1%, 2% and 3% IMBH, applying the same methodology that we use to find the best no-IMBH model. The radial velocity dispersion and surface brightness profiles of the best-fit models of different IMBH masses and also the ones for the best-fit no-IMBH model are shown in Figure 3.6 and Figure 3.7. The best-fit IMBH model is the one containing 2% of the stellar cluster mass starting initially with $\log(c) = 0.5$ and $r_{hp} = 12.8$ pc. As can be seen from Figure 3.6, the best-fit IMBH models with 1% and 3% of the cluster stellar mass do not fit the observed radial velocity dispersion well since they have lower or higher values than the observed velocity dispersion profile in the central part. A summary of best-fit models among all models including no-IMBH and

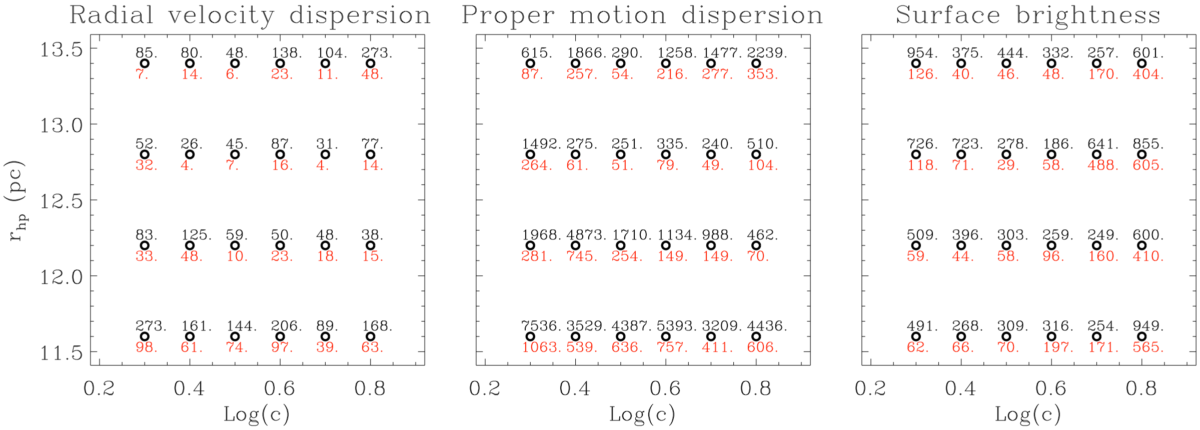

Figure 3.8: From left to right, the χ^2 map for the radial velocity, the proper motion dispersion and the surface brightness profiles, for models with an IMBH mass of 2% of the model cluster mass, over the grid of initial parameters space. The numbers in black are the absolute χ^2 over $400''$ radius. The absolute χ^2 values inside $40''$ are shown in red to visualize the goodness of the fit in the central region for each model.

IMBH are tabulated in Table 4.1. The chosen best-fit 2% mass IMBH model is highlighted with boldface.

The left panel in Figure 3.8 shows the radial velocity dispersion χ^2 map for models containing an IMBH mass of 2% of the cluster stellar mass. Models starting with an initial r_{hp} of 11.6 (13.4) pc always lie lower (higher) than the data at large radii because of the less (more) massive final cluster mass (see eq. 3.3). In contrast, models starting with r_{hp} of 12.2 and 12.8 fit the data much better at larger radii due to better cluster mass scaling when relaxation time is the same as for ω Centauri.

In addition to radial velocities, we calculate the proper motion dispersion (perpendicular component to the radial velocity in our models) with the weights and magnitude cut-offs explained in section 3.2.3 and 3.3.2. The χ^2 map for the proper motion dispersion for the 2% IMBH models is shown in the middle panel of Fig. 3.8. The right panel in Figure 3.8 depicts the χ^2 values of surface brightness for the models with an IMBH mass of 2% of the stellar mass. As it is shown in this figure, models starting with high initial concentrations such as $\log(c) = 0.7$ and 0.8 show a steeper cusp in the central part than the observation and do not describe the observed surface brightness well. For instance, models such as $\log(c) = 0.6$ with $r_{hp} = 12.2$ and 12.8 pc and also a model starting with $\log(c) = 0.7$ and $r_{hp} = 12.2$ pc show relatively small χ^2 in surface brightness map because of their large cores. A larger core gives a better fit at larger radii (around $80''$), though these models have a very poor fit in the central part due to a very steep rise. In addition, it should be noted that the number of data points at large radii is higher than at the center. Furthermore, the observational uncertainties are smaller at larger radii than in the central region, therefore, the χ^2 value can be small if a model has a good fit at large radii but an unsatisfactory fit in the central part. Thus, we choose models with smaller $\log(c)$ such

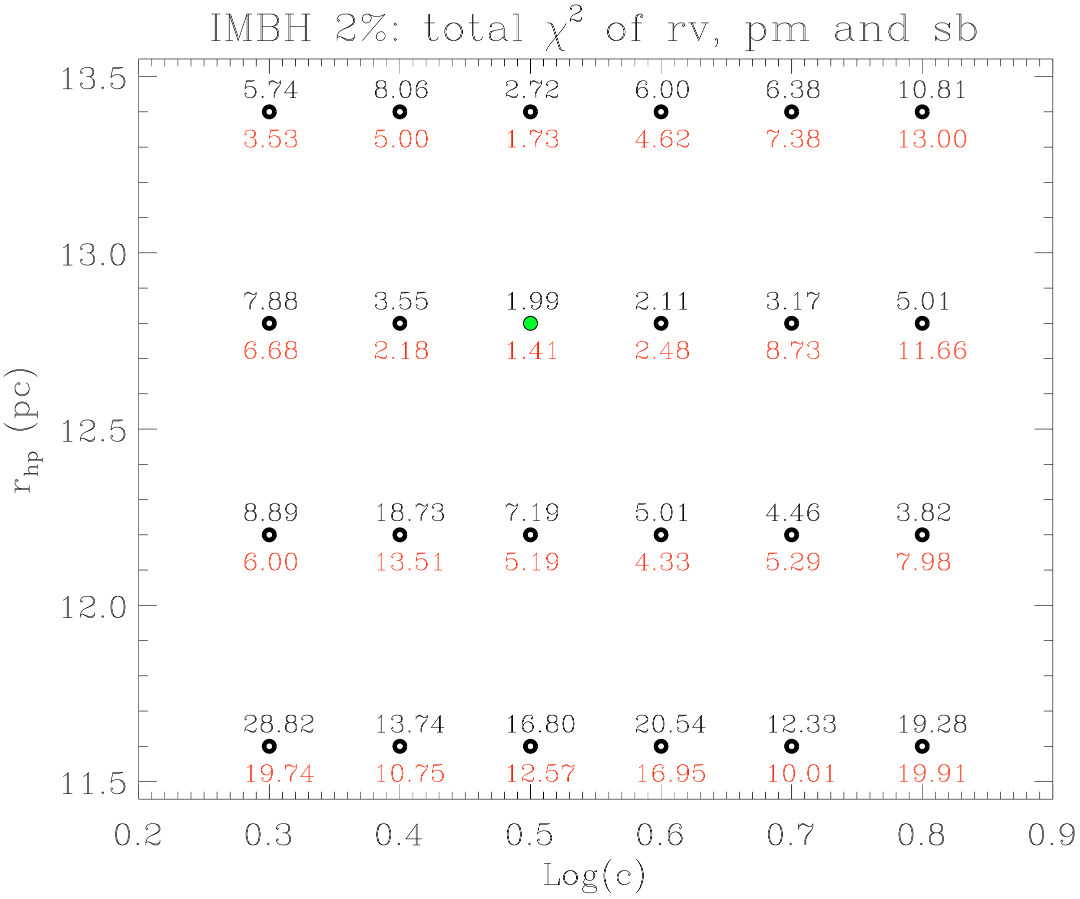

Figure 3.9: The final reduced, combined χ^2 map for models with an IMBH with a mass of 2% of the model cluster mass. This map is calculated based on equation 3.6, using the radial velocity, the proper motion dispersion and the surface brightness χ^2 maps in Fig 3.8. The best-fit model is marked in filled green.

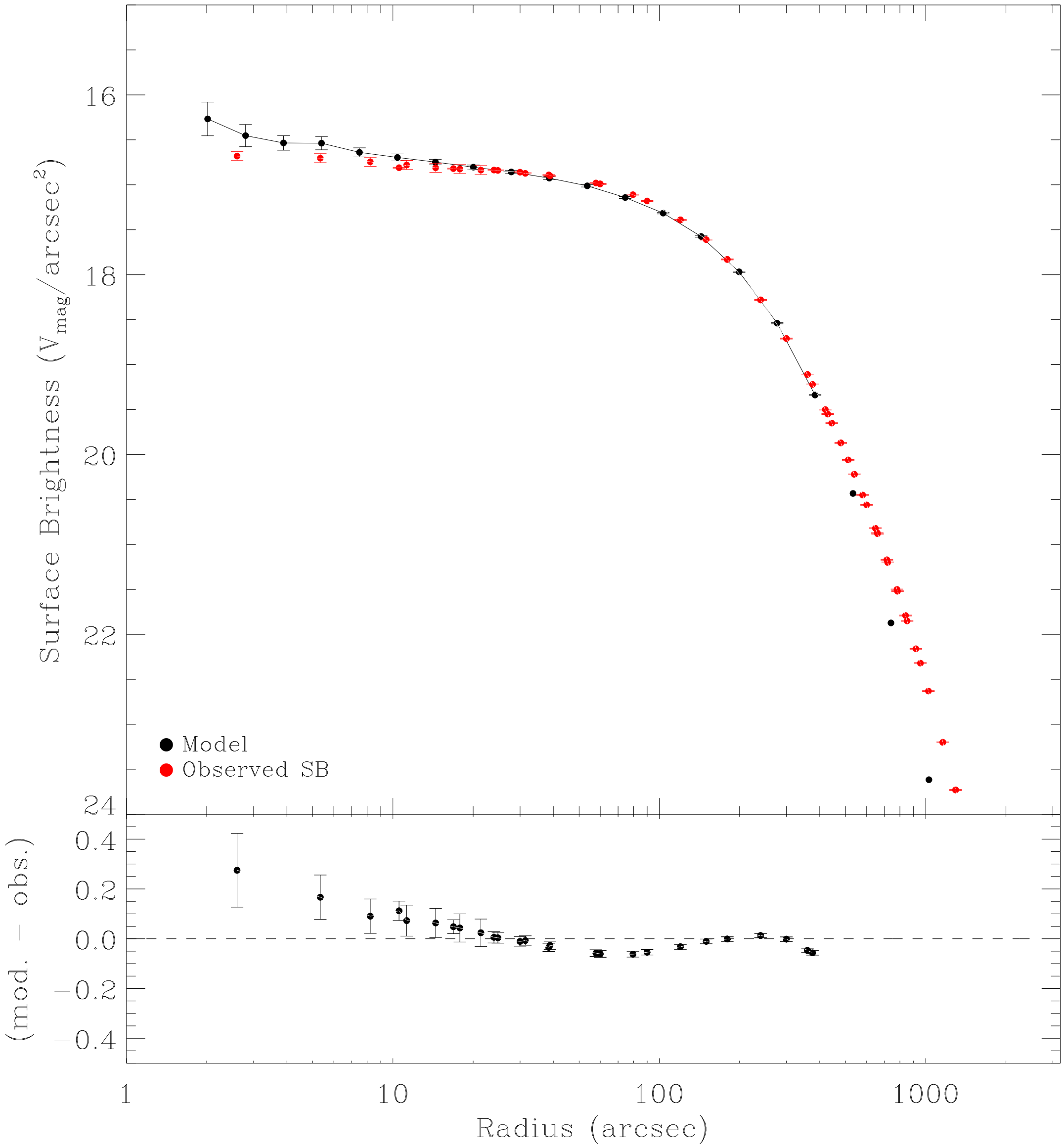

Figure 3.10: Upper panel: V-band surface brightness profile as a function of radius. The symbols are as in Fig. 3.11. Lower panel: residual of our model and the observed profile.

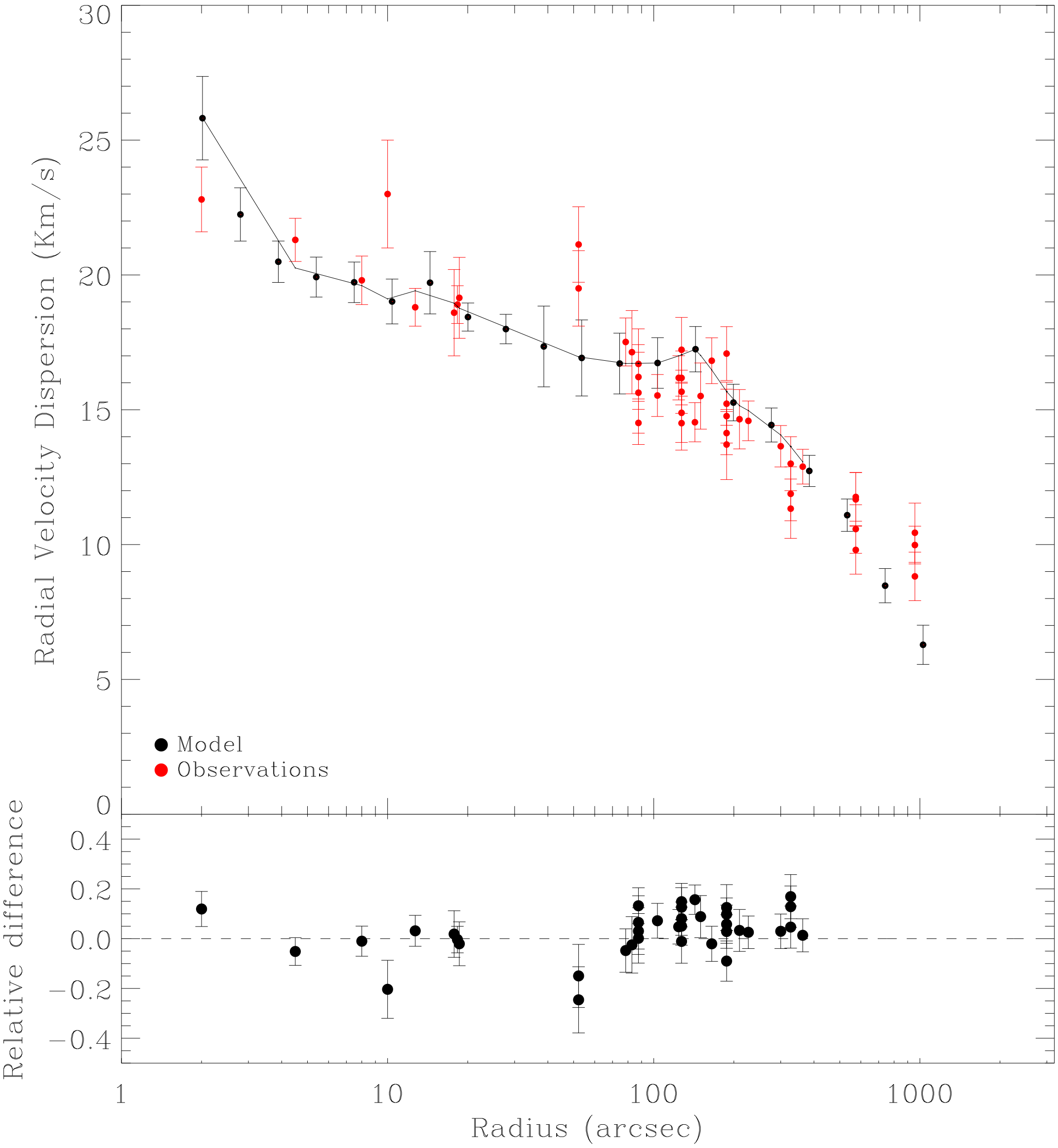

Figure 3.11: Upper panel: Velocity dispersion profile vs. radius in arcsecond. The red points are the observed data points relative to the kinematic center, taken from N10. The velocities for the best-fit model containing an IMBH mass of 2% of stellar mass is shown in black. Lower panel: the relative difference between our model and the observed profile.

as 0.4 and 0.5 as our best-fit models for representing of the surface brightness data. The fact that smaller core models such as $\log(c) = 0.4$ and 0.5 do not provide a better fit at larger radii in surface brightness is related to the initial King profile, which alone might not be sufficient to fit the density profile and is independent of having a central IMBH. In a future paper we intend to modify the initial density profile so that we take this effect into account, for instance by combining a King profile with a Sersic one.

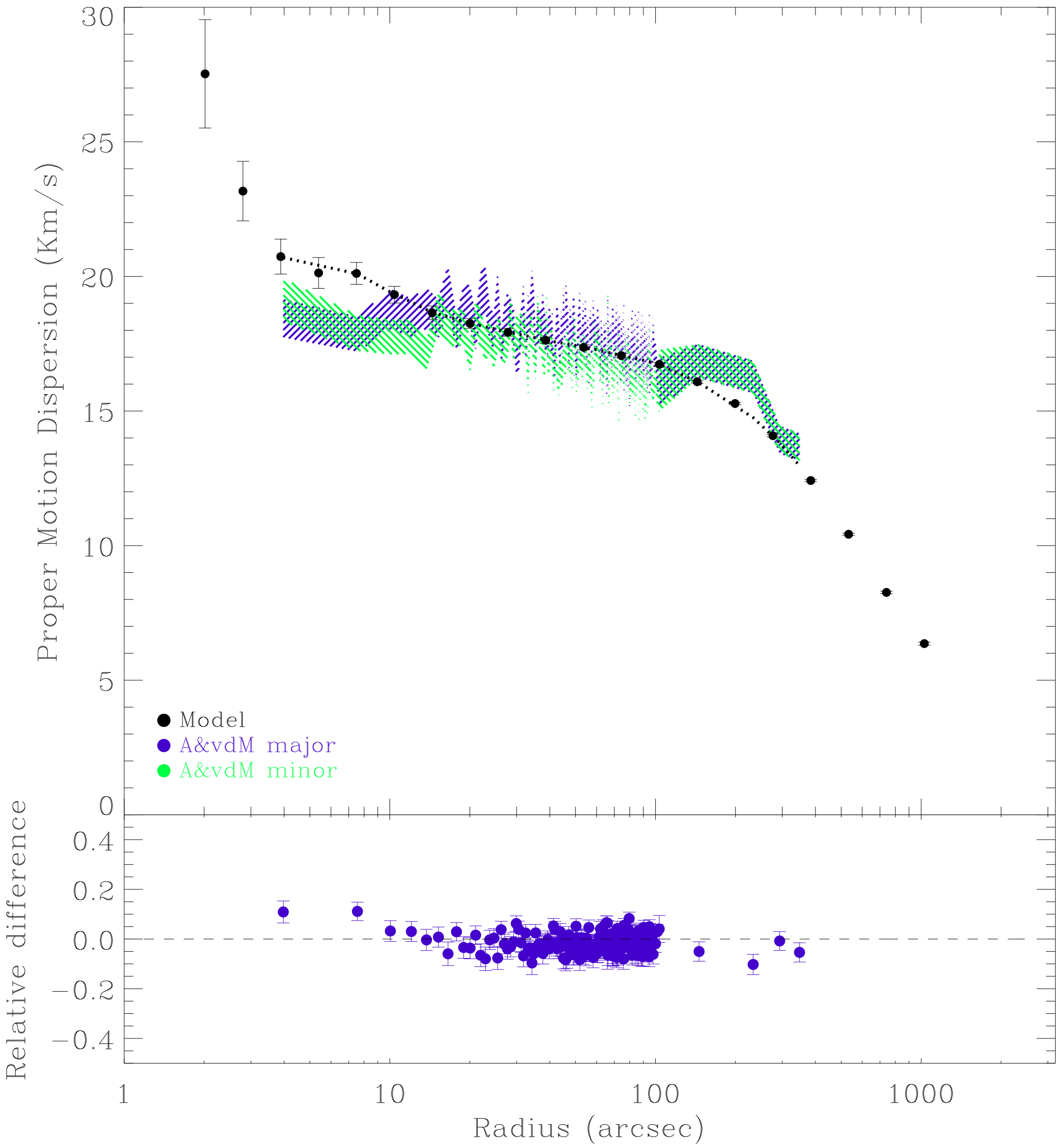

Figure 3.12: The proper motion dispersion profile for our best-fit IMBH model is shown in black. Shaded magenta and green are the observed proper motions for major and minor axes taken from vdMA10 but with respect to the kinematic center. The model proper motion dispersions for a cluster containing an IMBH mass of 2% of the stellar mass has a higher velocity dispersions than the observed one in the central 10″. The residual is illustrated only for major axis data for clarity.

Considering the above results, the model with initial $\log(c) = 0.5$ and $r_{hp} = 12.8$ pc fits better than the other models. However, it still has a slightly steeper surface brightness in the central region than the observed one. We show the final reduced combined χ^2 values (see eq. 3.6) for models with a 2% IMBH mass in Figure 3.9. The IMBH model starting

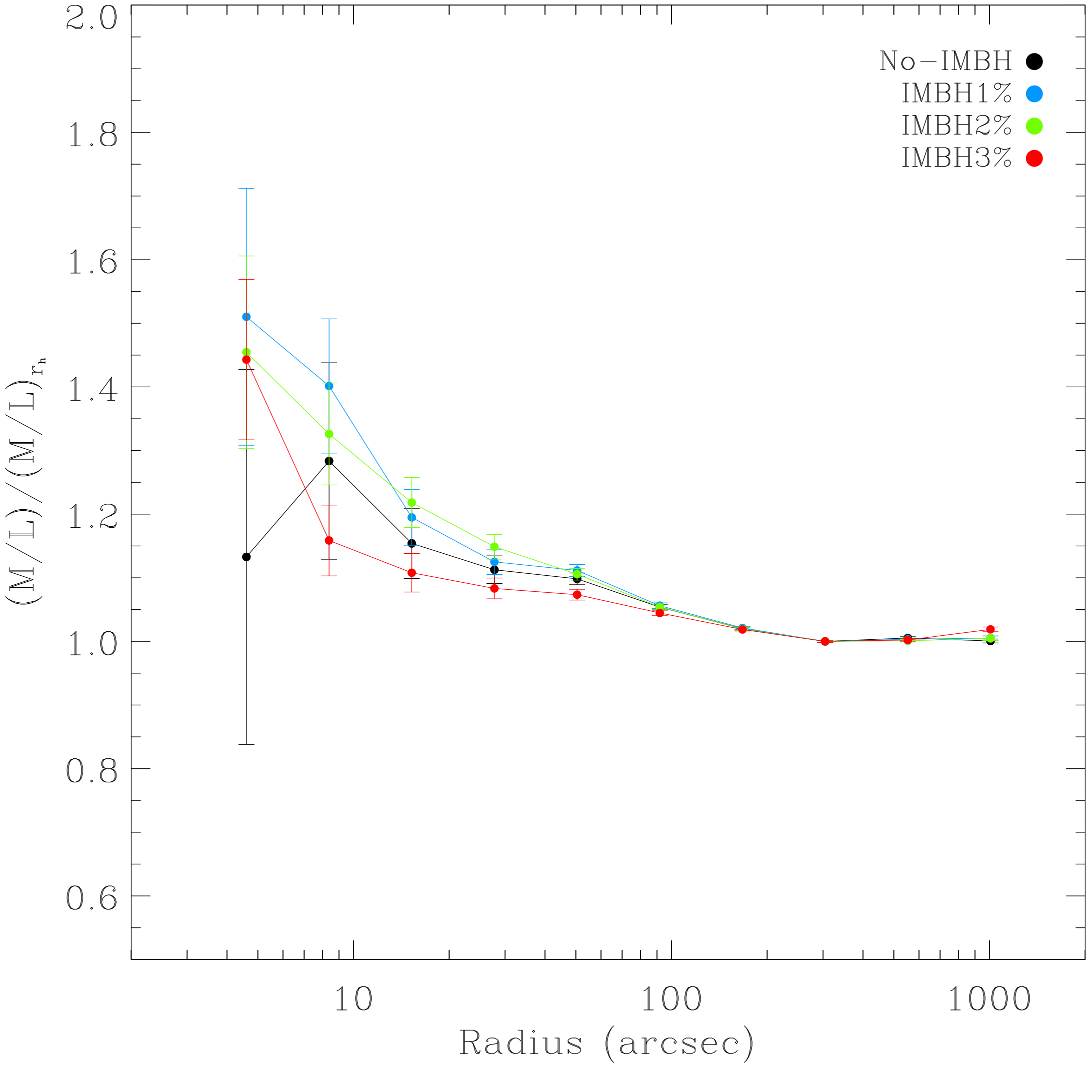

Figure 3.13: V-band stellar M/L ratio as a function of distance to cluster center for the best-fit models normalized by M/L at half-light radius. The M/L increases towards the center since massive white dwarfs are segregating inwards.

Table 3.2: Initial parameters and the χ^2 values for best-fit models containing different IMBH mass fractions.

Model	$\log(c)$	r_{hp} (pc)	χ^2_{rv}	χ^2_{pm}	χ^2_{sb}	red. χ^2_{total}[a]	red. $\chi^2_{total}(< 40'')$[b]
no-IMBH	0.9	12.8	84.74	283.22	248.61	2.14	1.87
1% IMBH	0.7	12.8	55.72	422.22	144.21	2.16	2.22
2% IMBH	**0.5**	**12.8**	**45.05**	**251.48**	**277.95**	**1.99**	**1.41**
3% IMBH	0.4	12.8	42.28	292.39	377.18	2.47	3.64

[a] This column is obtained by dividing the sum of absolute χ^2 on the total number of data points for all three observed profiles

[b] The same as the previous column but for the inner $40''$

with initial $\log(c) = 0.5$ and $r_{hp} = 12.8$ pc provides the best-fit to the observations. The profiles for the best-fit IMBH model are shown in Figures 3.10, 3.11 and 3.12. As can be seen in Figure 3.12, a model with an IMBH mass of 2% of the final cluster stellar mass shows higher central velocity dispersions than the observed proper motions. However, as mentioned before, the best-fit no-IMBH model might fit the proper motions better with respect to the AvdM10 center.

Furthermore, it is interesting to note that the radial versus transversal components of the velocities for our evolved clusters are the same. Thus, an initially isotropic cluster stays isotropic throughout its evolution even if a central IMBH is present.

In Fig. 3.13, we show the stellar V-band mass-to-light ratio profiles in our simulations for the best-fit models with an IMBH, and the model without an IMBH. Since the absolute value of M/L depends on the age of the stars, we calculated it using the same 20 snapshots, i.e. from 11 to 12 Gyr, for all the models in Fig. 3.13. As one might expect M/L is the same for all models at large radii since the initial mass function is the same in all models, and, the effect of IMBH is negligible in the outer region. The M/L ratio starts to rise towards the center due to the segregation of heavy-mass compact remnants and is about 1.3 times as large at $10''$ than at the half-mass radius.

As mentioned in Section 3.3, scaling the relaxation time and fixing the final present-day r_{hp} to the ones of ω Centauri, we obtain the final (present-day) total mass of the model cluster. We derive a cluster mass of $(2.5 \pm 0.1) \times 10^6 M_\odot$ if we use the best-fit model containing an IMBH of 2% of the cluster mass, which is in very good agreement with the determined $(2.5 \pm 0.3) \times 10^6 M_\odot$ mass for ω Centauri (vdV06).

3.5 Discussion and Conclusions

We have created a large set of evolutionary N-body models for ω Centauri with certain canonical assumptions which are usually applied as reasonable estimates for globular clusters, such as standard Kroupa IMF, with the aim of reproducing its observed properties. In particular, we examine whether we can explain the newly acquired observations for the central velocity dispersion profile with the presence of a central IMBH or whether a model without an IMBH is also consistent with the observations.

Following the method applied in Baumgardt et al. (2003a,b), we calculate models starting with spherical isotropic King conditions (King 1966) with different initial parameters. We do not include the tidal field of the Galaxy and primordial binaries in our models. Since we cannot simulate a star cluster of the size of ω Centauri by direct N-body simulations, we start with more extended clusters containing fewer number of stars than ω Centauri and scale our model clusters to the observed cluster such that the relaxation time is constant. As described in detail in Section 3.3, we measure physical quantities from our models such as velocity dispersion and surface brightness following the methods in observational studies, with the same magnitude cut-offs and luminosity weights. Using such careful magnitude weights and radial cut-offs in our models make the data-model comparisons and consequently the drawn conclusions more reliable. We use χ^2 values to compare the profiles of model clusters after 12 Gyr of evolution, with the observed ones. In Section 3.4, we present a grid of models for clusters containing an IMBH mass of 2% of the cluster stellar mass.

We show that the best-fit IMBH model, containing a $5\times10^4 M_\odot$ black hole, matches the data presented in Noyola et al. (2010) very well. In particular, we reproduce the observed rise in the central velocity dispersion as an indicator for the presence of an IMBH. We stress that relying on the profiles relative to the kinematic center in Noyola et al. (2010) makes it impossible to consistently fit the radial velocity dispersion over all radii without a central IMBH. Furthermore, we show that M/L is constant at large radii for all models independent of the presence of a central black hole. We predict a slight rise in M/L towards the center for all models due to the mass segregation of heavy-mass compact remnants. We do not claim that our best-fit model is unique. However, we examine more than 100 models to be confident about the initial parameters and the final chosen best-fit model.

A number of further details can be investigated or improved as a next step. Among the interesting issues are the study of rotation at different radii, especially in the central region. In principle such a study can be done using an axisymmetric model which is closer to ω Centauri, as an exception in Galactic star clusters. Fiestas & Spurzem (2010) investigated the evolution of rotating dense stellar systems containing massive black holes. Exploring rotation effects could help to better understand the observed discrepancy between proper motion and radial velocity dispersion. In addition, as described in previous studies (King & Anderson, 2002; Meylan, 1987), ω Centauri might not be well fitted by a King profile alone. We intend to investigate this in more detail in a future paper studying different initial configurations such as Sersic and double King profiles. Furthermore, to improve the model surface brightness profile at large radii, around the tidal radius, the tidal field of the Galaxy should be taken into account. In order to more tightly constrain the initial parameters for ω Centauri the above studies as well as trying different IMF distributions are necessary in addition to investigate a finer grid, though they will be computationally expensive.

Chapter 4

Orbit-based Models

Based on Jalali, B., Gebhardt, K., Kissler-Patig, M.,
Noyola, E., Lützgendorf, N., de Zeeuw, P. T., Baumgardt, H.,
in preparation

4.1 Introduction

To better understand and further constrain the dynamical structure of ω Centauri, we focus in this chapter on another specific method of dynamical modelling that is constructed to study the orbital structure of stellar systems. This method was invented by Schwarzschild (1979) and has been applied intensively during the last two decades to estimate black hole masses in galaxies and more recently to study their dark matter halos. This method allows to model galaxies using a certain general symmetry assumptions, basically about the shape of the potential and the dimensions of the velocity ellipsoid. The main advantage is that unlike the Jeans modelling which requires prior restrictions, such as a specific anisotropy form, the Schwarzschild method reconstructs the structure of stellar systems by super-position of orbits and constructing the collisionless distribution function. The orbital weights are chosen so that the model can match the observed light and kinematic of the system as well as possible. More detailed reviews on the history and technical aspects is provided in Gebhardt (2004) and Thomas (2010) and references therein.

Schwarzschild models, also known as orbit-based models, provide important information on the structure of massive galaxies. Historically, codes based on this method were implemented to measure the black hole masses in galaxies (Kormendy & Richstone, 1995; van der Marel et al., 1998; Gebhardt et al., 2003; Krajnović et al., 2005) and then further developed to also perform dark matter modelling of galaxies (Thomas et al., 2004, 2005,

2007) and further, to cover more general symmetries such as triaxial rather than only axisymmetric ones (van den Bosch et al., 2008; van den Bosch & de Zeeuw, 2010).

We note that for star clusters such as ω Centauri, by assuming a specific distribution function (King spherical models in this case) we could also follow the time evolution of the system (presented in Chapter 3) which in principle can be extended to a point at which it is not necessary to assume any prior symmetry such as the work in N-body simulations for merging galaxies (Barnes & Hernquist, 1992). Thus, the applied model in this chapter is covering other aspects of dynamical modelling for stellar systems than N-body simulations.

Orbit-based models have been used before for a couple of star clusters such as ω Centauri (van de Ven et al., 2006) and M15 (van den Bosch et al., 2006). For this thesis, we follow the approach of Gebhardt et al. (2003). In addition to some differences in the technical issues with respect to the models in the above studies, we use the most up to date kinematics for the central region which we recently obtained and analysed in Noyola et al. (2010) (see Chapter 2). In fact, the main focus of the model in van de Ven et al. (2006) is on modelling the structure at large radii and to derive global information such as inclination, dynamical distance and total cluster mass, where by using new kinematic data we attempt to investigate the central dynamic in particular the presence of a possible IMBH in more detail.

As a result of performing orbit-based models on many nearby galaxies, there is no doubt about the existence of supermassive black holes at the center of galaxies. Further, there are tight correlations between the mass of supermassive black holes and the properties of the host galaxies such as the velocity dispersion (Gültekin et al., 2009). One of the most interesting questions about such correlations is whether they can be extended to smaller systems such as star clusters and therefore further link these systems with giant massive galaxies. To address this question we perform orbit-based models for ω Centauri, one of the most well studied star clusters in the Milky Way, due to its close distance which allows us to better resolve the influence radius of the possible black hole. Furthermore, this cluster shows many spectacular properties as mentioned in Chapter 1, such as having a very high central velocity dispersion and being the most massive Milky Way cluster, which make this object one of the most interesting Galactic clusters to investigate with such a goal.

4.2 Data

For this work, we use the same data-sets as described in detail in Chapter 2, and also used for our N-body simulations in Chapter 3. We summarise them briefly:
The data for ω Centauri consist of HST photometry (used to obtain surface brightness profile), and stellar kinematics taken by VLT-FLAMES for the central $10''$ and a compilation of ground-based observations at large radii.

High resolution imaging is necessary to obtain the stellar surface brightness profile in particular for the central region. We use the star catalog of Anderson & van der Marel (2010), which is constructed by using HST images, performing star counts in the central regions ($R < 20''$) with respect to our kinematic center. We use stars brighter than 19.5

mag and an adaptive kernel density estimator for the star counts. The magnitude cut is applied to limit the incompleteness. Our center is stable for this magnitude cut-off (more detailed discussions are in Chapter 2 and 3). We adjust our star count profile to the Meylan (1987) and Trager et al. (1995) profiles at larger radii which compile the surface brightness data for ω Centauri from different sources in the literature (Meylan, 1987; Trager et al., 1995). In Noyola et al. (2008) a surface brightness profile is obtained with integrated light from HST-ACS data within the central $40''$. We use their data from radii larger than $20''$, i.e. the data from $20''$ to $40''$ comes from integrated light measurements and the inner $20''$ comes from star counts.

As presented in Chapter 2, we obtained kinematics in the central region of ω Centauri using integral field spectroscopy. We measure the velocity dispersion from integrated light using VLT-FLAMES with a spectral resolution of ∼10,000 in the Ca-triplet wavelength (Noyola et al., 2010). We use the velocity dispersions with respect to the kinematic center as presented in Table 1 of Noyola et al. (2010). In addition, we use Gemini-GMOS data which Noyola et al. (2008) obtain with integrated light using the same approach as for the VLT-FLAMES data.

At larger radii, van de Ven et al. (2006) collect individual velocity measurements from different sources (Suntzeff & Kraft (1996); Mayor et al. (1997); Reijns et al. (2006); Xie and Gebhardt (private communication)). Most of the above authors measure the velocities of luminous (giants) stars. As an input for the next Section, we use the velocity dispersions presented in Table 4 of van de Ven et al. (2006).

To further constrain the internal dynamics of this object, in particular the degree of anisotropy, proper motions are a useful additional information and we intend to include them in our orbit-based modelling (Section 5). In addition to available ground-based data from van de Ven et al. (2006), we use HST proper motions from AvdM10 at the central $80''$.

4.3 Dynamical Model

There are a number of preliminary steps necessary to prepare the data as inputs for the orbit-based model: 1) deprojecting the observed surface brightness profile to construct a light distribution in three-dimensional space, 2) the reduction of spectra at different locations on the sky to finally obtain projected line-of-sight velocity distributions (LOSVDs).

The first step is to deproject the two-dimensional surface brightness to obtain the internal three-dimensional luminosity density. The luminosity density of a stellar system, $\nu(r)$, is the luminosity per unit volume at position $\mathbf{r}$ (Binney & Tremaine, 2008). Similarly, surface brightness, I(R), could be defined as the system's luminosity per unit area (observationally this normally is reported in terms of magnitude per square arcsecond). Assuming spherical symmetry these two quantities are related to each other as follows

$$I(R) = 2\int_R^\infty dr \frac{r\nu(r)}{\sqrt{r^2 - R^2}}. \tag{4.1}$$

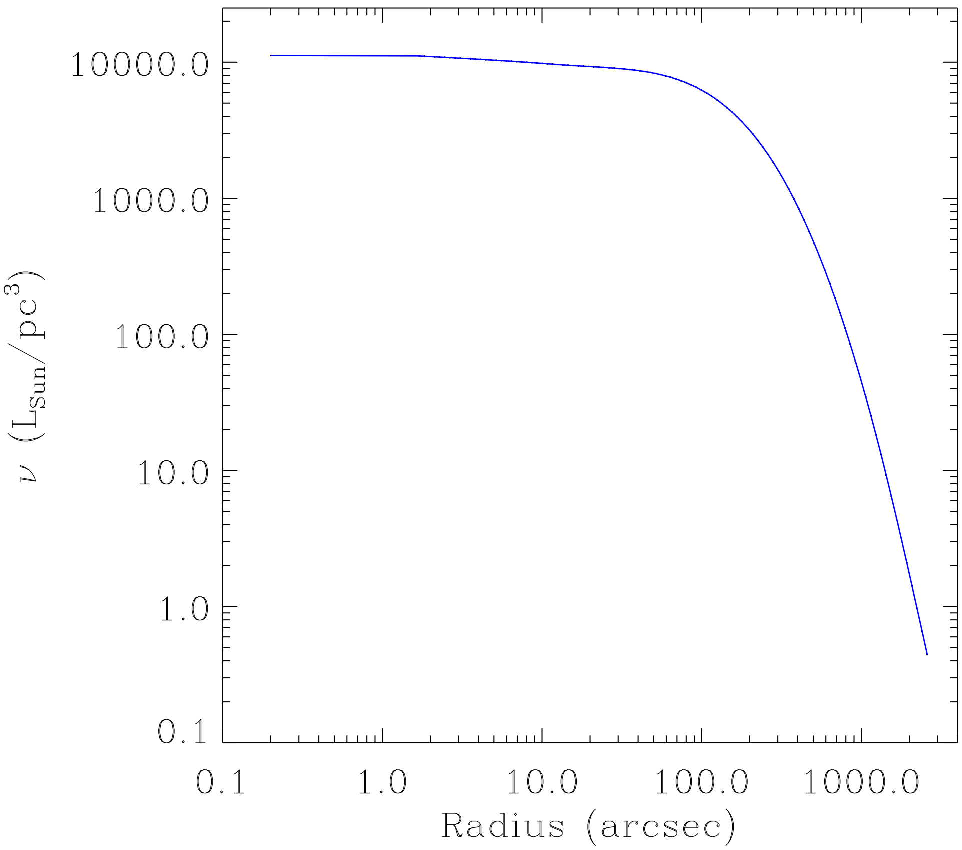

Figure 4.1: Internal light for ω Centauri as a function of distance to the cluster center. The deprojection of the observed surface brightness profile to construct the three-dimensional light distribution is performed non-parametrically following the method presented in Gebhardt et al. (1996).

For a spherical system one can invert the above equation using Abel's integral to obtain luminosity density from surface brightness profile:

$$\nu(r) = -\frac{1}{\pi}\int_r^{\infty} \frac{dR}{\sqrt{R^2 - r^2}}\frac{dI}{dR} \tag{4.2}$$

It is important to note that the central mass concentration will be increased by a central massive dark object, thus the luminosity density provides a lower limit for the mass concentration (Gebhardt 1996).

While the solution of the above Abel's integral will be simpler numerically, in practice any noise in the data is amplified by the construction of $\nu(r)$. In Gebhardt et al. (1996) and references therein there are intensive discussions about the disadvantages and pitfalls of parametric deprojections of surface brightness data.
We thus follow Gebhardt et al. (1996) approach to perform the deprojection by a non-parametric Abel inversion, assuming axisymmetry and the inclination angle of $i \sim 50°$. This method basically uses a smoothing spline to the data in order to numerically integrate and solve equation 4.2. Figure 4.1 shows the obtained internal luminosity density for our star cluster.

For the second step, to extract the projected LOSVDs, we apply a Maximum Penalised Likelihood (MPL) estimator that is discussed in details in Gebhardt et al. (2000b) and Pinkney et al. (2003). Here, we describe again the main steps. It is important to consider that in order to obtain reliable kinematics from MPL method the S/N should be sufficiently high. We bin the pixels as in Gebhardt et al. (2003) into angular and radial bins by luminosity-weighted averaging of the spectra to optimise the S/N. We then perform the MPL method on the binned spectra as following.

First, by dividing out the continua we normalise the spectra of cluster and stellar template. The combined stellar template is then convolved with a binned initial LOSVD. Starting from velocity bins of about 8 km/s, we adjust the height of each LOSVD bin to define a sample LOSVD. The LOSVD and the weights of the templates are iteratively varied until the convolved combined spectrum match the cluster data. For the template, we use two individual stars taken in our IFU set up. These are a normal late-type giant star and a hot star (shown in Chapter 2). The program then determines the relative weight of these two stars. The kinematical analysis we use are described in Noyola et al. (2008, 2010). We fit the second Ca-Triplet line in our spectra to derive the LOSVDs. The above fit is done by minimising the penalised χ^2: $\chi_p^2 = \chi^2 + \alpha P$. The penalty function P is the integral of squared second derivative of the LOSVD.

A certain level of smoothing is applied to the LOSVD. The smoothing parameter α determines the level of regularisation and its value depends on the velocity dispersion of the cluster and the S/N of the data. We estimate the appropriate smoothing for our data from the kinematic analysis of a large data-set of model cluster spectra. These models are created by broadening the template spectrum with a velocity dispersion of similar to our expected velocity dispersion.

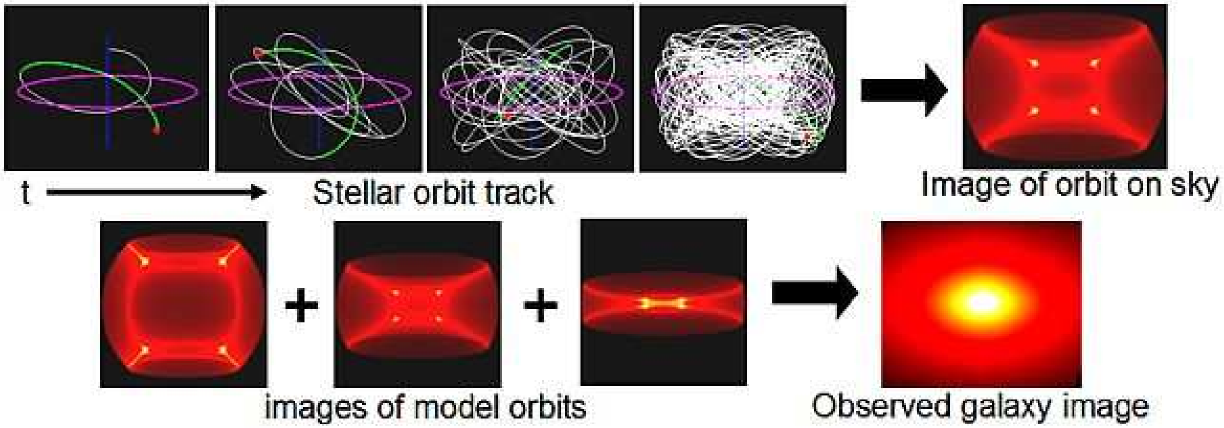

Figure 4.2: A schematic representation for the orbit-based superposition method applied to model an elliptical galaxy (from Cappellari et al., 2004). The main recipe is to derive the time-averaged density distributions of several thousand orbits with different energies and angular momenta. Iteratively repeating this procedure for a range of M/L ratios and central black hole masses will determine the final M/L ratio and black hole mass such that the obtained model light and kinematic profiles match as good as possible with the observed ones.

To calculate uncertainties for each LOSVD we perform Monte Carlo realisations of the cluster spectra. These spectra are obtained by convolving the measured LOSVD with the stellar templates. Each spectrum differs from the others in the amount specified by a Gaussian noise added to the spectrum at each wavelength position. An LOSVD is extracted from every spectrum, and used to estimate the errors.

The resulting LOSVDs can be biased by several systematic effects, including the choice of stellar template, continuum shape, spectral range used in the fit, and amount of smoothing. These are discussed by Pinkney et al. (2003). In general, the most significant bias is probably template mismatch. However, we observed the spectra in the Ca II near-triplet region (8500 $\AA$), and in this region the LOSVD is not very sensitive to template variations.

For the next step, assuming a stellar M/L ratio and a central black hole of mass M_{BH} we construct the mass density from the obtained three-dimensional light distribution. This approach generally allows us to also include dark matter into the models, but we have not done it for the scope of this thesis. The gravitational potential can then be derived by integrating Poisson's equation of the following mass density

$$\rho(r,\theta) = M_{BH}\delta(r) + \gamma\nu(r,\theta) + \rho_{\mathrm{DM}}(r) \tag{4.3}$$

where ν is the stellar luminosity distribution, γ is the mass-to-light ratio (M/L), and ρ_{DM} is the dark matter density profile. We assume a constant stellar M/L throughout the cluster as a good estimate considering our N-body simulations result in the previous chapter.

Thus, varying M_{BH} and M/L values construct a grid of dynamical models. Each model with a given potential of such a grid consists of a superposition of representative orbits

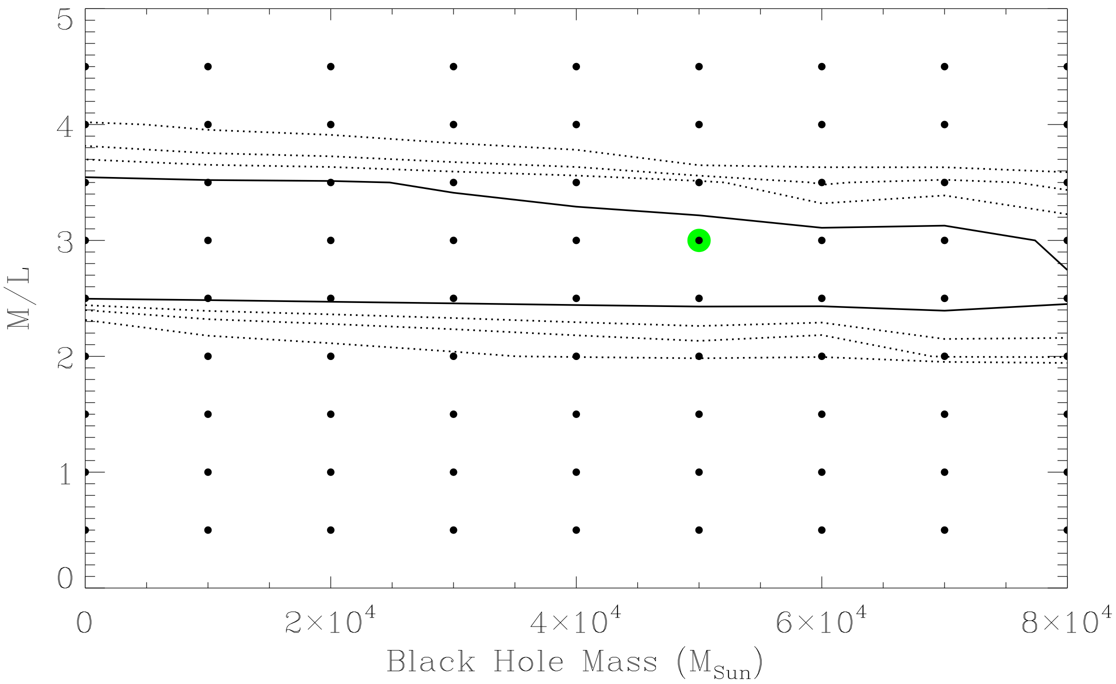

Figure 4.3: χ^2 contour map in terms of black hole mass and stellar M/L for our dynamical models. Each dot represents a model. The green symbol corresponds to the "best" model with minimum $\chi^2 = 21.464$. The contour levels are drawn for $\Delta\chi^2 = \chi^2 - \chi^2_{min}$ equal to 1.0 (dashed), 2.71, 4.0, and 6.63, corresponding to confidence levels of 68%, 90%, 95%, and 99%, respectively for one degree of freedom (marginalized over M/L).

that is appropriately weighted to match the observed data. We use $N \sim 7000$ orbits in each model. We use a maximum-entropy technique as described in Gebhardt et al. (2003) to minimize χ^2 using non-negative orbit weights. For each model, we determine $\chi^2_{(M_{BH},M/L)}$ to choose the best-fit model which match both photometry and kinematic of ω Centauri. The minimum of χ^2 determines the best combination of M_{BH} and M/L for the cluster. A schematic view of the above steps is shown in Figure 4.2.

The $\Delta\chi^2 = 1$ contour on the $\chi^2_{(M_{BH},M/L)}$ map determines the "1σ" confidence of black hole mass parameter. The total number of parameters is 234 that is the result of multiplying of 18 for LOSVDs times 13 for the number of velocity bins.

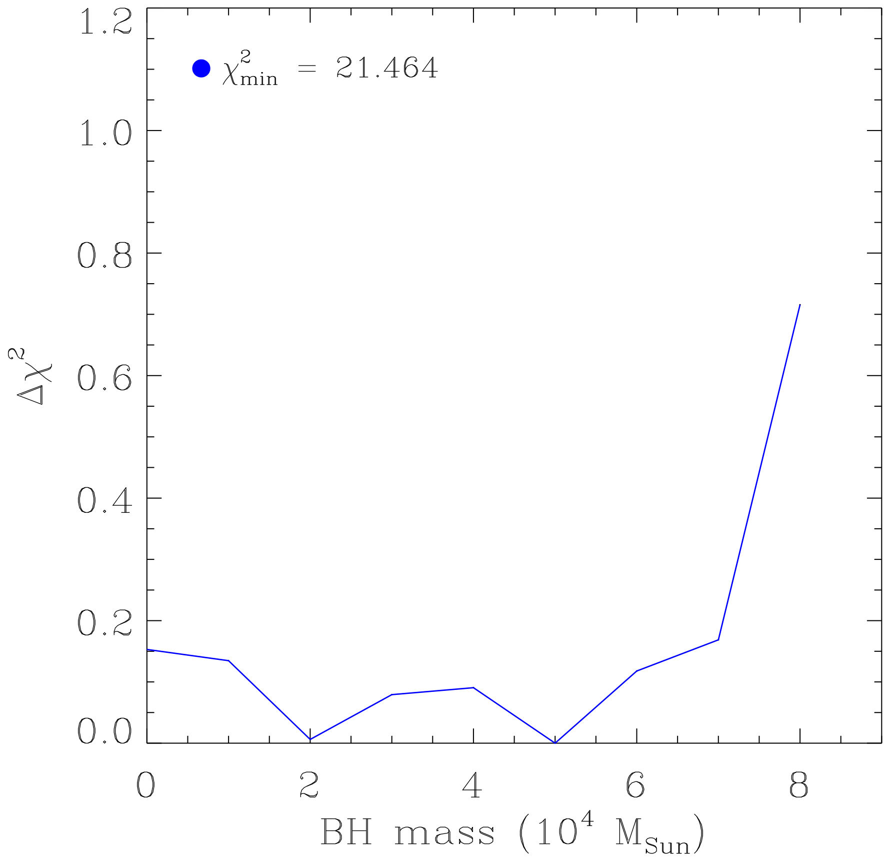

Figure 4.4: χ^2 values vs. different black hole masses obtained by marginalizing χ^2 space over the M/L. The small variations in χ^2 values is also expected by the huge range of black hole masses within the 1σ contour in the previous figure. Hence, obtaining the uncertainty of black hole mass is currently not possible and calls for including the proper motions to tighter constrain the black hole mass (see Section 5).

4.4 Results for ω Centauri from line-of-sight velocities

4.4.1 IMBH mass

As described above, we construct a grid of models by varying M_{BH} and M/L. Such a grid is shown in Figure 4.3 where black hole masses are in the range of 0 to $8 \times 10^4 M_\odot$ and the M/L covers values reasonable for Galactic star clusters. The upper mass limit of our black holes is consistent with extrapolating the black hole mass versus velocity dispersion relation (Gültekin et al., 2009) for galaxies to smaller systems such as dwarf galaxies and globular clusters. The existence of an IMBH more massive than a few $10^4 M_\odot$ is not expected.

Our covered M/L range ensures that we are investigating around reasonable values. Our values for M/L are within the range of most stellar population models such as Maraston (1998) and is also consistent with the dynamical value derived for ω Centauri in van de Ven et al. (2006). Furthermore, our results from the N-body simulations (Chapter 3) showed a rather constant M/L over entire cluster radii, justifying our constant M/L assumption in our orbit-based models.

Figure 4.3 presents the two-dimensional distribution in χ^2 space as a function of black hole mass and M/L. The contours are based on the χ^2 values of the underlying grid points. The marginalized χ^2 distribution as a function of M_{BH} is shown as the blue line in Figure 4.4. The best-fit value for M_{BH} and its uncertainty can be determined from the marginalized distribution over M/L. However, as can be seen in both Figs. 4.3 and 4.4 there is a huge range of possible black hole masses with similar small χ^2 values. Hence, we intend to include proper motions to possibly tighten constraints on the black hole mass (see Section 5).

4.4.2 Anisotropy

One of the important applications of orbit-based modelling is to inspect the internal orbital structure of stellar systems under general axisymmetry assumptions of the distribution function. We examine the ratio of radial over tangential dispersion, σ_r/σ_t for ω Centauri which, represents the shape of the velocity dispersion tensor. In Figure 4.5, we compare the internal dispersion ratio σ_r/σ_t for the best-fit models with and without an intermediate-mass black hole. Random and ordered motion contribute in the tangential dispersion. Thus it is given by

$$\sigma_t = \sqrt{\frac{V_\theta^2 + (V_\phi^2 + v_\phi^2)}{2}}. \tag{4.4}$$

This figure is plotted by averaging σ_r/σ_t over five angular bins. As an example, the details for our five angular bins and their correspondent velocities for the best-fit black hole mass, i.e. $5 \times 10^4 M_\odot$, are listed in Table 4.1.

As can be seen in Figure 4.5, the red curve is the σ_r/σ_t ratio without an IMBH as a function of distance from the cluster center. In the absence of a central black hole, the pronounced feature is the strong radial anisotropy in the central regions to reproduce the

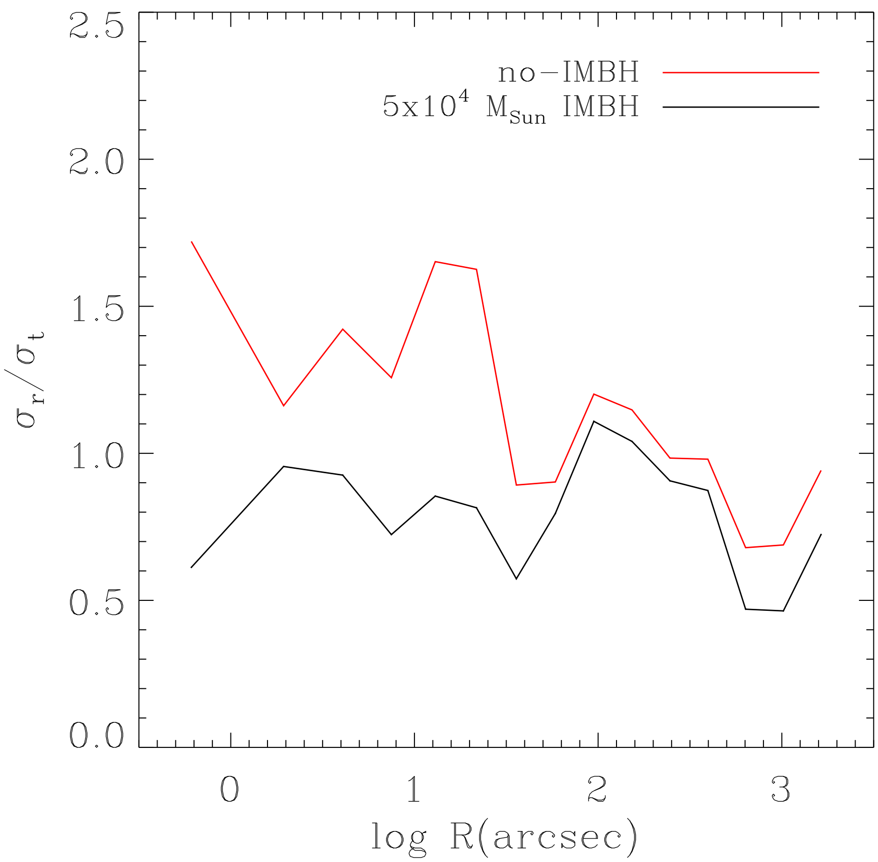

Figure 4.5: The ratio of radial over tangential internal moments as a function of distance to the cluster center. The black line is our best-fit model including a black hole of $5 \times 10^4 M_\odot$ mass with stellar V-band $M/L = 3$. The red line indicates a no-IMBH model with the same $M/L = 3$ as black curve. Note the strong radial anisotropy in the central region in the absence of an IMBH which, is expected to not be a stable configuration over the life time of the cluster.

observed rise in the radial velocity dispersions profile (Chapter 2). The central σ_r/σ_t ratio is closer to being isotropic in the case of a $5 \times 10^4 M_\odot$ IMBH. The strong radial anisotropy as the main alternative to the existence of the black hole is highly unstable for a star cluster such as ω Centauri with relaxation time of about a few Gyr. In the other words, this radial anisotropy is expected to be erased by two-body relaxation process over one or two Gyr (Baumgardt; private communications). In fact, the presence of an IMBH might cause a slight tangential orbital configuration in the central $10''$ as is the case here (black line in Figure 4.5).

As we describe in Section 3 reproducing the observed light and kinematic of our cluster is the essential goal of our modelling with a certain potential (with or without a central IMBH). We depict such a data-model LOSVD fit for our best-fit model containing a $5 \times 10^4 M_\odot$ IMBH in Figure 4.6.

4.5 Summary and Future work

As we show in Figure 4.3 while we could constrain the stellar M/L very well, there is a wide range of black hole masses which apparently can fit the data almost equally well (Figure 4.4). There are a few future steps which can possibly help to improve this situation.

The most important one is to include proper motions data to the models, which as described in Chapter 2 and 3 they are available at almost all radii. We intend to use proper motions on minor and major axis separately such as the method we presented here for the line-of-sight velocities. Comparing the results of these intermediate steps can help us to better understand the role of anisotropy and constrain its contribution versus black hole mass. The next step could of course be to consider all three components of velocities at the same time which provide complete three-dimensional information on the kinematics. Therefore, basically including proper motions might remarkably help us to limit the range of allowed black hole masses by providing additional information.

Investigating the rotation in more detail is the second step which provide extra information on the velocity components particularly on proper motions in the central region of ω Centauri. Currently the total 1D proper motion results in Anderson & van der Marel (2010) could possibly underestimate the rotation because of the small spatial window they used for measuring the proper motions. This could also explain their smaller velocity dispersions comparing to our radial ones. In our analysis of the recent radial velocities taken by VLT-FLAMES we see a rotation by an amplitude of about 5 km/s. This, however, needs further careful analysis. In addition, considering different components of proper motions (major and minor), we see that their peak in velocity dispersions do not lie on top of each other, which together with the small spatial window of proper motion measurements in Anderson & van der Marel (2010), could be another hint for their underestimating the contribution of rotation.

Hence, including properly the proper motions and also carefully investigate the effects of rotation, we hope to make a firmer step on constraining the possible black hole mass in ω Centauri using orbit-based modelling.

Table 4.1: Different components of internal velocities over 5 angular bins for our best-fit model including a $5 \times 10^4 M_\odot$ IMBH.

R	Θ	V_r	V_θ	$V_r V_t$	V_ϕ	v_ϕ	β
0.61	5.77	90.2761	53.3242	0.0000	115.2791	0.0000	0.0102
1.94	5.77	58.9579	55.0421	0.0000	48.8753	0.0000	0.2206
4.07	5.77	32.1012	30.6502	0.0000	32.5514	0.0000	0.0301
7.49	5.77	22.1961	28.3132	0.0000	28.0217	0.0000	-0.6105
12.98	5.77	19.0604	19.9074	0.0000	23.4391	0.0000	-0.3015
21.77	5.77	14.0082	15.5241	0.0000	14.7774	0.0000	-0.1705
35.87	5.77	13.1377	21.0947	0.0000	23.7806	0.0000	-1.9273
58.48	5.77	19.4739	22.6509	0.0000	25.9290	0.0000	-0.5629
94.74	5.77	20.6964	16.6123	0.0000	20.1167	0.0000	0.2055
152.88	5.77	18.4815	15.8667	0.0000	16.8117	0.0000	0.2177
246.10	5.77	16.4393	17.1743	0.0000	13.9465	0.0000	0.0944
395.58	5.77	13.3132	14.5276	0.0000	11.5194	0.0000	0.0303
635.27	5.77	8.7827	16.7028	0.0000	13.4775	0.0000	-1.9858
1019.62	5.77	6.7999	15.0988	0.0000	14.2700	0.0000	-3.6672
1635.91	5.77	5.8548	8.3951	0.0000	9.4137	0.0000	-1.3206
0.61	17.56	86.1150	57.6372	0.0000	113.5300	0.0000	-0.0930
1.94	17.56	56.8250	55.0031	0.0000	46.9172	0.0000	0.1907
4.07	17.56	29.2119	30.2942	0.0000	33.9119	0.0000	-0.2116
7.49	17.56	21.0599	28.3433	0.0000	28.2023	0.0000	-0.8023
12.98	17.56	17.7170	19.9735	0.0000	20.2795	0.0000	-0.2906
21.77	17.56	12.2489	15.5839	0.0000	13.8342	0.0000	-0.4471
35.87	17.56	12.2171	21.0110	0.0000	23.6899	0.0000	-2.3589
58.48	17.56	19.6769	22.4802	0.0000	26.7755	0.0000	-0.5784
94.74	17.56	20.9227	16.4401	0.0000	19.8921	0.0000	0.2393
152.88	17.56	18.2946	15.8574	0.0000	16.0838	0.0000	0.2379
246.10	17.56	16.1774	17.3032	0.0000	14.3641	0.0000	0.0338
395.58	17.56	13.2393	14.6413	0.0000	11.7565	0.0000	-0.0058
635.27	17.56	8.8522	16.8293	0.0000	13.9439	0.0000	-2.0478
1019.62	17.56	7.3082	15.1159	0.0000	13.1503	0.0000	-2.7580
1635.91	17.56	6.1418	8.3753	0.0000	8.0096	0.0000	-0.7801
0.61	30.22	79.4429	66.0682	0.0000	139.9402	0.0000	-0.8973
1.94	30.22	53.8616	55.9051	0.0000	39.8513	0.0000	0.1876
4.07	30.22	31.5720	30.9814	0.0000	25.7040	0.0000	0.1871
7.49	30.22	20.2161	28.2636	0.0000	26.2839	0.0000	-0.8225
12.98	30.22	15.9033	19.9494	0.0000	18.5972	0.0000	-0.4705
21.77	30.22	11.3253	15.6959	0.0000	15.0959	0.0000	-0.8487
35.87	30.22	12.1154	20.3525	0.0000	26.2112	0.0000	-2.7513

Table 4.1: continued.

R	Θ	V_r	V_θ	V_rV_t	V_ϕ	v_ϕ	β
58.48	30.22	19.6535	21.8647	0.0000	26.0878	0.0000	-0.4998
94.74	30.22	20.1545	16.1606	0.0000	18.3869	0.0000	0.2624
152.88	30.22	17.2162	15.8472	0.0000	15.4860	0.0000	0.1718
246.10	30.22	15.3299	17.4904	0.0000	15.3477	0.0000	-0.1520
395.58	30.22	12.4427	14.8757	0.0000	12.5415	0.0000	-0.2226
635.27	30.22	7.8300	17.0121	0.0000	15.2060	0.0000	-3.2460
1019.62	30.22	7.0561	15.2543	0.0000	14.4183	0.0000	-3.4246
1635.91	30.22	6.3873	8.4951	0.0000	7.1114	0.0000	-0.5042
0.61	45.00	27.8204	71.5407	0.0000	118.4561	0.0000	-11.3711
1.94	45.00	38.7407	57.1357	0.0000	49.3097	0.0000	-0.8976
4.07	45.00	23.8687	31.3694	0.0000	32.1668	0.0000	-0.7717
7.49	45.00	18.4352	29.0510	0.0000	29.3158	0.0000	-1.5060
12.98	45.00	17.2233	20.3284	0.0000	21.8604	0.0000	-0.5020
21.77	45.00	13.0293	15.8485	0.0000	15.8690	0.0000	-0.4815
35.87	45.00	12.1799	20.3849	0.0000	18.7885	0.0000	-1.5903
58.48	45.00	17.0091	21.7520	0.0000	23.1416	0.0000	-0.7433
94.74	45.00	17.5027	15.9975	0.0000	16.5372	0.0000	0.1359
152.88	45.00	15.1907	16.0932	0.0000	15.9917	0.0000	-0.1153
246.10	45.00	13.9419	17.9477	0.0000	16.3232	0.0000	-0.5140
395.58	45.00	10.8397	15.2876	0.0000	13.7704	0.0000	-0.8015
635.27	45.00	6.0603	17.0824	0.0000	17.3005	0.0000	-7.0473
1019.62	45.00	6.4542	15.3524	0.0000	15.4636	0.0000	-4.6993
1635.91	45.00	5.9378	8.5463	0.0000	9.2257	0.0000	-1.2428
0.61	71.57	8.4159	26.7313	0.0000	131.3987	0.0000	-125.9282
1.94	71.57	40.1192	38.8553	0.0000	71.5028	0.0000	-1.0572
4.07	71.57	27.2411	22.7275	0.0000	39.4718	0.0000	-0.3978
7.49	71.57	20.3841	21.7702	0.0000	34.0540	0.0000	-0.9658
12.98	71.57	16.8653	15.1714	0.0000	22.6226	0.0000	-0.3042
21.77	71.57	11.8630	12.9806	0.0000	17.7791	0.0000	-0.7217
35.87	71.57	12.1584	20.6654	0.0000	19.9247	0.0000	-1.7872
58.48	71.57	16.9078	21.8678	0.0000	20.0166	0.0000	-0.5372
94.74	71.57	16.3669	16.1829	0.0000	15.4015	0.0000	0.0684
152.88	71.57	13.7963	17.1619	0.0000	14.0010	0.0000	-0.2887
246.10	71.57	12.8788	20.4877	0.0000	14.8798	0.0000	-0.9328
395.58	71.57	10.7891	18.0813	0.0000	11.8283	0.0000	-1.0053
635.27	71.57	6.1538	17.5558	0.0000	16.6018	0.0000	-6.7085
1019.62	71.57	6.8336	15.4707	0.0000	15.0620	0.0000	-3.9918
1635.91	71.57	6.0836	8.5455	0.0000	8.0913	0.0000	-0.8710

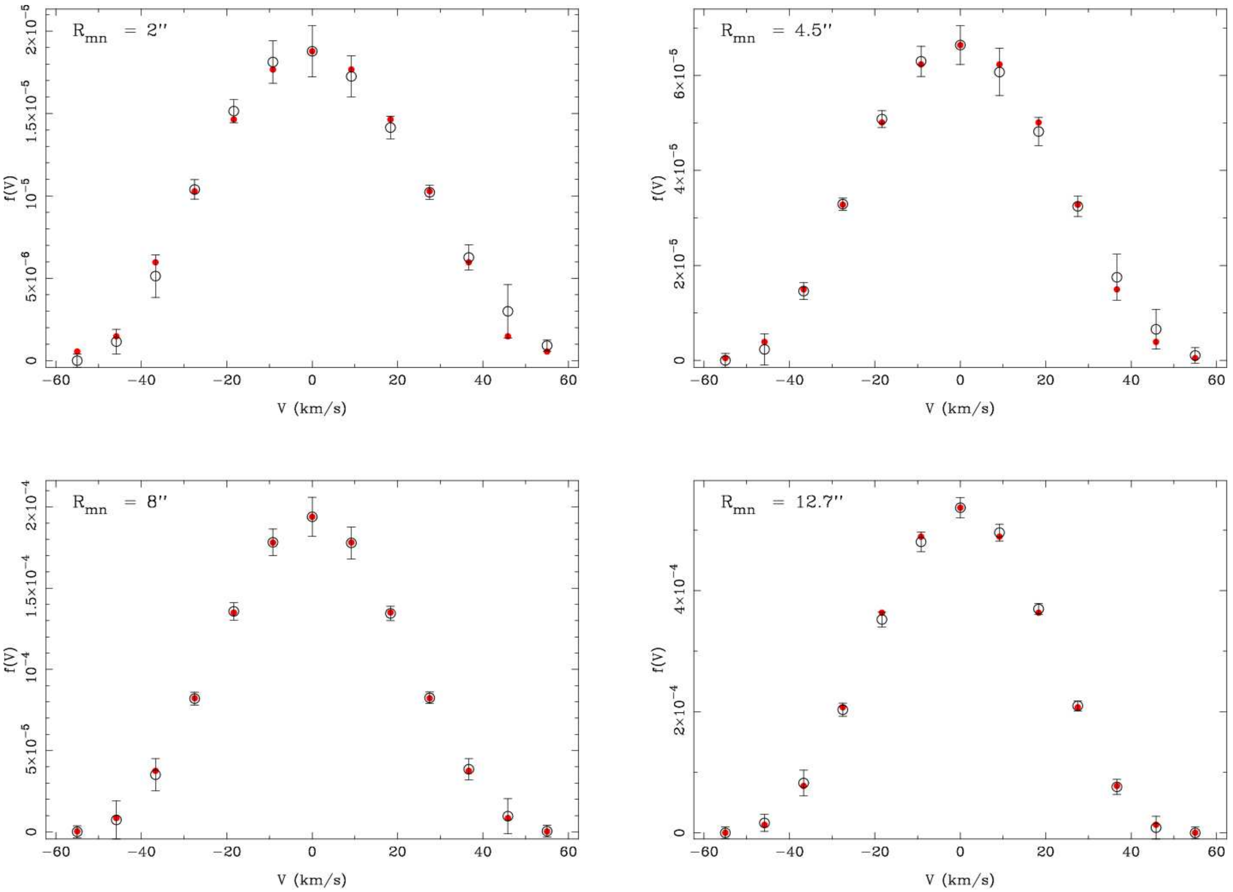
R_{mn} = 2″
f(V)
0
5×10^{-6}
10^{-5}
1.5×10^{-5}
2×10^{-5}
V (km/s)
−60
−40
−20
0
20
40
60
R_{mn} = 4.5″
f(V)
0
2×10^{-5}
4×10^{-5}
6×10^{-5}
V (km/s)
R_{mn} = 8″
f(V)
0
5×10^{-5}
10^{-4}
1.5×10^{-4}
2×10^{-4}
V (km/s)
R_{mn} = 12.7″
f(V)
0
2×10^{-4}
4×10^{-4}
V (km/s)

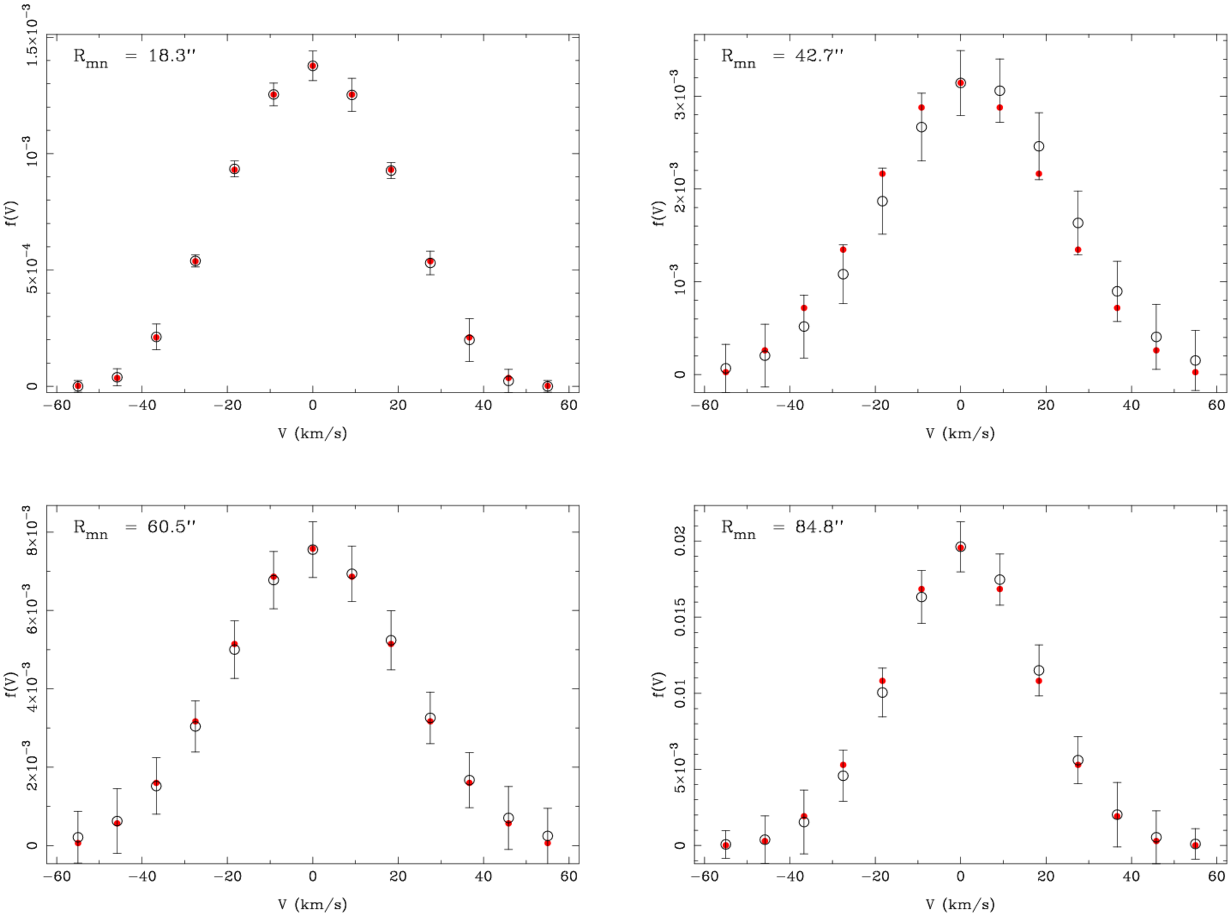
R_mn = 18.3″
R_mn = 42.7″
R_mn = 60.5″
R_mn = 84.8″
f(V)
V (km/s)
−60
−40
−20
0
20
40
60
0
5×10⁻⁴
10⁻³
1.5×10⁻³
10⁻³
2×10⁻³
3×10⁻³
2×10⁻³
4×10⁻³
6×10⁻³
8×10⁻³
5×10⁻³
0.01
0.015
0.02

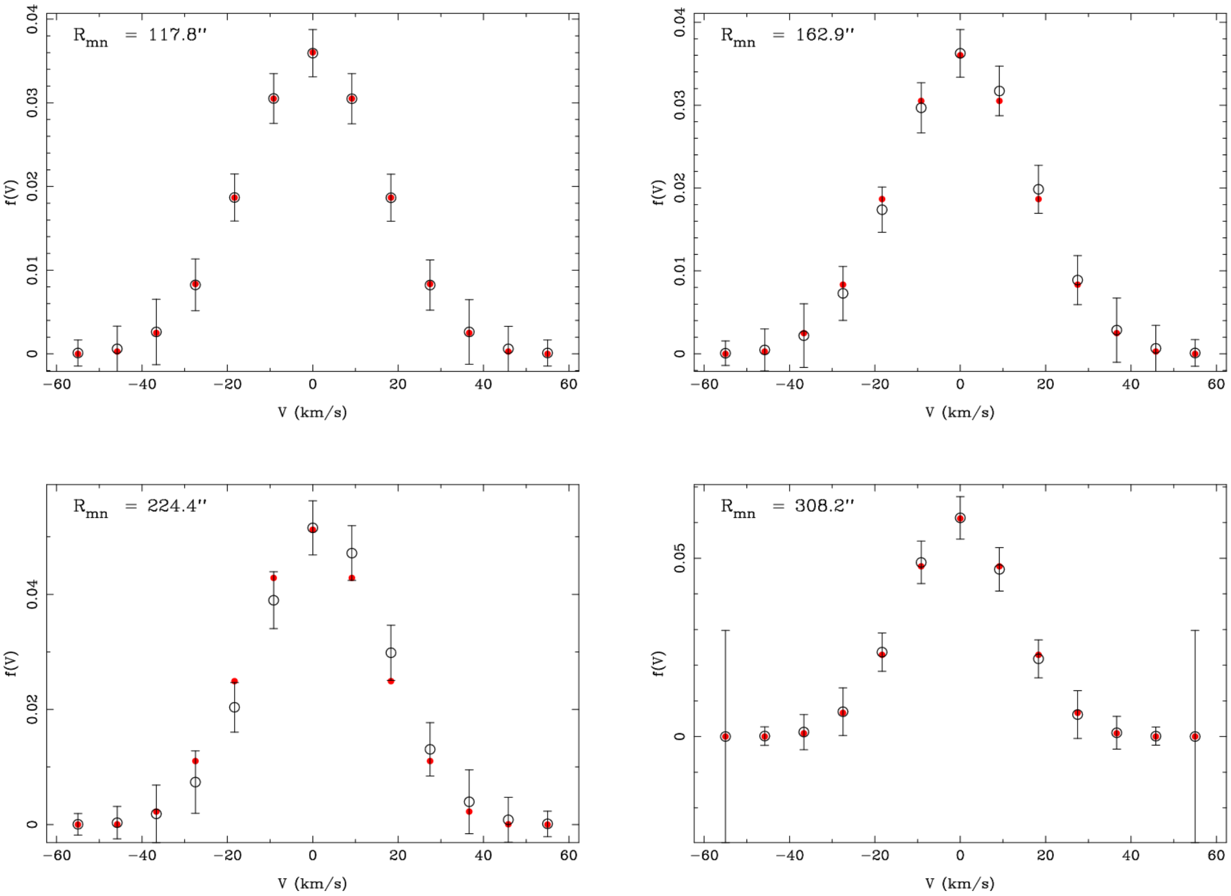

Figure 4.6: Projected LOSVDs at several radii. The radii are given at the upper left part of each sub-panel. Open circles are the data extracted as described in Section 3. The model values are shown in filled red points. The area is normalized to total light in the given bin.

Chapter 5

Conclusions and Outlook

IMBHs could be the missing links between stellar mass BHs and SMBHs. Thus, strong observational signatures of the existence of IMBHs could have important consequences both on the dynamical evolution of the host systems and also on the formation and growth of SMBHs. In this context, massive star clusters such as globular clusters and nuclear star clusters are among the best targets to look for an IMBH. ω Centauri as the most massive Galactic star cluster, and at the close distance of only 5 kpc, is one of the most interesting objects for such studies.

5.1 Evidence for a central IMBH in ω Centauri

We measure the central kinematics for ω Centauri using the Ca-triplet lines around ~ 850 nm with the VLT-FLAMES integral field spectrograph. We resolve the influence radius of a $5 \times 10^4 M_\odot$ black hole at the distance of our cluster. The measured line-of-sight velocity dispersion shows a continuous rise towards the center of this cluster. This rise is also seen in the measured velocity dispersion from integral field spectroscopic data taken by Gemini-GMOS as an independent data-set (Noyola et al. 2008). This gradual rise starting from ~ 17 km/s at the core radius ($\sim 100''$) inwards to 22.8 km/s at the inner most region ($2''$) provides significant evidence for a central massive black hole.

This thesis present three stellar dynamical methods to model the observations, and to study the signatures of an IMBH:
We construct spherical isotropic Jeans models assuming different IMBH masses, and compare the model velocity dispersion profiles with the observed one. We could well reproduce the observed velocity dispersion profile with a model containing a $5 \times 10^4 M_\odot$ IMBH.

To further investigate a consistency of the existence of an IMBH in this cluster with the observations, we create a large set of evolutionary N-body models. In these simulations we follow the dynamical evolution of stars (including stellar evolution) directly in a star-by-star way over 12 Gyr. We study in detail the effects of an IMBH on the dynamical evolution of model clusters, on both the light profile as well as velocity dispersion profile of such model clusters. The model clusters are then compared to our newly acquired

VLT-FLAMES data, as well as to the rich data from the literature.

Starting with spherical isotropic King conditions (King 1966) with different initial parameters, with and without an IMBH, we measure physical quantities from our models such as velocity dispersion and surface brightness following the methods in observational studies, meaning with the same magnitude cut-offs and luminosity weights. Using such careful analysis of our models make the data-model comparisons and consequently the drawn conclusions more reliable.

We show that the best-fit IMBH model, containing a $5 \times 10^4 M_\odot$ black hole, matches the kinematic data presented in Noyola et al. (2010) very well. In particular, we reproduce the observed rise in the central velocity dispersion as an indicator for the presence of an IMBH. We stress that relying on the profiles relative to the kinematic center in Noyola et al. (2010) makes it impossible to consistently fit the line-of-sight velocity dispersion over all radii without a central IMBH. Furthermore, as a result of our N-body simulations, we show that M/L is constant at large radii for all models independent of the presence of a central black hole. We predict a slight rise in M/L towards the center for all models due to mass segregation of heavy-mass compact remnants.

In addition, studying the temporal stability conditions of alternative configurations such as the concentration of smaller dark objects (white dwarfs and neutron stars) against the presence of a massive black hole is only possible by performing N-body simulations. We intend to investigate such models in the near future. In order to further constrain the initial parameters for ω Centauri, we will probe different stellar initial mass functions in the models.

ω Centauri is slightly flattened, i.e. not completely spherical. Thus, a certain amount of anisotropy could in principle also reproduce the observed kinematics. Therefore, as another modelling method, we apply axisymmetric orbit-based models which allow us a general freedom in the anisotropy values as a function of radius of the cluster. We construct trial potentials with a grid of black hole masses versus stellar mass-to-light ratios. The preliminary result of the models reproduce the obtained line-of-sight velocity dispersion profile as well as the HST surface brightness profile with a $5 \times 10^4 M_\odot$ IMBH, again consistent with the above independent approaches. We intend to include the obtained proper motion dispersions as an extra observational information to set tighter constraints on the IMBH mass, and therefore, improve the robustness of the IMBH detection.

5.2 The VLT-FLAMES kinematic survey of Galactic globular clusters

The goal of our team is to identify the best candidate globular clusters for hosting IMBHs and to systematically investigate their central kinematics in order to detect or set tight upper mass limits on their central black holes. We therefore intend to considerably enlarge the sample of IMBH demography on the lower mass end of the $M_{BH} - \sigma$ relation using both observational and model approaches (Figure 5.1).

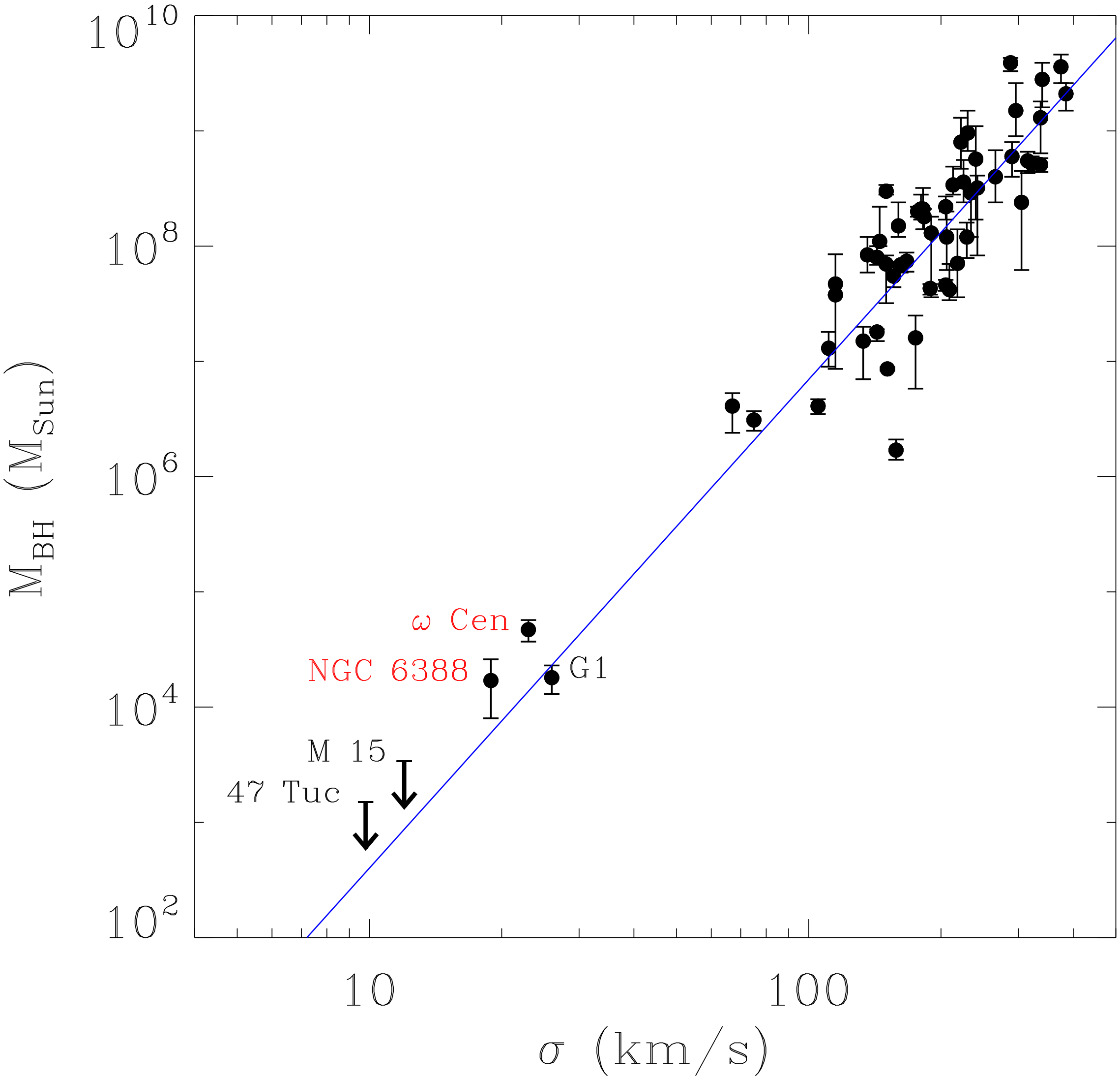

Figure 5.1: Sample of dynamically detected black hole masses versus the central velocity dispersion of the host systems for galaxies and star clusters. The data for galaxies, and the fit (blue line) are taken from Gültekin et al. (2009) and reference therein. The parameters of M15, 47 Tuc and G1 are from van den Bosch et al. (2006); McLaughlin et al. (2006); Gebhardt et al. (2005), respectively. The black hole mass and velocity dispersion for ω Centauri are taken from this thesis. The values of NGC 6388 are from Lützgendorf et al. (2011) as part of our survey.

Table 5.1: Some of the main characteristics of our sample. The central slope of the surface brightness profile ρ_0 is taken from Noyola & Gebhardt (2006). The heliocentric distance, velocity dispersion σ, and total cluster mass M are from Pryor & Meylan (1993).

ID	distance (kpc)	slope of ρ_0 profile	σ_0 (km/s)	$\log(M)$ ($M_\odot$)
NGC 5139	4.9	-0.08 ± 0.03	23.0	6.6
NGC 6388	11.0	-0.13 ± 0.07	15.0	6.2
NGC 6266	5.5	0.03 ± 0.05	14.3	5.8
NGC 2808	9.2	-0.06 ± 0.07	13.4	6.2
NGC 5286	9.3	-0.28 ± 0.11	8.0	5.5
NGC 1851	12.2	-0.38 ± 0.11	10.4	6.0
NGC 6093	8.4	-0.16 ± 0.07	12.5	6.0

I review briefly some theoretical points based on which we selected the clusters for which we collected kinematical data for a few Galactic star clusters:
Baumgardt et al. (2005) and Noyola & Baumgardt (submitted) have analyzed detailed N-body simulations of star clusters with and without central black holes. Their models predict that the presence of an IMBH induces a shallow cusp in the density profile. Hence, clusters showing shallow cusps are among the best candidates for harboring an IMBH. Furthermore, Miocchi (2007) investigated the effect of an IMBH on horizontal branch morphologies. A central black hole that strips some stars of their outer envelope during close passages, could be one avenue for producing an extended horizontal branch (EHB). Finally, preliminary results of Noyola et al. (to be submitted) by Gemini-GNIRS integral field data for M54 (a cluster which also presents a shallow cusp and an EHB) shows an important central rotation signature. Current best model fits predict a black hole of $10^4 M_\odot$ for this object, which is confirmed by Ibata et al. (2009) using velocity dispersions from VLT-FLAMES. It is quite important to find out if central rotation is a common signature to clusters that are candidates to host IMBHs as this could give important clues to the formation channels of both the host and the IMBHs.

Hence, we are looking for globular clusters that 1) show shallow cusps in their surface brightness profile, 2) have anomalies in their stellar populations such as EHB, and 3) are candidates for central rotation. Table 5.1 lists our sample of globular clusters which we think are good candidates to harbor an IMBH.

Figure 5.2 shows as an example the surface brightness profiles of NGC 1851 and NGC 2808 that show shallow cusps in their HST data (Noyola & Gebhardt 2006). Both of the above clusters show anomalies in their stellar populations. NGC 1851 shows a double sub-giant branch (Milone et al., 2008), while NGC 2808 shows a triple main sequence (Piotto et al., 2007). Moreover, these two clusters show anomalies in their horizontal branches.

In addition, most of these clusters lie relatively close to us, within ~ 10 kpc, that allows us to spatially resolve and investigate their radius of influence of a possible IMBH.

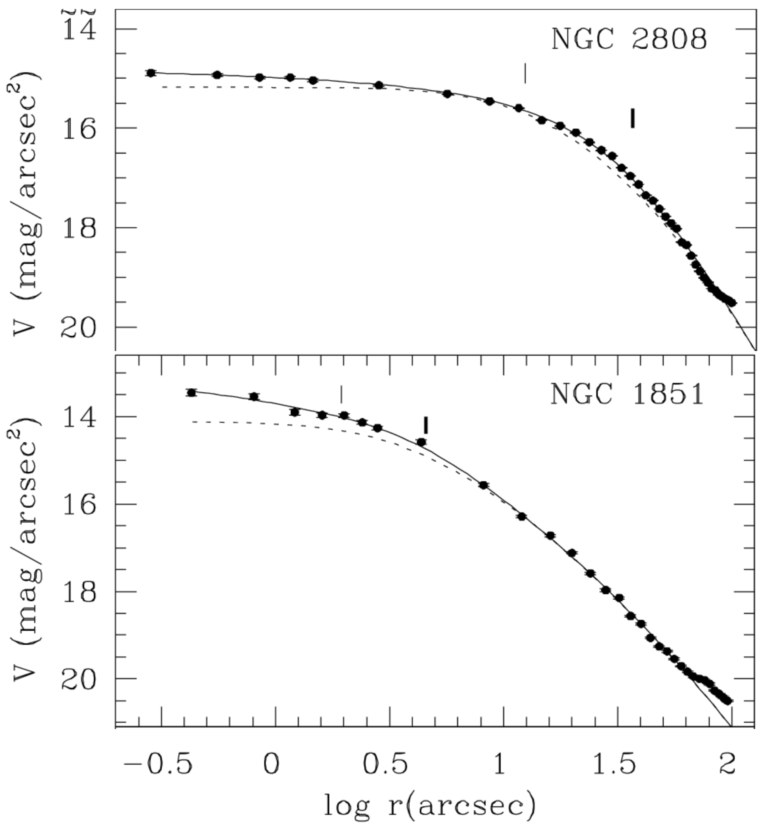

Figure 5.2: Surface brightness profiles of two globular clusters in our sample taken from Noyola & Gebhardt (2006). The photometric measurements on the HST images are marked by circles, and a fit to the photometric points is shown as solid line. The core radius where the central flux falls to half of its value is marked by a thin vertical bar. The break radius where the second derivative of the profile with respect to the radius reaches a minimum is marked by a thick vertical bar. The deviation (shallow cusp) from a flat classical King profile in the central region (dotted line) is part of our selection criterion.

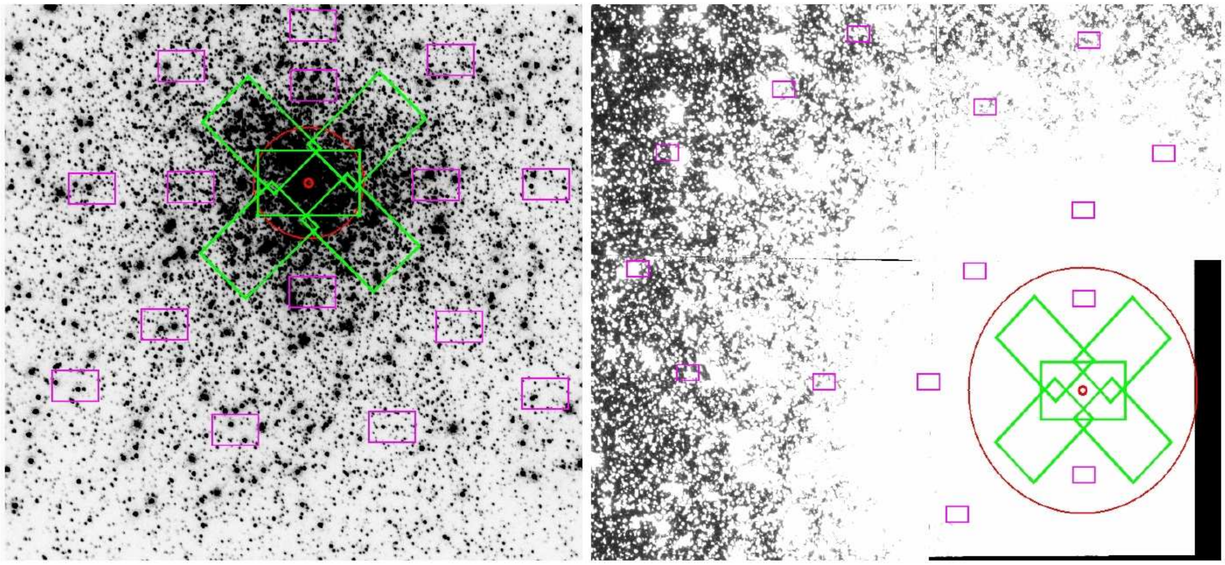

NGC 1851 ***NGC 2808***

Figure 5.3: The observing strategy for our two observed targets: NGC 1851 and NGC 2808. The centre and the core radius are marked in red, the proposed ARGUS pointings in green, and the proposed IFU pointings in pink.

Considering their high velocity dispersions, extrapolation of the $M_{BH} - \sigma$ relation predicts black hole masses of several $10^3 M_\odot$ for most of these objects and this in turn is equivalent to a radius of influence of about $2'' - 3''$ at their respective distances.

Therefore, FLAMES-ARGUS at the VLT provides both sufficient spectral and spatial resolution and also the necessary field of view to study the central dynamics of our samples. Moreover, the used Ca-triplet lines around $\sim$ 850 nm have excellent strong features for kinematic measurements as it is depicted in Figure 2.8 in Chapter 2. They are sharp absorption lines with little sky contamination. The two pointing maps of our proposed FLAMES-ARGUS for the above two clusters are presented in Figure 5.3.

Characterizing the low-mass end of the $M_{BH} - \sigma$ relation might also indicate the link between IMBHs and galaxy formation and evolution. Further, such ideas will contribute to our understanding of the formation of nuclear clusters, their ability to host IMBHs and the role of IMBHs as seeds for the formation of SMBHs that are intimately linked to the formation and evolution of galaxies. In this context, we have compiled the most promising sample of Galactic star clusters. We aim to make conclusive constraints on the dynamics of central regions, and on possible IMBHs of this sample using different dynamical methods that are constructed and presented in this thesis for ω Centauri.

Bibliography

Aarseth, S. J. 1999, PASP, 111, 1333

Aarseth, S. J. 2003, Gravitational N-Body Simulations, ed. Aarseth, S. J.

Abramowski, A., Acero, F., Aharonian, F., et al. 2011, ApJ, 735, 12

Anderson, J. 2002, in Astronomical Society of the Pacific Conference Series, Vol. 265, Omega Centauri, A Unique Window into Astrophysics, ed. F. van Leeuwen, J. D. Hughes, & G. Piotto, 87

Anderson, J. & van der Marel, R. P. 2010, ApJ, 710, 1032

Barnes, J. E. & Hernquist, L. 1992, ARA&A, 30, 705

Barth, A., Ho, L., & Sargent, W. 2004, in Astronomical Society of the Pacific Conference Series, Vol. 311, AGN Physics with the Sloan Digital Sky Survey, ed. G. T. Richards & P. B. Hall, 91

Baumgardt, H., Hut, P., Makino, J., McMillan, S., & Portegies Zwart, S. 2003a, ApJ, 582, L21

Baumgardt, H., Makino, J., & Ebisuzaki, T. 2004a, ApJ, 613, 1133

Baumgardt, H., Makino, J., & Ebisuzaki, T. 2004b, ApJ, 613, 1143

Baumgardt, H., Makino, J., & Hut, P. 2005, ApJ, 620, 238

Baumgardt, H., Makino, J., Hut, P., McMillan, S., & Portegies Zwart, S. 2003b, ApJ, 589, L25

Baumgardt, H. & Mieske, S. 2008, MNRAS, 391, 942

Baumgardt, H., Portegies Zwart, S. F., McMillan, S. L. W., Makino, J., & Ebisuzaki, T. 2004c, in Astronomical Society of the Pacific Conference Series, Vol. 322, The Formation and Evolution of Massive Young Star Clusters, ed. H. J. G. L. M. Lamers, L. J. Smith, & A. Nota, 459

Bedin, L. R., Piotto, G., Anderson, J., et al. 2004, ApJ, 605, L125

Beers, T. C., Flynn, K., & Gebhardt, K. 1990, AJ, 100, 32

Bekki, K. & Norris, J. E. 2006, ApJ, 637, L109

Bender, R., Burstein, D., & Faber, S. M. 1992, ApJ, 399, 462

Binney, J. & Tremaine, S. 2008, Galactic Dynamics: Second Edition, ed. Binney, J. & Tremaine, S. (Princeton University Press)

Bombaci, I. 1996, A&A, 305, 871

Brown, G. E. & Bethe, H. A. 1994, ApJ, 423, 659

Cappellari, M., van den Bosch, R. C. E., Verolme, E. K., et al. 2004, Coevolution of Black Holes and Galaxies

Carney, B. W., Aguilar, L. A., Latham, D. W., & Laird, J. B. 2005, AJ, 129, 1886

Carr, B. J. & Lidsey, J. E. 1993, Phys. Rev. D, 48, 543

Casertano, S. & Hut, P. 1985, ApJ, 298, 80

Charles, P. 2001, in Black Holes in Binaries and Galactic Nuclei, ed. L. Kaper, E. P. J. van den Heuvel, & P. A. Woudt, 27

Colbert, E. J. M. & Ptak, A. F. 2002, ApJS, 143, 25

Da Costa, G. S. 1979, AJ, 84, 505

D'Antona, F., D'Ercole, A., Marino, A. F., et al. 2011, ApJ, 736, 5

Dinescu, D. I., Girard, T. M., & van Altena, W. F. 1999, AJ, 117, 1792

Dinescu, D. I., Majewski, S. R., Girard, T. M., & Cudworth, K. M. 2001, AJ, 122, 1916

Ebisuzaki, T., Makino, J., Tsuru, T. G., et al. 2001, ApJ, 562, L19

Eggleton, P. P., Tout, C. A., & Fitchett, M. J. 1989, ApJ, 347, 998

Fabbiano, G., Zezas, A., King, A. R., et al. 2003, ApJ, 584, L5

Faber, S. M. & Jackson, R. E. 1976, ApJ, 204, 668

Fan, X., Narayanan, V. K., Lupton, R. H., et al. 2001, AJ, 122, 2833

Ferrarese, L. & Merritt, D. 2000, ApJ, 539, L9

Ferraro, F. R., Sollima, A., Pancino, E., et al. 2004, ApJ, 603, L81

Ferraro, F. R., Sollima, A., Rood, R. T., et al. 2006, ApJ, 638, 433

Fiestas, J. & Spurzem, R. 2010, MNRAS, 405, 194

Filippenko, A. V. & Ho, L. C. 2003, ApJ, 588, L13

Freeman, K. C. 1993, in Astronomical Society of the Pacific Conference Series, Vol. 48, The Globular Cluster-Galaxy Connection, ed. G. H. Smith & J. P. Brodie, 608

Freeman, K. C. & Rodgers, A. W. 1975, ApJ, 201, L71

Fryer, C. L. 1999, ApJ, 522, 413

Fryer, C. L., Woosley, S. E., & Heger, A. 2001, ApJ, 550, 372

Fukugita, M., Hogan, C. J., & Peebles, P. J. E. 1998, ApJ, 503, 518

Gascoigne, S. C. B. & Burr, E. J. 1956, MNRAS, 116, 570

Gebhardt, K. 2004, Coevolution of Black Holes and Galaxies, 248

Gebhardt, K., Adams, J., Richstone, D., et al. 2011, ApJ, 729, 119

Gebhardt, K., Bender, R., Bower, G., et al. 2000a, ApJ, 539, L13

Gebhardt, K., Rich, R. M., & Ho, L. C. 2005, ApJ, 634, 1093

Gebhardt, K., Richstone, D., Ajhar, E. A., et al. 1996, AJ, 112, 105

Gebhardt, K., Richstone, D., Kormendy, J., et al. 2000b, AJ, 119, 1157

Gebhardt, K., Richstone, D., Tremaine, S., et al. 2003, ApJ, 583, 92

Genzel, R., Thatte, N., Krabbe, A., Kroker, H., & Tacconi-Garman, L. E. 1996, ApJ, 472, 153

Georgiev, I. Y., Hilker, M., Puzia, T. H., Goudfrooij, P., & Baumgardt, H. 2009, MNRAS, 396, 1075

Ghez, A. M., Becklin, E., Duchjne, G., et al. 2003, Astronomische Nachrichten Supplement, 324, 527

Giersz, M. & Heggie, D. C. 1996, MNRAS, 279, 1037

Giersz, M. & Heggie, D. C. 2003, MNRAS, 339, 486

Gies, D. R. & Bolton, C. T. 1986, ApJ, 304, 371

Gillessen, S., Eisenhauer, F., Trippe, S., et al. 2009, ApJ, 692, 1075

Godet, O., Barret, D., Webb, N. A., Farrell, S. A., & Gehrels, N. 2009, ApJ, 705, L109

Gratton, R. G., Bonifacio, P., Bragaglia, A., et al. 2001, A&A, 369, 87

Gültekin, K., Richstone, D. O., Gebhardt, K., et al. 2009, ApJ, 698, 198

Haehnelt, M. G., Natarajan, P., & Rees, M. J. 1998, MNRAS, 300, 817

Haiman, Z. & Loeb, A. 2001, ApJ, 552, 459

Häring, N. & Rix, H. 2004, ApJ, 604, L89

Harris, W. E. 1996, AJ, 112, 1487

Hasani Zonoozi, A., Kuepper, A. H. W., Baumgardt, H., et al. 2010, ArXiv e-prints

Heger, A. & Woosley, S. E. 2002, ApJ, 567, 532

Hilker, M., Kayser, A., Richtler, T., & Willemsen, P. 2004, A&A, 422, L9

Hughes, S. A. & Blandford, R. D. 2003, ApJ, 585, L101

Hurley, J. R. 2007, MNRAS, 379, 93

Hurley, J. R., Pols, O. R., & Tout, C. A. 2000, MNRAS, 315, 543

Hut, P., McMillan, S., Goodman, J., et al. 1992, PASP, 104, 981

Ibata, R., Bellazzini, M., Chapman, S. C., et al. 2009, ApJ, 699, L169

Iorio, L. 2008, Ap&SS, 315, 335

King, A. R., Davies, M. B., Ward, M. J., Fabbiano, G., & Elvis, M. 2001, ApJ, 552, L109

King, I. R. 1966, AJ, 71, 64

King, I. R. & Anderson, J. 2002, in Astronomical Society of the Pacific Conference Series, Vol. 265, Omega Centauri, A Unique Window into Astrophysics, ed. F. van Leeuwen, J. D. Hughes, & G. Piotto, 21

King, I. R., Hedemann, Jr., E., Hodge, S. M., & White, R. E. 1968, AJ, 73, 456

Kormendy, J. 1993, in The Nearest Active Galaxies, ed. J. Beckman, L. Colina, & H. Netzer, 197–218

Kormendy, J. & Gebhardt, K. 2001, in American Institute of Physics Conference Series, Vol. 586, 20th Texas Symposium on relativistic astrophysics, ed. J. C. Wheeler & H. Martel, 363–381

Kormendy, J. & Richstone, D. 1995, ARA&A, 33, 581

Krajnović, D., Cappellari, M., Emsellem, E., McDermid, R. M., & de Zeeuw, P. T. 2005, MNRAS, 357, 1113

Kroupa, P. 2001, MNRAS, 322, 231

Kroupa, P. 2008, in IAU Symposium, Vol. 246, IAU Symposium, ed. E. Vesperini, M. Giersz, & A. Sills, 13–22

Lacey, C. G. & Ostriker, J. P. 1985, ApJ, 299, 633

Larson, R. B. 1998, MNRAS, 301, 569

Lee, H. M. 1987, ApJ, 319, 801

Lu, T.-N. & Kong, A. K. H. 2011, ApJ, 729, L25

Madau, P. & Rees, M. J. 2001, ApJ, 551, L27

Magorrian, J., Tremaine, S., Richstone, D., et al. 1998, AJ, 115, 2285

Maoz, E. 1995, ApJ, 447, L91

Maoz, E. 1998, ApJ, 494, L181

Maraston, C. 1998, MNRAS, 300, 872

Mashchenko, S. & Sills, A. 2005, ApJ, 619, 243

Mateo, M. L. 1998, ARA&A, 36, 435

Matsumoto, H., Tsuru, T. G., Koyama, K., et al. 2001, ApJ, 547, L25

Mayor, M., Meylan, G., Udry, S., et al. 1997, AJ, 114, 1087

McLaughlin, D. E., Anderson, J., Meylan, G., et al. 2006, ApJS, 166, 249

Merloni, A., Heinz, S., & di Matteo, T. 2003, MNRAS, 345, 1057

Merritt, D., Meylan, G., & Mayor, M. 1997, AJ, 114, 1074

Meylan, G. 1987, A&A, 184, 144

Meylan, G. 2002, in Astronomical Society of the Pacific Conference Series, Vol. 265, Omega Centauri, A Unique Window into Astrophysics, ed. F. van Leeuwen, J. D. Hughes, & G. Piotto, 3

Meylan, G., Mayor, M., Duquennoy, A., & Dubath, P. 1995, A&A, 303, 761

Meza, A., Navarro, J. F., Abadi, M. G., & Steinmetz, M. 2005, MNRAS, 359, 93

Miller, M. C. 2003, in American Institute of Physics Conference Series, Vol. 686, The Astrophysics of Gravitational Wave Sources, ed. J. M. Centrella, 125–134

Miller, M. C. & Hamilton, D. P. 2002, MNRAS, 330, 232

Milone, A. P., Bedin, L. R., Piotto, G., et al. 2008, ApJ, 673, 241

Miniutti, G., Ponti, G., Dadina, M., et al. 2006, MNRAS, 373, L1

Miocchi, P. 2007, MNRAS, 381, 103

Norris, J. E. & Da Costa, G. S. 1995, ApJ, 447, 680

Noyola, E. & Gebhardt, K. 2006, AJ, 132, 447

Noyola, E. & Gebhardt, K. 2007, AJ, 134, 912

Noyola, E., Gebhardt, K., & Bergmann, M. 2008, ApJ, 676, 1008

Noyola, E., Gebhardt, K., Kissler-Patig, M., et al. 2010, ApJ, 719, L60

Pasquini, L., Avila, G., Blecha, A., et al. 2002, The Messenger, 110, 1

Pinkney, J., Gebhardt, K., Bender, R., et al. 2003, ApJ, 596, 903

Piotto, G., Bedin, L. R., Anderson, J., et al. 2007, ApJ, 661, L53

Piotto, G., Villanova, S., Bedin, L. R., et al. 2005, ApJ, 621, 777

Pooley, D. & Rappaport, S. 2006, ApJ, 644, L45

Portegies Zwart, S. F., Baumgardt, H., Hut, P., Makino, J., & McMillan, S. L. W. 2004, Nature, 428, 724

Portegies Zwart, S. F., Baumgardt, H., McMillan, S. L. W., et al. 2006, ApJ, 641, 319

Portegies Zwart, S. F., Makino, J., McMillan, S. L. W., & Hut, P. 1999, A&A, 348, 117

Portegies Zwart, S. F. & McMillan, S. L. W. 2002, ApJ, 576, 899

Pryor, C. & Meylan, G. 1993, in Astronomical Society of the Pacific Conference Series, Vol. 50, Structure and Dynamics of Globular Clusters, ed. S. G. Djorgovski & G. Meylan, 357

Rees, M. J. 1984, ARA&A, 22, 471

Reijns, R. A., Seitzer, P., Arnold, R., et al. 2006, A&A, 445, 503

Sargent, W. L. W., Young, P. J., Lynds, C. R., et al. 1978, ApJ, 221, 731

Sawyer Hogg, H. 1947, JRASC, 41, 69

Schneider, R., Ferrara, A., Natarajan, P., & Omukai, K. 2002, ApJ, 571, 30

Schödel, R., Ott, T., Genzel, R., et al. 2002, Nature, 419, 694

Schwarzschild, M. 1979, ApJ, 232, 236

Seth, A., Agüeros, M., Lee, D., & Basu-Zych, A. 2008, ApJ, 678, 116

Seth, A. C., Cappellari, M., Neumayer, N., et al. 2010, ApJ, 714, 713

Silk, J. & Rees, M. J. 1998, A&A, 331, L1

Sollima, A., Pancino, E., Ferraro, F. R., et al. 2005, ApJ, 634, 332

Soria, R., Hau, G. K. T., Graham, A. W., et al. 2010, MNRAS, 405, 870

Sparke, L. S. & Gallagher, III, J. S. 2006, Galaxies in the Universe - 2nd Edition, ed. Sparke, L. S. & Gallagher, J. S., III

Spitzer, L. 1987, Dynamical evolution of globular clusters, ed. Spitzer, L.

Suntzeff, N. B. & Kraft, R. P. 1996, AJ, 111, 1913

Tanaka, T. & Haiman, Z. 2009, ApJ, 696, 1798

Thomas, J. 2010, ArXiv e-prints

Thomas, J., Saglia, R. P., Bender, R., et al. 2005, MNRAS, 360, 1355

Thomas, J., Saglia, R. P., Bender, R., et al. 2007, MNRAS, 382, 657

Thomas, J., Saglia, R. P., Bender, R., et al. 2004, MNRAS, 353, 391

Trager, S. C., King, I. R., & Djorgovski, S. 1995, AJ, 109, 218

Tremaine, S., Gebhardt, K., Bender, R., et al. 2002, ApJ, 574, 740

Ulvestad, J. S., Greene, J. E., & Ho, L. C. 2007, ApJ, 661, L151

Usuda, T., Kobayashi, N., Terada, H., et al. 2001, in Astronomical Society of the Pacific Conference Series, Vol. 245, Astrophysical Ages and Times Scales, ed. T. von Hippel, C. Simpson, & N. Manset, 454

van de Ven, G., van den Bosch, R. C. E., Verolme, E. K., & de Zeeuw, P. T. 2006, A&A, 445, 513

van den Bosch, R., de Zeeuw, T., Gebhardt, K., Noyola, E., & van de Ven, G. 2006, ApJ, 641, 852 van den Bosch, R. C. E. & de Zeeuw, P. T. 2010, MNRAS, 401, 1770

van den Bosch, R. C. E., van de Ven, G., Verolme, E. K., Cappellari, M., & de Zeeuw, P. T. 2008, MNRAS, 385, 647

van der Marel, R. P. & Anderson, J. 2010, ApJ, 710, 1063

van der Marel, R. P., Cretton, N., de Zeeuw, P. T., & Rix, H.-W. 1998, ApJ, 493, 613

Vesperini, E. & Trenti, M. 2010, ApJ, 720, L179

Volonteri, M., Madau, P., & Haardt, F. 2003, ApJ, 593, 661

Walcher, C. J., van der Marel, R. P., McLaughlin, D., et al. 2005, ApJ, 618, 237

White, R. E. & Shawl, S. J. 1987, ApJ, 317, 246

Wiersema, K., Farrell, S. A., Webb, N. A., et al. 2010, ApJ, 721, L102

Zezas, A. & Fabbiano, G. 2002, ApJ, 577, 726

Acknowledgements

Properly appreciating the support and help of my friends during these three years is impossible to express in a few words. But I would like to first thank Dr. Markus Kissler-Patig very much, for his patience, and for his always constructive strategical advice. Without his support this project would have not been possible at ESO. Markus, you were always a very kind supporter and I hope I could learn the main ingredients that are necessary for doing scientific research.

I would like to thank my collaborators especially Prof. Karl Gebhardt, who I had a chance to work with during my PhD, and hosted me in Texas university at Austin in April 2010. I am also grateful to Dr. Holger Baumgardt who strongly contributed to this thesis, and for his hospitality during my stay in Bonn in two visits in 2009. I thank Dr. Eva Noyola very much for the things I learned with her and many discussions we had which were necessary for the development of my thesis. Chapter 2 is heavily based on her contribution on obtaining the kinematics of ω Centauri. I will not forget the exciting times we had while observing with the VLT. I acknowledge Dr. Nadine Neumayer for carefully reading my introduction and conclusion chapters that has improved my manuscript. I thank Nora Luetzgendorf, especially for nicely translating my abstract into German. I would also like to thank Prof. Tim de Zeeuw for his kind advice and his great support. I thank Prof. Barbara Ercolano for accepting to be my second thesis referee and review my PhD dissertation.

During the last three years, I have had many nice memories with friends that I have met from around the world. Greetings to my friends in Garching who made the time I spent here enjoyable, especially for all the coffee breaks, ping-pong matches and biking trips: Renzo Capelli, Gregor Rossmanith, Heike Modest, Luca Ricci, Alex Boehnert, Ingo Misgeld, Carolina Nunez, Tania Penuela, Iva Karovic, Matthias Frank, Ulf Seemann, Lu Feng, Anna Raiter, Mariya Lyubenova, Camilla Juul Hansen, Eli Bressert, Fei Zhao and many more to list here.

I feel extremely lucky to meet Matthias Frank at ESO whose smart ideas and positive justifications improved and broadened my knowledge in astronomical world as well as in general. Matthias, it was indeed lots of fun to chat with you about all the social things. I also thank my friend Dr. Kambiz Fathi for all the discussions and fun chats we had together which helped me keep going on.

My special thanks will go to Mohammad Zamaninasab, as my best friend and as my first physics teacher who positively affects my life since the very beginning we have met.

I could only make it to now with the non-stop moral support of my family especially my mother, Shahla, and my dear sister, Banafsheh. I will always remember the emotions and the moments we spent together. Ati, I really appreciate you for your kind patience.

Curriculum Vitae

Behrang Jalali

Personal Information:

First Name:	Behrang
Last Name:	Jalali
Date of Birth:	19 September 1981
Gender:	Male
Nationality:	Iranian
Marital status:	Married to Fatemeh Motalebi

Education:

- April 2008 - September 2011
PhD in Astronomy
European Southern Observatory & Ludwig-Maximilians-Universität, München, Germany

- September 2005 - January 2008
M. Sc. in Physics at Sharif University of Technology, Iran

- September 2000 - January 2005
B. Sc. in Physics at Isfahan University of Technology, Iran

Refereed Publications:

1. "Very Large Telescope Kinematics for Omega Centauri: Further Support for a Central Black Hole"
Noyola, E., Gebhardt, K., Kissler-Patig, M., Lützgendorf, N., **Jalali, B.**, de Zeeuw, P. T., Baumgardt, H. 2010, ApJL, 719, 60

2. "A Dynamical N-body Model for the Central Region of ω Centauri"
   Jalali, B., Baumgardt, H., Kissler-Patig, M., Gebhardt, K., Noyola, E., Lützgendorf, N., de Zeeuw, P. T., submitted to A&A

3. "Kinematic signature of an intermediate mass black hole in the globular cluster NGC 6388"
   Lützgendorf, N., Kissler-Patig, M., Noyola, E., **Jalali, B.**, de Zeeuw, P. T., Gebhardt, K., Baumgardt, H., accepted for publication in A&A

4. "Central Black Hole of ω Centauri: More Evidence from Orbit-Based Models"
   Jalali, B., Gebhardt, K., Kissler-Patig, M., Noyola, E., Lützgendorf, N., de Zeeuw, P. T., Baumgardt, H., in final preparation

Research Interests:

- Dynamical Structure and Evolution of Stellar Systems:
  Observational Projects and Numerical Modelling
- Galaxy Formation and Evolution
- Instrumentation:
  Integral Field Units, Adaptive Optics, Fabry-Perot

Observations:

- PI of 17h visitor mode observations with VLT/FLAMES (086.D-0573); observed in February 2011
- CoI of two proposals in visitor mode observations with VLT/FLAMES (083.D-0444 and 085.D-0928); taken in June 2009 and May 2010
- Observing with VLT/FLAMES in June 2009

Technical Skills:

- **Operating Systems:** good knowledge of Linux and Windows
- **Programming languages:** good knowledge of C/C++, familiar with Fortran
- **Data reduction softwares/packages:** IRAF/DS9, DAOPHOT (photometry on VLT-NACO data: Fabry-Perot behind Adaptive Optics) and NBODY6 (simulations package)
- **Miscellaneous tools:** IDL, LaTeX, familiar with Gnuplot and Maple